THE POSSIBLE COMMON ORIGIN OF THE STILLWATER COMPLEX AND BUSHVELD COMPLEX

A Senior Honors Thesis

Submitted in Partial Fulfillment of the Requirements for the degree of

Bachelor of Science with Distinction in Geological Sciences at

The Ohio State University

By

Andrew Rathbun

The Ohio State University

2003

Approved by

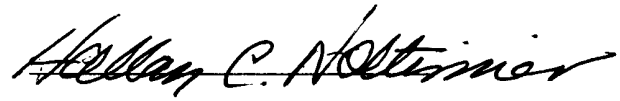

Dr. Hallan C. Noltimier

Department of Geological Sciences

Abstract

A pre-Rodinia Supercontinent first proposed by Rogers and Santosh, (2002), and further discussed by Zhao et al., (2002) contained both the Wyoming and Kaapvaal Cratons possibly in close proximity. This investigation looks at the possibility that the Wyoming and Kaapvaal Cratons may have been connected by exploring the geology of the Stillwater and Bushveld Complexes. A reconstruction is presented based on previous reconstructions by Zhao et al., (2002)

It has been concluded that these two unique intrusions were not coeval at formation, due to age differences, platinum group element ratios in ore minerals, ore mineralogy, and contact metamorphism. However, this study may contribute to revision of the few proposed Archean supercontinent reconstructions.

GEOLOGIC TIME SCALE (2003)

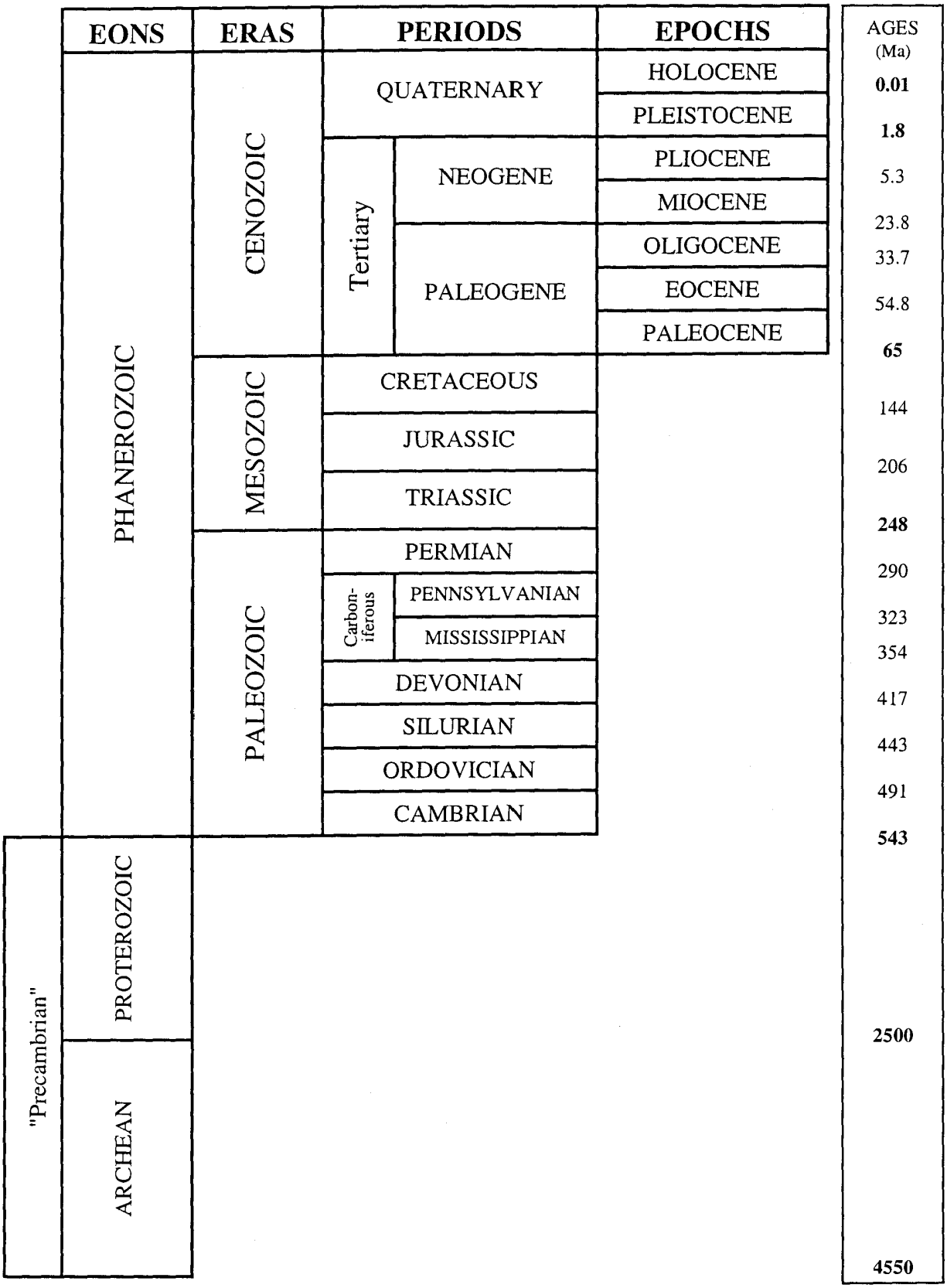

Acknowledgments

I would like to thank my advisor, Dr. Hallan C. Noltimier for giving me the opportunity to work on this project. His guidance, support, access to ore samples collected in South Africa and Montana, and patience have been much valued and needed throughout the project and time spent.

I would also like to thank Dr. Ennis Geraghaty and all of the geologists at Stillwater Mining Company for their time, tour of the mine and operations, and provision of additional samples. The time and samples provided from Paul Linton, Senior Geologist, Dr. Chris A. Lee, Division of Consulting Geologist, Gordon Chunnett, Manger of Exploration, Anglo American Platinum Corp. Ltd. Johannesburg, RSA, and Alan S. Page Mining Engineer, Anglo American Platinum Corp. Ltd. Rustenburg, RSA

The reviews of my committee of Dr. Martin Caffrey and Dr. Douglas Pride are much appreciated along with all of their input and guidance.

Most importantly I would like to thank my parents and family for giving me the opportunity and support needed to attend Ohio State University.

Support for this project has been supplied by, Sigma-Xi Chapter at Ohio State University, the Ohio State Honors Program, and the Friends of Orton Hall Fund of the Ohio State Department of Geological Sciences.

TABLE OF CONTENTS

LIST OF FIGURES

LIST TABLES

Chapter 1

Introduction

1.1 Introduction

This thesis project focuses on the Stillwater Complex of Montana and Bushveld Complex of South Africa and their relation to the tectonic history and discussion of an Archean pre-Rodinia supercontinent. Both complexes are layered igneous intrusions with unique igneous stratigraphy and mineralization. Within these two complexes are some of the world's richest chromitite and platinum group element mines and reserves as well as other important mineral resources.

The Stillwater Complex was emplaced ca. 2,700 Ma (Premo et al., 1990) and the Bushveld at 2,060 Ma (Cawthorn and Walraven, 1998). Both are mafic to ultramafic complexes with layering from a few mm to km in scale. Rock types are norite, gabbro, bronzitite, harzburgite, dunite, and anorthosite, to name some of the major rock types. In both complexes platinum-palladium mineralization is related to the appearance of anorthosite rocks.

1.2 Purpose of Investigation

The mining geology and history of both the Stillwater and Bushveld complexes has been studied in detail, with limited information released to the scientific community.

Occurrences of ore mineralization are strikingly similar within the complexes. The purpose of this investigation is three fold; to focus on the similarities, contrast the differences and relate possible locations of the complexes when they formed.

1.3 Methodology

1.3.1 Laboratory Studies

Studies were conducted in the MARC Lab at Ohio State University by Dr. John Olesik on the ICP-MS for platinum group elements, V, Cr, and Ni. Dr. Sreenivas Bhattiprolu of the MARC facility analyzed samples of both complexes on the scanning electron microscope, for mineral identification. Results of the ICP-MS analysis are given in Appendix A and SEM analysis in Appendix B. Chromitite samples from the Mouat Mine within the Stillwater complex were observed under reflected light microscopy for mineralization and textures.

1.3.2 Research

Most work for this thesis was done as literature research. A wealth of literature has been published on most issues considered within this thesis and much effort was been expended to find relevant research by major authors concerning both complexes. Original correlation and investigation was carried out based on these published sources.

Chapter 2

Bushveld and Stillwater Complexes

2.1 Bushveld Complex Geology and Stratigraphy

The Bushveld Igneous Complex (BIC) is located in the northeast part of the Kaapvaal Craton in the eastern Republic of South Africa, around 100 km northwest of Johannesburg. The layered igneous intrusion was emplaced at 2,060 Ma (Cawthorn and Walraven, 1998). At the time of intrusion into the Transvaal Supergroup, the Craton was stable. The age of the supergroup is 2,551 to 2,204 Ma (Cawthorn and Walraven, 1998). The BIC is the largest known layered intrusion on Earth with an area of 61,000-65,000 km^2, or around a 290 km diameter. The overall area is more than 310 times larger than the Stillwater Complex, MT, USA. The average thickness of the complex is seven to nine km for the layered mafic rocks. The complex has undergone little to no metamorphism since its intrusion. The BIC is composed of both layered mafic and ultramafic rocks at the base. Commonly called the Rustenburg Layered Suite, layered felsic rocks overlie the Rustenburg Layered Suite.

2.1.2 Emplacement and Crystallization

The Bushveld Igneous Complex formed from multiple injections of magma likely from different feeders. It has been proposed that the magma was emplaced over a period of about 75,000 years (Cawthorn and Walraven, 1998). The volume of rock in the Eastern and Western Limbs is 370,000 km^3 to 600,000 km^3, but it is thought that

significant volumes are missing, original volumes could have been over 1,000,000 km^3 (Cawthorn and Walraven, 1998). It is thought that the BIC was the intrusive equivalent of a flood basalt related to a mantle plume. Cawthorn and Walraven, (1998) calculated cooling rates assuming six different injections of magma, but the actual number of injections is not known. Crystallization times are estimated to be around 200,000 years for the Rustenburg Layered Suite (Cawthorn and Walraven, 1998).

The BIC intrudes the Pretoria Group of the Transvaal Supergroup. Figure 2.1 shows the stratigraphy and intrusion geometry of the BIC. The Transvaal Supergroup consists of quartzites, ironstone, shales, with basaltic and acid volcanic rock at the top. The Bushy Bend Lava Member at the base of the group has been dated at 2,350 Ma from zircon studies (Eriksson et al., 1995). Some have hypothesized that the intrusion occurs on a regional unconformity (Eales and Cawthorn, 1996). The BIC is still relatively unmetamorphosed and undeformed (Cawthorn and Walraven, 1998). Dips throughout the complex range from 10° to 35°. Figure 2.2 shows a generalized geologic cross section through the East Limb of the BIC.

Studies in the far Western Limb of the BIC indicate contact metamorphic conditions between 646 and 740°C and pressures of 210-320 MPa, but likely under 220 MPa from field relationships (Engelbrecht, 1990), with partial melting seen throughout the top of the BIC (Eriksson et al., 1995). The limits of contact metamorphism are around 10 km to the north of the limb and 45 km to the southwest. Beyond this zone, lower greenschist facies regional metamorphism has taken place. The intrusion of the BIC metamorphosed rock of the Pretoria Group into hornfels, slates, and amphibolites.

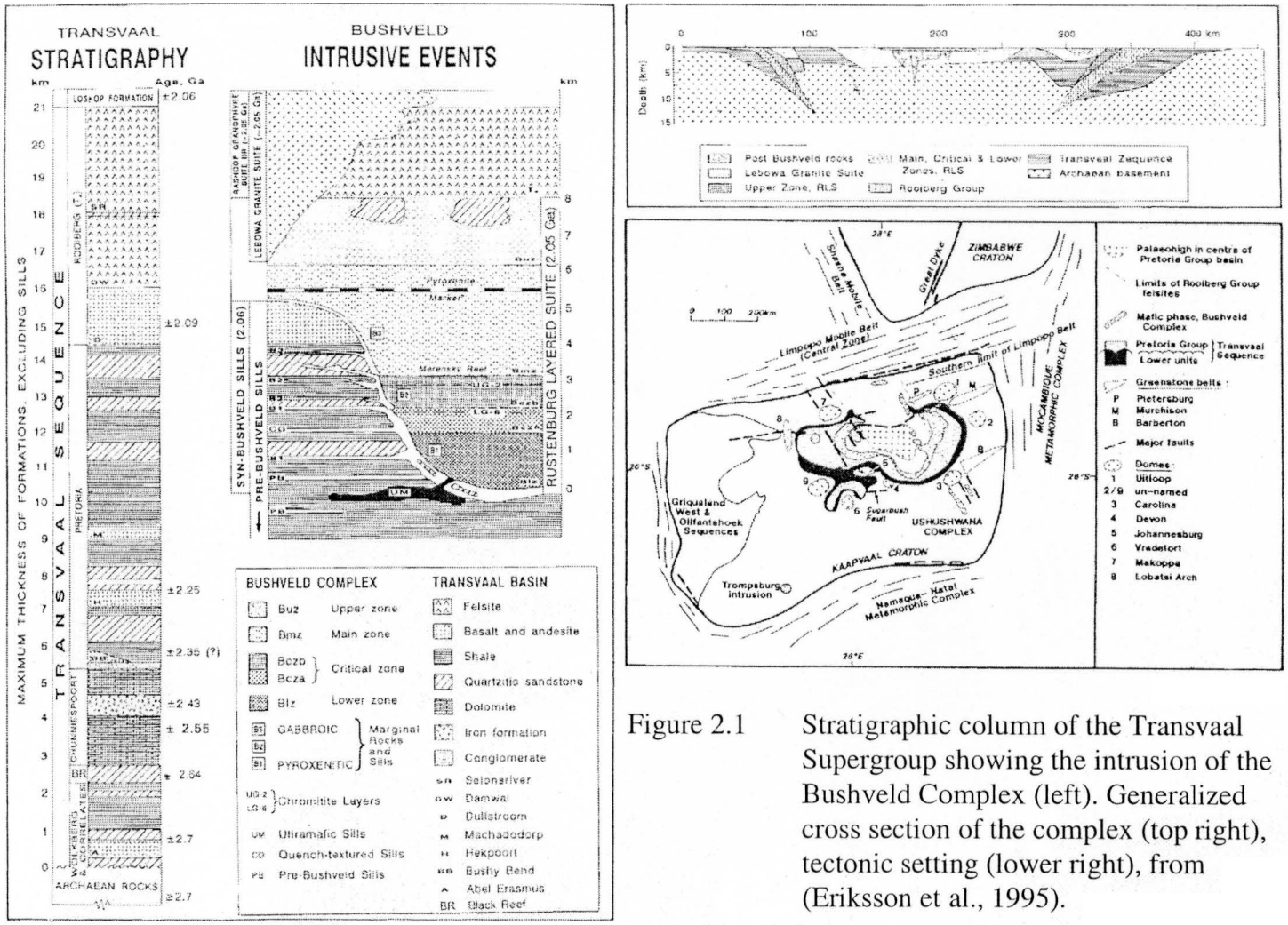

Figure 2.1 Stratigraphic column of the Transvaal Supergroup showing the intrusion of the Bushveld Complex (left). Generalized cross section of the complex (top right), tectonic setting (lower right), from (Eriksson et al., 1995).

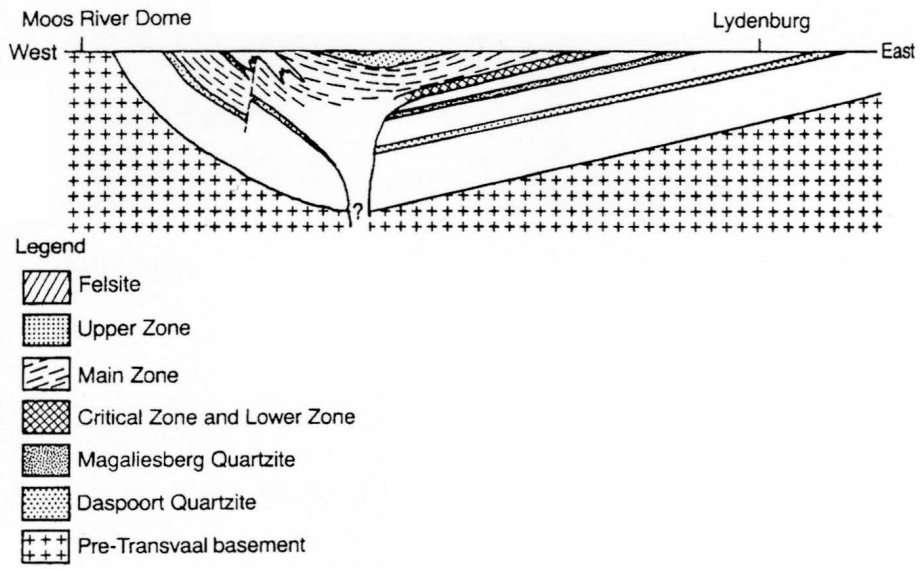

Figure 2.2 Generalized cross section through the Eastern Limb of the Bushveld Complex from (Guilbert and Park, 1986).

The Pretoria Group consists mainly of alternating sequences of shale and sandstone interbedded with lava flows and some carbonates, diamictites, and conglomerates. One flow near the base of the group has been dated at 2,350 Ma (Eriksson et al., 1995). The sandstone has often been metamorphosed to quartzite.

2.1.3 Stratigraphy

The igneous stratigraphy of the BIC is long and complex. A great portion of the work on the stratigraphy has been completed in conjunction with mining operations and is not readily available. In areas without mining activity little is known. In these areas observations are almost solely based on surface exposures. A complete overview of the stratigraphy of the Rustenburg Layered Suite will be given in this section. The major zones of the BIC are the Marginal, Lower (LZ), Critical (CZ), Main (MZ), and Upper (UZ), the CZ is divided into the Lower Critical Zone (C_LZ) and Upper Critical Zone (C_UZ). Figure 2.3 gives a generalized stratigraphic column of the East and West Limbs as well as cumulus phases. The BIC consists of four major limbs with one that underlies younger sedimentary rocks (Eales and Cawthorn, 1996). Figure 2.4 shows the location of the major limbs of the BIC along with a simplified geologic map. The most studied and well known limb is the Western and Far Western. The other limbs are the Eastern, Northern or Potgietersrus, and the unexposed Southern or Bethal Limb (Eales and Cawthorn, 1996). Some researchers argue that it is likely that the Eastern and Western Limbs were connected but it can not be shown whether the Potgietersrus and

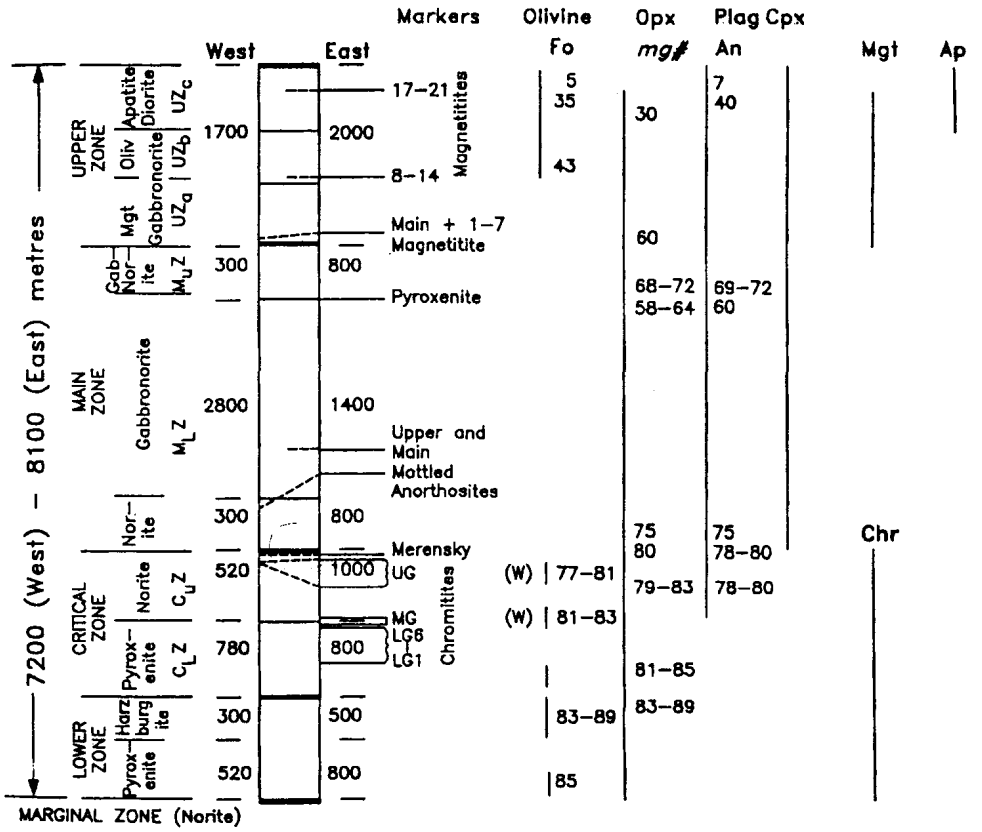

Figure 2.3 Stratigraphic column showing maximum thickness of units in the East and West Limbs, occurrence of minerals and cumulus percentages from (Eales and Cawthorn, 1996).

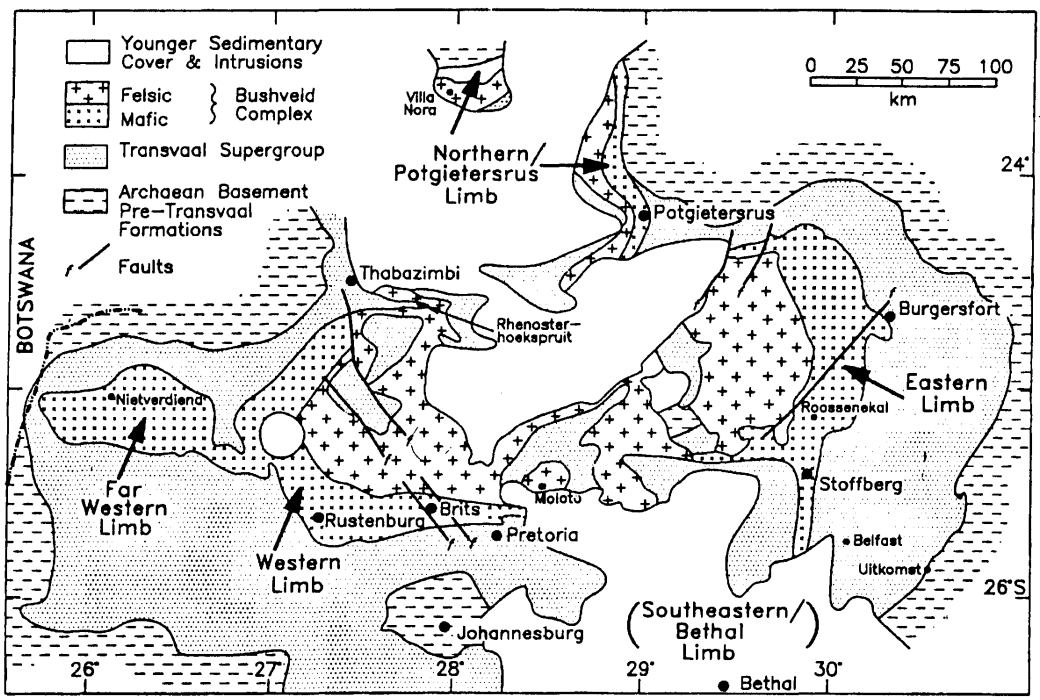

Figure 2.4 Map showing major limbs and rocks of the Bushveld Complex from (Eales and Cawthorn 1996).

Bethal Limbs were synchronous or whether they postdated or predated the two major limbs (Cawthorn and Walraven, 1998).

The Marginal Zone attains a maximum thickness of 800 m. Rocks of the Marginal Zone consist of norite and pyroxenite with abundant xenoliths of further metamorphosed metasedimentary rock. This zone is absent north of Potgietersrus and in a locality in the Eastern Limb (Cawthorn and Walraven, 1998, Eales and Cawthorn, 1996).

The Lower Zone is a relatively poorly studied layer of the BIC. Existing topography of the floor of the complex likely controlled thickness of deposition of the LZ. The LZ is not present throughout the entire complex, but best exposures are on the eastern side of the BIC. Major rock types include pyroxenite, harzburgite, and dunite. At its thickest, the LZ is 1,700 m in the Potgietersrus Limb and 800 m to 1,300 m in the East to West Limbs. LZ cyclic units consist of olivine, chromite, and orthopyroxene cumulates. Only in the Potgietersrus Limb are significant occurrences of PGE's found; these occurrences are related to chromite layering. The top of this layer is defined as the change from two to six percent interstitial plagioclase in pyroxene, however this change is not found in the Western Limb so the top of the sequence is marked by the lack of significant olivine (Eales and Cawthorn, 1996).

The Critical Zone contains the rich platinum ore bodies of the BIC. The CZ attains a maximum thickness of 1,800 m in the Eastern Limb and is divided into the Lower Critical Zone (C_LZ) and Upper Critical Zone (C_UZ). This zone is home to both the UG2 and Merensky reef in the 800 m thick Upper Critical Zone (Eales and Cawthorn, 1996). The layering of the complex is best developed within the CZ (Guilbert and Park

1986). The CZ is also host to all of the chromite layers of the BIC. Chromite layers of the C_LZ are called LG1 through LG7. These layers are generally less than one meter thick and are associated with either harzburgite or pyroxenite (Schurmann et al., 1998). The C_LZ is characterized by the cumulus pyroxene. Other rock types include norite, and peridotites (Guilbert and Park, 1986). In the Western Limb of the BIC these chromite layers decrease in thickness from the northwest to the southeast. A change is also seen in the Eastern Limb of the complex, but is not as defined. In the Potgietersrus Limb the C_LZ does not have an obvious equivalent, but variations may have made it indistinguishable from the LZ. The CZ wedges out toward the north of the complex (Eales and Cawthorn, 1996).

Above the LG1-7 chromite layers lies the Middle Group (MG) chromite, which are termed MG1 through MG4. The transition from C_LZ to C_UZ occurs between the MG2 and MG3. This transition is the first instance of cumulus plagioclase rock. This anorthosite first occurs in the BIC at the base of C_UZ. The zone is around 900 m thick and like the C_LZ is strongly layered. Norite and anorthosite are the most common rock types along with the chromite layers. In addition to the MG chromites the C_UZ contains the Upper Group chromites, UG1 and UG2, in the Eastern Limb UG3 is present (Guilbert and Park, 1986). Around 100 m from the top of the C_UZ is the Merensky Cyclic Unit. The Merensky Cyclic Unit contains a basal chromite, a pyroxenite, which can contain olivine, norite, and anorthosite. This unit contains the PGE rich Merensky Reef. A complete description of the Merensky Reef and UG2 layer can be found elsewhere in this thesis. Above the Merensky Cyclic Unit is the Bastard Cyclic Unit. This unit is similar to

the Merensky in most respects, but has subeconomic levels of ore minerals. Also chromite is locally absent (Eales and Cawthorn, 1996, Cawthorn and Walraven, 1998).

The division between the Main Zone and CZ is difficult to define, but is marked by the top of a mottled anorthosite layer with large oikocrysts of pyroxene, up to 10 cm in diameter. This layer is termed the Giant Mottled Anorthosite. The MZ is divided into two different zones, the Lower Main Zone (M_LZ) and Upper Main Zone (M_UZ). The MZ is a thick succession of cumulates, with the absence of both olivine and chromite as cumulate minerals. This zone lacks the fine scale layering of the CZ and also the diversity of the zone. Overall the MZ is attains a maximum thickness of 3,400 m in the Western Limb and 3,000 m in the Eastern Limb (Eales and Cawthorn, 1996, Cawthorn and Walraven, 1998).

The MZ has a basal norite ranging from 300 m to 800 m west to east. This norite contains cumulus augite then pigeonite toward the top. Above this layer, norite in the west and gabbronorite in the east is interbedded with the Main and Upper Mottled Anorthosites. The Upper Mottled Anorthosite is absent in the west of the complex. The Main Mottled Anorthosite is a strong magnetic marker allowing it to be traced throughout the complex. Above the gabbronorite zone is a one km thick interval containing both orthopyroxene and pigeonite, another one km above this pigeonite is replaced by orthopyroxene, this orthopyroxene-rich layer is called the Pyroxenite Marker (Eales and Cawthorn, 1996, Cawthorn and Walraven, 1998).

The Upper Zone is defined by the appearance of cumulus magnetite. Some have argued that isotopic definition of the zone would place the base at the Pyroxenite Marker, but most literature uses the magnetite layer. The UZ is between 1,700 m and 2,000 m as a

maximum thickness east to west, sometimes divided into subzones a, b, and c. The MZ is well layered intermittently with 25 magnetite layers in the Eastern Limb. The magnetite layers have sharp bases with magnetite grading out with height in the layers. The thickest of these layers is six m. Subzone a is composed of anorthosite and ferrogabbro with magnetite layering. Iron rich olivine marks the transition form subzone a to b. Within subzone b are anorthosite, troctolite, and ferrogabbro in addition to magnetite layers. Subzone c is marked by cumulus apatite, with olivine diorite, anorthosite, magnetite diorite and magnetite layers. The UZ magnetite is currently mined for the vanadium in the magnetite (Eales and Cawthorn, 1996, Cawthorn and Walraven, 1998).

2.2 Stillwater Complex Stratigraphy and Geology

The Stillwater Complex (SIC) is located in the Beartooth Mountains in southwest Montana of the Wyoming Craton. The SIC was emplaced around 2,700 Ma at depths of around six to seven km with an area of 194 km^2. The maximum width of the complex is eight km and the length is about 47 km. The SIC trends northwest to southeast with a dip of 45-60° to the north. It is not uncommon for dips to be close to 90° or even be over turned. The complex has three major series, the Basal, Ultramafic, and Banded. The Banded Series is divided into three subseries, the Lower Banded Series, Middle Banded Series, and Upper Banded Series. The SIC is intruded into Archean metasedimentary rocks in the west, in other areas the complex is in contact with younger Archean intrusions. In the north the Stillwater Complex is in contact with Paleozoic and Mesozoic sedimentary rocks. Figure 2.5 shows the placement of the Stillwater Complex and a

general geologic map (McCallum, 1987, McCallum, 1996, Guilbert and Park, 1986, Raedeke, 1982).

2.1.2 Emplacement

Studies have shown ages of 2701±8 Ma using Sm-Nd isotopes on mineral separates (DePaolo and Wasserburg, 1979). A study of zircons in the Basal Series determined an age of 2713±3 Ma (Nunes, 1981). The Sill/Dyke Suite associated with the Basal Series was dated at 2705±4 Ma using U-Pb zircon dating (Premo et al., 1990).

The Stillwater Complex was intruded into metasedimentary rock consisting of pelitic schist, iron formation, graywacke, quartzite and argillite. In many places the contact of the SIC and metamorphic rock is marked by a fault. The complex of metasediments is called the Boulder River Complex and contains iron formation, quartzite, schist, and hornfels with contact metamorphism occurring as far as 10 km distant. Assemblages indicate maximum temperatures of contact metamorphism at 825° C, with no partial melting seen in the pelitic rocks. Pressures indicated by the metamorphic rocks are around 200 MPa, or a depth of six to seven km (Labotka and Kath, 2001).

The iron formation and schist are discontinuous bodies near the intrusion of the SIC. Contacts generally are iron formation and hornfels to the northeast and hornfels to the southwest. Some bodies of iron formation do occur within the hornfels. The hornfels is found as far as four km from the complex. These assemblages are unfoliated with porphyroblasts of cummingtonite or hypersthene. Medium grained moderately foliated

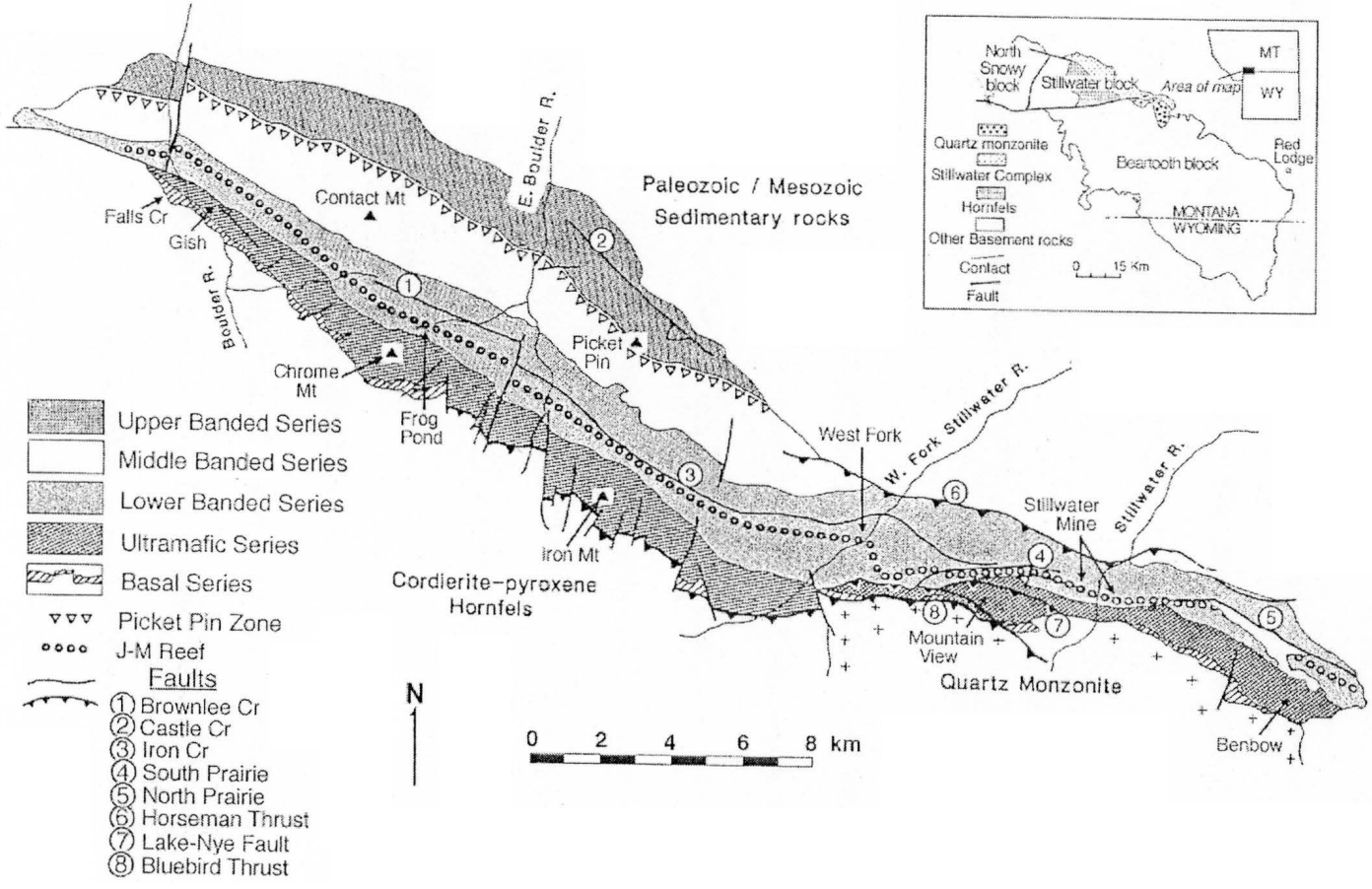

Figure 2.5 Map showing the geology and location of the Stillwater Complex from (McCallum, 1996).

biotite schists are seen more than four km away from the SIC. Cummingtonite, mica, and amphibole are randomly oriented with respect to the foliation plane. The hornfelsic texture may have been emplaced over regionally metamorphosed rocks that have relic sillimanite grades of metamorphism. This regional metamorphism may have taken place at 2,750 Ma (Labotka and Kath, 2001).

2.1.3 Stratigraphy

When dealing with the stratigraphy of the SIC it is important to keep the different naming schemes consistent. At least four common naming systems are used with the SIC and several others can also be found in the literature. This thesis will use the system of Todd et al., (1982) as it is most common in relevant literature. However, a recent trend to use the system of McCallum, Raedeke, and Mathez, (1980) can be seen because of the absence of some of Todd et al., (1982) layers in some areas of the SIC. Figure 2.6 contrasts the common naming schemes.

The stratigraphy of the SIC is complicated by faulting with deformation related to Cretaceous Larmide uplift. Figure 2.7 shows a cross section of the eastern section of the Complex in the Mountain View area. The faulting has broken and displaced stratigraphy throughout the Complex. The Bluebird thrust has placed Ultramafic Series rocks against Banded Series Rocks, the Lake-Nye Fault has offset the entire SIC a distance of almost one km. The Horseman Thrust forms the northern boundary of the Complex and thrusts a portion of it over younger sediments (McCallum, 1996).

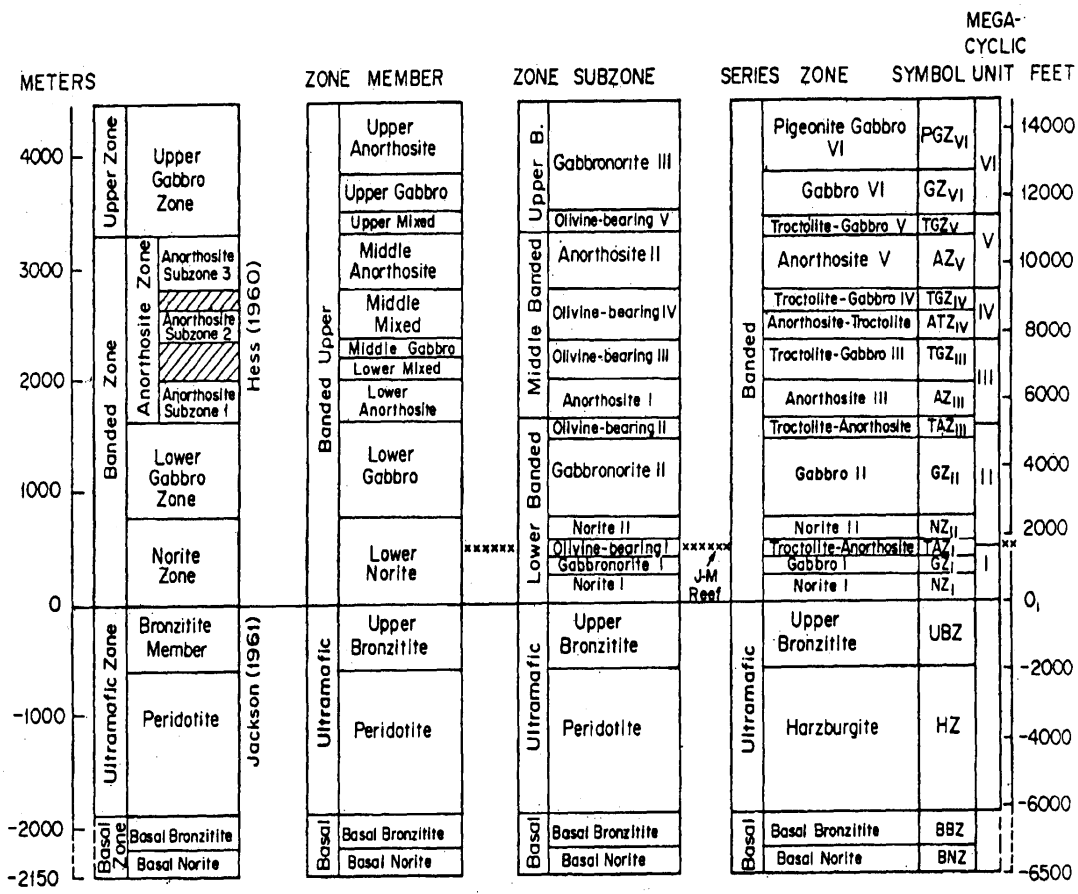

Jones, Peoples and Howland (1960)

Segerstrom and Carlson (1977, 1970,1980)

McCallum, Raedeke and Mathez (1980)

Todd et al., (1982)

Figure 2.6 Correlation of stratigraphic divisions of the Stillwater complex from (Todd et al., 1982).

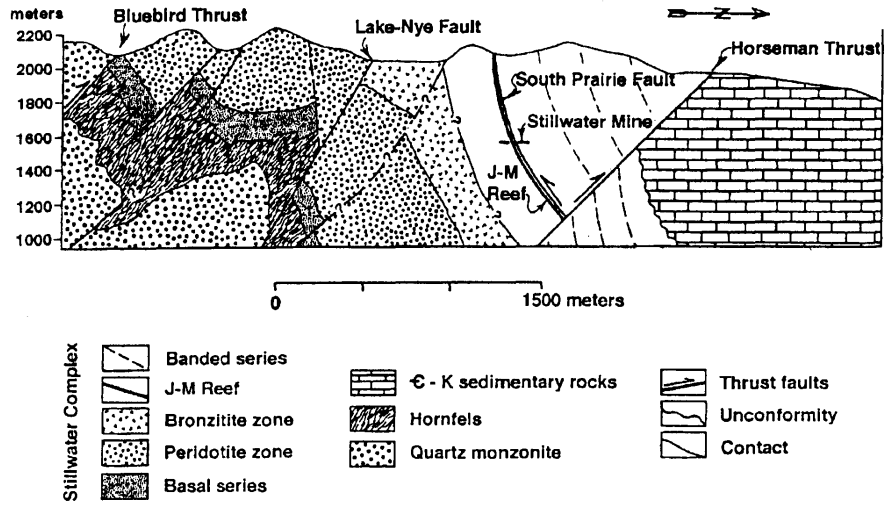

Figure 2.7 Cross Section through the Stillwater Complex in the Mountain View Area (from McCallum, 1996)

Figure 2.8 shows the stratigraphy of the SIC including cumulus phases. The Basal Series is irregular and not present in some areas of the complex. Thickness and presence of this series is controlled by numerous small and large scale faults. The thickness is between 18 and 400 m with an average of 160 m. This series is composed of two separate subseries: Basal Norite and Basal Bronzitite. The Basal Norite is a heterogeneous norite with many different cumulates with some orthopyroxene, plagioclase, augite, and olivine. Throughout the Basal Series, xenoliths of cordierite orthopyroxene hornfels are found. The Basal Bronzitite is defined by bronzitite being the only cumulus mineral present. Discontinuous zones of chromite seams are found in the upper levels of the Bronzitite subseries. Sulfides of copper and nickel are present throughout the series but decrease with height in the series (McCallum, 1996, McCallum, 1987, Raedeke, 1982, Zientek et al., 1985).

The Sill/Dyke Suite is associated with the Basal Series. These intrusions occur into the metasedimentary rock that underlies the SIC. In this suite two distinct types of sills and dykes exist. The first type has a diabasic texture with compositions of norite to gabbronorite. Sulfides are rare in this type of sill and dyke. The second type has two to 40 percent sulfide with a composition of norite. It is thought that both of these were related to the main intrusion of the SIC (McCallum, 1996).

The base of the Ultramafic Series is defined by the first occurrence of significant cumulus olivine. This series ranges from around 1,000 m to 2,000 m in thickness. This basal contact is only preserved in the west of the complex and only locally elsewhere. This series is divided into an upper Bronzitite Zone and lower Harzburgite Zone by Todd et al., (1982), or Peridotite Zone by McCallum, Raedeke, and Mathez, (1980).

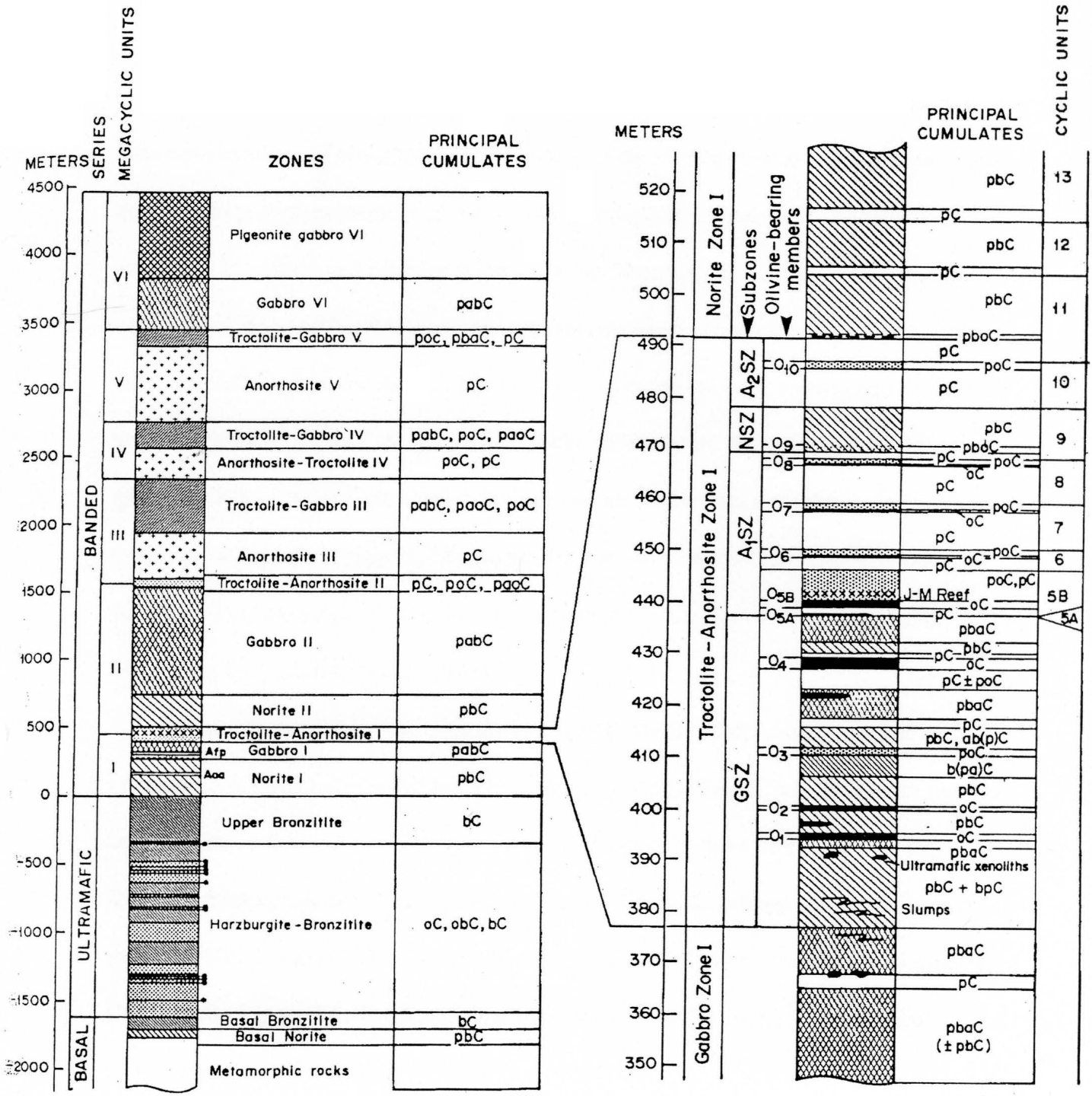

Figure 2.8 Stratigraphic column of the Stillwater Complex with exploded view of TAZ1. Abbreviations: cumulate (C), plagioclase (p), olivine (o), bronzite (b), augite (a). Solid circles in the Ultramafic Series denote chromitite layers from (Irvine et al., 1983).

The Harzburgite Zone is characterized by cyclic units of repeating olivine and bronzite cumulates. Through each cyclic unit olivine decreases with height then abruptly becomes important at the base of the next unit. Within this zone eight to 21 cyclic units have been identified and range in thickness from 50 to 150 m. Rock types are poikilitic harzburgite, granular harzburgite, and bronzite. Associated with the olivine cumulates thin chromitite layers are present. These layers are named A to K; mining activity has been restricted to layers G and H only. The chromitite layers range in thickness from a few crystals to a meter. The layers can thick and thin over distance, with some layers even separating into sublayers. The Bronzitite Zone is almost exclusively pyroxene cumulate. Post cumulus minerals include plagioclase and augite (McCallum, 1996, McCallum 1987, Zientek et al., 1985).

The transition from the Ultramafic Series to the Banded Series is marked by the appearance of cumulus plagioclase. The Banded Series is divided into the Lower Banded Series (LBS), Middle Banded Series (MBS), and Upper Banded Series (UBS). The Banded Series comprised about 2/3 the thickness of the SIC. Names will be given in the system of Todd et al., (1982), but can be correlated to McCallum, Raedeke, and Mathez, (1980) using Figure 2.6. The Banded Series is the only series in the SIC where cumulus plagioclase rocks are present.

The LBS can be split into six zones, these are Norite I, Gabbro I Troctolite-Anorthosite I (TAZ_I), Norite II, Gabbro II, and Troctolite-Anorthosite II. Zone TAZ_I is of special importance because it contains the platinum-palladium bearing J-M reef. Detailed stratigraphy of this layer can be found elsewhere in this thesis. The LBS is around 1,500 m thick and is well layered. Fine rhythmic layering, modal grading, cross bedding,

channel structures, and slump structures can all be seen. The lowest unit, Norite Zone I, consists of bronzite-plagioclase cumulates and is traceable throughout the entire complex. Cumulus augite marks the start of Gabbro Zone I, which also contains cumulus plagioclase and bronzite. TAZ_I, or Olivine bearing zone I of some authors, is a secession of olivine, plagioclase, bronzite, and augite bearing cumulates and pegmatoids. This is the first occurrence of cumulus olivine above the Ultramafic Series. The TAZ_I can be traced throughout the entire complex but the subzones within it are discontinuous. Above the TAZ_I is the Norite II, this zone is characterized by plagioclase-bronzite cumulate and one m thick rhythmic layering. Above this zone is the Gabbro Zone II, the thickest zone of the Banded Series. The top zone of the LBS is Troctolite-Anorthosite II, this unit, composed of plagioclase cumulates and olivine bearing cumulates thickness to the east of the complex (McCallum, 1996, Zientek et al., 1985).

The MBS can be divided into five zones. This series is around 2,000 m thick throughout the complex. The first zone, Anorthosite Zone III is a thick plagioclase cumulate. This layer is very distinctive because of 10 cm across oikocrysts of pyroxene. Above this zone is Troctolite-Gabbro Zone III. This zone is a mixture of plagioclase-augite, plagioclase-olivine-augite, and plagioclase-olivine-augite-bronzite cumulates. Above this is Anorthosite-Troctolite IV, which is composed of plagioclase cumulate, which grades into Troctolite-Gabbro Zone IV a plagioclase-olivine-augite cumulate which can contain bronzite. Above Troctolite-Gabbro Zone IV is Anorthosite V, another thick plagioclase cumulate zone similar to Anorthosite Zone III. This zone contains the subeconomic Picket Pin deposit. The Picket Pin deposit is traceable for 22 km with pipes

of sulfide minerals. These pipes occur to a depth of 150 m in the anorthosite and lead to lenses. No mining has taken place in this zone (McCallum 1996, Zientek et al., 1985).

The UBS is the thinnest of the Banded Series. This subseries is only around 1,000 m thick. It can be divided into Troctolite-Gabbro V, Gabbro VI, and Pigeonite Gabbro VI. The first zone, Troctolite-Gabbro V is a sequence of olivine bearing cumulates and serves as a distinctive marker layer for the SIC. The top two zones are not divided by most authors of the SIC. They consist of two pyroxene gabbro and plagioclase cumulate throughout the complex. These rocks can become fine grained locally with plagioclase forming phenocrysts (McCallum 1996, Zientek et al., 1985).

Chapter 3

Mining Geology

3.1 Mining Geology of the Bushveld Complex

The Bushveld Complex holds half of the Earth's known reserves of platinum, palladium and the other PGE's along with large amounts of iron, titanium, vanadium, and tin (Cawthorn et al. 2002). The most important PGE layers are the Merensky Reef and the UG2 Chromitite. The average grade of the PGE is five to seven g/t over 100 km of strike length. Grades are very similar on both the eastern and western side of the complex. However, most of the mining has taken place on the western side (Cawthorn et al., 2002). Figure 3.1 shows the Bushveld Complex with platinum mineralization and mining. Both the Merensky Reef and UG2 are part of the Upper Critical Zone of the complex. Another important PGE layer, the Platreef, is located in the base of the Main Zone and occurs on the Potgietersrus limb. This layer has not been widely studied. Figure 3.2 contrasts the Eastern and Western Limbs to the Potgietersrus Limb and location of the Platreef.

3.1.2 Mineralogy

The Merensky Reef has been traced for a strike length of 283 km and ranges in thickness from a few centimeters to 14 m with potholes increasing it to greater thicknesses (Viljoen and Schurmann 1998). The rock types of this layer are generally feldspathic pyroxenite pegmatoids bounded by thin chromitite layers. The chromite

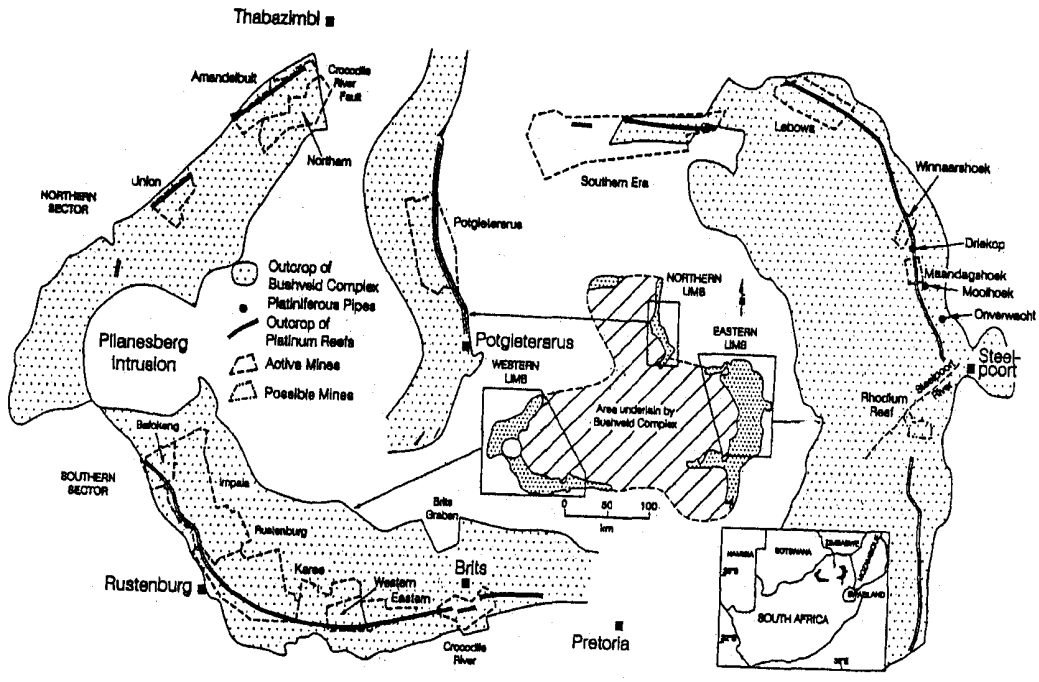

Figure 3.1 Map of the Bushveld Complex showing mines and platinum bodies from (Cawthorn et al., 2002)

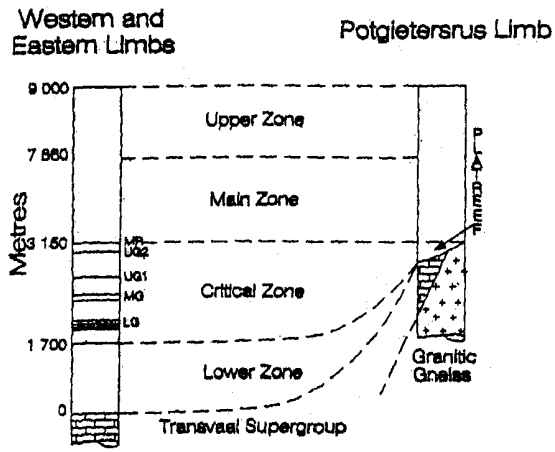

Figure 3.2 Correlation of Zones from the Western and Eastern Limbs to the Potgietersrus Limb from (Cawthorn et al., 2002).

layers are on the order of one cm thick. Other rock types hosting the Merensky Reef include harzburgite, melanorite, and norite with a footwall of either anorthosite or norite. The reef is composed of orthopyroxene, clinopyroxene, olivine, plagioclase, and chromite. Minor minerals include phlogopite, quartz, orthoclase, apatite, zircon, tremolite, talc, and serpentine with two to four percent sulfide (Cawthorn et al.2002).

The ore mineralogy of the reef over the entire complex is roughly 60 percent pyrrhotite, pentlandite, and pyrite, and 40 percent PGM and alloys. Throughout the complex, Pt is generally hosted in solid solution with pyrrhotite and as distinct minerals. Palladium and Rh occur in solid solution with pentlandite and discrete minerals, whereas pyrite hosts all PGE's but in small amounts. (Guilbert and Park 1986). The percentages of PGM's in seven current mines are shown in Figure 3.3. Within the chromite bounding layers laurite is common. Grain size of PGM's are on the scale of 10-350μm (Viljoen and Schurmann 1998). The ratio of Pt:Pd varies greatly within the complex, but the overall trend is around 2.4:1 platinum to palladium. Grades of the Merensky reef are on average six to nine g/t, but can be higher locally, the grade can be seen in Table 3.1. (Cawthorn et al., 2002).

The UG2 or Upper Group 2 Chromitite is 15 m below the Merensky Reef on the Western Limb of the complex and 400 m on the Eastern Limb, and the layer can be traced for over 280 km. The thickness is highly vairable between 70 and 250 cm with potholes increasing the depth significantly in places (Viljoen and Schurmann 1998, McLaren and Villiers 1982). Pyroxenite, melanorite, and anorthosite underlie the chromitite. Several leaders of chromitite are also present in the footwall and contain subeconomic platinum mineralization (Viljoen and Schurmann 1998).

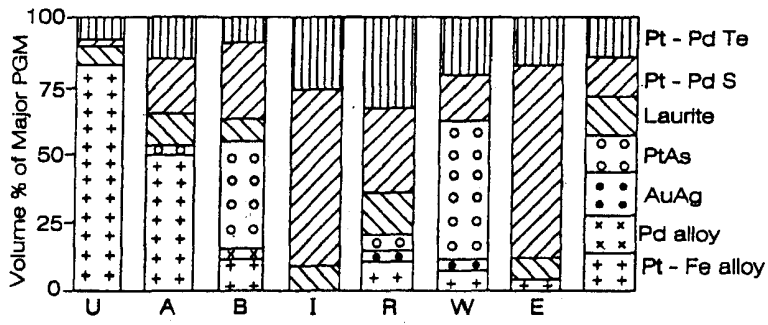

Figure 3.3 Percentages of PGM from the Union (U), Amandelbult (A), Bafokeng-Rasimone (B), Impala (I), Rustenburg (R), Western (W) of the Western Limb, and Lebowa (E) of the Eastern Limb from (Cawthorn et al., 2002).

Mine	PGE (g/t) mining width	PGE (g/t) best grade	Thickness of best grade	Pt %	Pd %	Ru %	Rh %	Ir %	Os %
Western limb									
Amandelbult	6.7	7.9	100	58	28	7	4	1.5	1.0
Union	9.2	7.4	130	59	24	8	5	1.8	1.0
Northam	6.1			61	26	7	3	1.3	2.0
Bafokeng	7.3								
Impala	6.8			59	27	7	5	1.7	1.4
Rustenburg	6.9	8.5	40	59	27	8	4	1.3	0.9
Western	5.6			62	28	6	3	1.0	0.3
Eastern limb									
Messina	4.9			48	41	5	3	2	n.a.
Lebowa	5.9	6.8	65	61	25	8	4	1.3	1.0
Winnaarshoek	5.9			54	30	6	3	1.4	n.a.

Table 3.1 Thickness in cm and grade of ore in g/t of mines in the Western and Eastern Limbs of the Bushveld Complex from (Cawthorn et al., 2002).

Chromite makes up 60-90 percent of the UG2 layer with pentlandite, and chalcopyrite, plus minor pyrrhotite, pyrite, arsenopyrite, bornite, chalcocite, covellite, galena, and millerite. Laurite also is a common inclusion in chromite. Grains sizes are on the order of 30μm (Viljoen and Schurmann 1998). Table 3.2 shows the grade of the UG2 layer throughout the complex. Grades for the UG2 are, on average, five to seven g/t but can be much higher. (Cawthorn et al. 2002). The grades of both the Merensky Reef and UG2 layer are shown at seven mines in the BIC in Figure 3.4. The UG2 contains over 50 percent of the PGE resources in the Bushveld Complex (McLaren and Villiers 1982).

The Platreef occurs on the northern or Potgietersrus limb of the complex. It is considered to be a local equivalent to the Merensky Reef. The Platreef is divided into three reefs, A, B and C. The upper, C reef, is usually barren of PGE's. Overall the occurrence of PGM's is sporadic with tellurides making the majority of the "ore" mineralization.

Potholes occur in both the UG2 and Merensky Reef. These structures are broad subcircular structures that cut footwall stratigraphy. The potholes of the Merensky Reef can range from one to 10m deep and 10m to one km across. These potholes often have a planar base and are economic to mine. The largest and most common potholes occur in the northern section of the complex (Cawthorn et al. 2002). Merensky potholes can show slightly higher grades of mineralization especially along the base, but not the slope. In some mines a higher proportion of Pt-Pd sulfides is present in potholes than in the normal reef. Overall the grade of the potholes is equal to the rest of the reef (Cawthorn et al. 2002).

Platinoids	UG2 data – southwestern and eastern lobes (%)	UG2 data – average of the whole Bushveld Complex (%)
Pt-Pd sulphides	44	35
Laurite	25	30
Pt-Fe alloy and intergrowths	15	21
Rh sulphides	14	11
Palladium alloys	2	3

Table 3.2 PGM in the UG2 of the Eastern and Southern Limbs in comparison to the whole Bushveld Complex from (Viljoen and Schurmann, 1998)

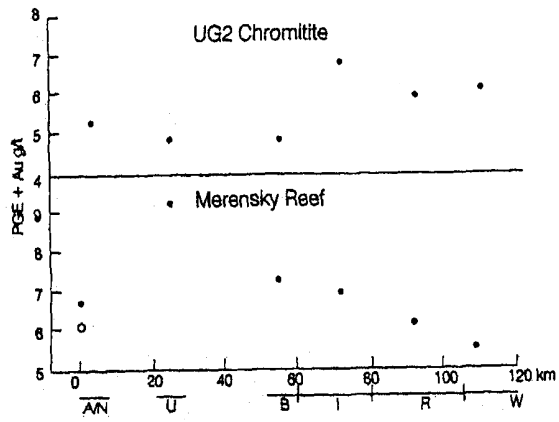

Figure 3.4 Grade of PGE+Au in g/t contrasted for the UG2 and Merenskey Reef. Union (U), Amandelbult (A), Bafokeng-Rasimone (B), Implala (I),Rustenburg (R), Western (W), locations can be seen on figure 2.1 from (Cawthorn et al., 2002).

The UG2 potholes are smaller and are usually in a different form. The bases are not usually planar and often are in the form of rolls or depressions. There seems to be no correlation between the overlying and underlying potholes, with the exception of where separation between the Merensky and UG2 layers is only 15 m (McLaren and Villiers 1982, Cawthorn et al. 2002). Figure 3.5 shows the mineralization of a pothole in the UG2.

3.2 Mining Geology of the Stillwater Complex

The ore mineralogy of the Stillwater Complex exists in two unique phases. The dominant PGE element, palladium exists in solid solution about 80 percent of the time, whereas platinum occurs as either metal alloys or PGM almost 100 percent of the time (Stillwater information sheet, Mann and Lin, 1985). The J-M reef is enriched from 0.25-5 percent by volume in Pd-Pt with an average Pt:Pd ratio of 1:3.4. In 2001, the average grade was 21.3 g/t (0.62 troy oz per ton (opt)). Proven reserves are 2,778,000 tons at 24.3 g/t (0.71 opt) with probable reserves of 32,864,000 tons at 24.3 g/t (0.71 opt) (Stillwater information sheet, 2001).

3.2.2 Stratigraphy of the reef

The J-M reef is located in Troctolite-Anorthosite Zone I (TAZ I) in the Lower Banded Series. TAZ I has been divided into four subzones that are recognizable in most areas of the complex. Some authors do not use the subdivisions, but choose to instead just

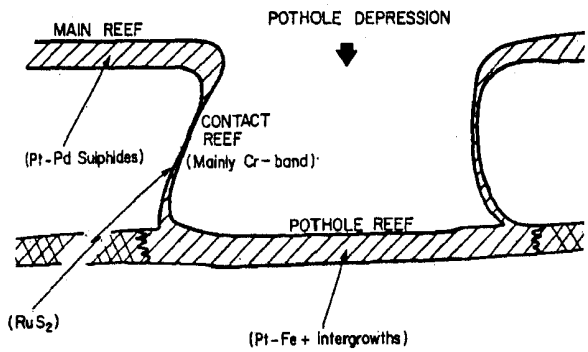

Figure 3.5 Mineralization in the potholes of the Merensky UG2 layer from (Kinloch 1982).

refer to the reef package (Turner et al. 1984). TAZ I is divided into Gabbro subzone (GSZ), Anorthosite 1 subzone (A_1SZ), Norite subzone (NSZ), and Anorthosite 2 subzone (A_2SZ) (Todd et al. 1982). The J-M reef is located in A_1SZ near the base of the subzone (Figure 2.8). It is most commonly in Olivine Member O_{5B}, but this is variable (LeRoy, 1984). The J-M reef is defined by one to two percent sulfide by volume over one to three m in thickness (Todd et al., 1982). Therefore it is not restricted to a particular layer, but only sulfide abundance and presence. Member O_{5B} contains a cumulus olivine layer 0.5-2 m thick at the base with plagioclase olivine cumulate two to five m thick at the top (LeRoy, 1984). The most common minerals of the reef are plagioclase (labradorite), orthopyroxene (bronzite), clinopyroxene (augite), and olivine. The olivine is often serpentinized with magnetite. Minor minerals include phlogopite, and chromite (Stillwater information sheet, 2002).

3.2.3 Mineralization

The PGE's generally occur with sulfide minerals or in association with them in the Stillwater Complex. The most common minerals are chalcopyrite, pyrrhotite and pentlandite. These minerals can be found in several different modes within the complex, and in many different layers of the complex. In the platinum-palladium-rich area of the intrusion palladium usually occurs in solid solution with pentlandite and platinum as an alloy, or as a platinoid mineral associated with chalcopyrite, pentlandite and occasionally pyrrhotite.

Palladium is hosted in pentlandite about 80 percent of the time, and in sulfides such as vysotskite [(Pd,Ni,Pt)S], braggite [(Pt,Pd,Ni)S], and cooperite [(Pt,Pd,Ni)S] about15 percent of the time. Around five percent of the palladium occurs as the telluride moncheite [(Pt,Pd)(Te,Bi)$_2$]. Other minerals in the J-M reef include pyrite, marcasite, millerite, cubanite, covellite, sphalerite, galena, stibnite, Cu, Au, chromite, magnetite, graphite, argentian tetrahedrite, cobaltian violarite, Pd-Au alloy, Pt-Fe alloy, sperrylite, kotulskite, telluropalladinite, keithconnite, zvyaginsevite, rustenburgite, and palladoarsenide, (Page et. al., 1984, Stillwater information sheet, 2002).

The J-M reef is highly variable in thickness with a range from six through 18 m. Ore mineralization occurs in three major styles; coarse blebs and segregations, interstitial networks, and fine disseminated grains and to a lesser extent as secondary mineralization. The least important of these are the segregations. Ore mineral size ranges from around one cm in diameter to three by 17 cm. The segregations occur in proximity to pegmatoidal pyroxene grains or in coarse grained areas of cumulus olivine. Occurrences of ore minerals are erratic with values below 34 g/t Pt and Pd. The second mode of occurrence is as interstitial sulfide. Networks of sulfide mineralization are associated with cumulus subhedral to euhedral plagioclase. The sulfide forms branching lamellae with clusters up to four cm in diameter. Analyses have indicated concentrations of more than 34 g/t Pt and Pd, or a little over two percent of the rock. The last major mode of occurrence is disseminated sulfide minerals. Sizes are one mm or less, but are present in greater abundances in the upper part of the J-M reef. Secondary mineralization is associated with diabase intrusions and contains few ore metals (Mann & Lin, 1984).

Sulfides with PGE minerals are commonly found in four environments (Turner et al., 1984). Early authors in PGE studies often use the term pothole, but care should be taken in the case of Stillwater in applying this term. The "potholes" are not direct equivalents of potholes in the Bushveld Complex. Recent authors use ballrooms to describe Stillwater (Geraghy, pers. communications 2002). For the purposes of this section the term pothole will be used as it is common in most relevant literature.

The first environment of PGE mineralization is the pothole. In the pothole itself sulfides have accumulated in the base of the pothole. Stratified reef rock has filled depressions in the footwall. Above average grades of PGE's are found in these structures. The second environment is the pothole margin. Sulfide mineralization is found in layered footwall gabbro adjacent to the contact with the reef, this type of mineralization exhibits above average grades of PGE's. The next area is the pothole apron. What are termed "boulders" by Turner et al. (1984) are spread erratically on the slope of the pothole. These boulders contain hydrous silicates and suggest volatile streaming as a mechanism for formation. Mineralization is erratic in the boulders. The last major area of occurrence is in cross cutting veins of the footwall gabbro. Sulfides are found as narrow veins that cross cut layers as far as 100 m below the reef (Turner et al. 1984).

Chapter 4

Implications for a pre-Rodinia Supercontinent

4.1 Introduction

All references from this section are from Zhao et al., (2002) unless otherwise noted. Kaapvaal and Kalahari refer to the same craton.

Several authors have argued for pre-Rodinia supercontinents, most notably Rodgers and Santosh (2002), and Zhao et al., (2002). Their proposed name of this supercontinent is Columbia and will be refereed to as such hereafter (Rodgers and Santosh 2002). Evidence for Columbia can be seen on all present continents. Central to these arguments are the placement of both the Wyoming (SIC) and Kaapvaal (BIC) cratons and their relation to global tectonics. The cratonic blocks of South Africa and the Limpopo Belt can be seen in Figure 4.1. The Wyoming Craton is welded together with the Superior Craton during the Trans-Hudson orogen at 2,000-1,800 Ma, this is presented in Figure 4.2. It is important to note that some authors prefer the term Kalahari Craton instead of Kaapvaal Craton for reconstructions of Rodinia and Columbia.

The formation of Rodinia was completed by ca. 1,000 Ma with the completion of the Grenvillian and age-equivalent orogens. Evidence has been given that major collisional orogenic events occurred from 2,100-1,800 Ma. These events include the Transamazonian Orogen of South American, the Eburnean Orogen of West Africa, the Svecofennian and Kola-Karelia Orogens of Europe, the Akitan and Central Aldan

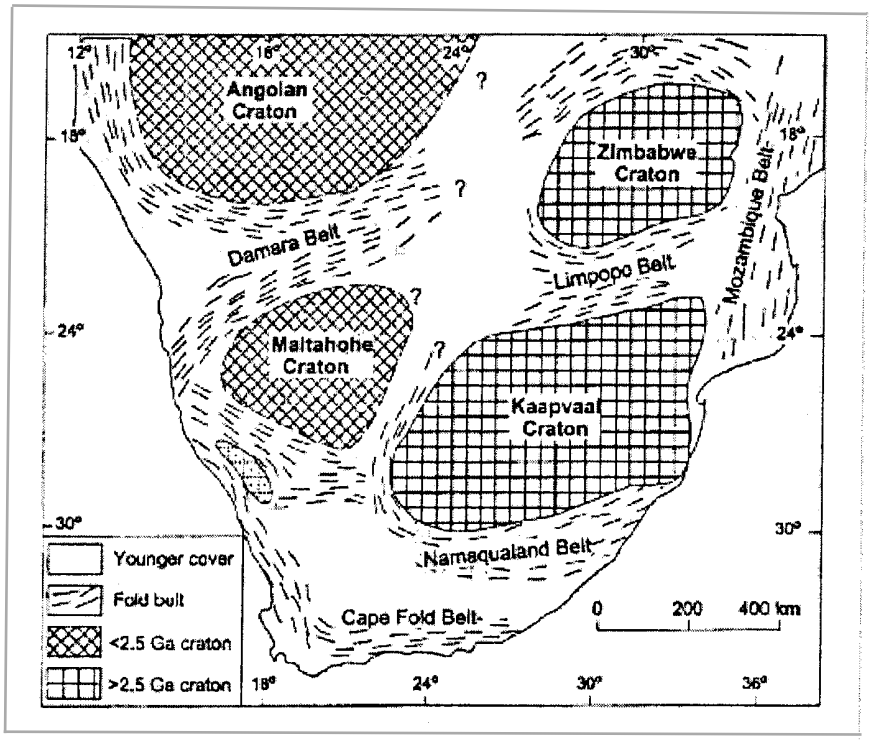

Figure 4.1 Southern Africa showing major cratons and orogenic belts from (Zhao et al., 2002).

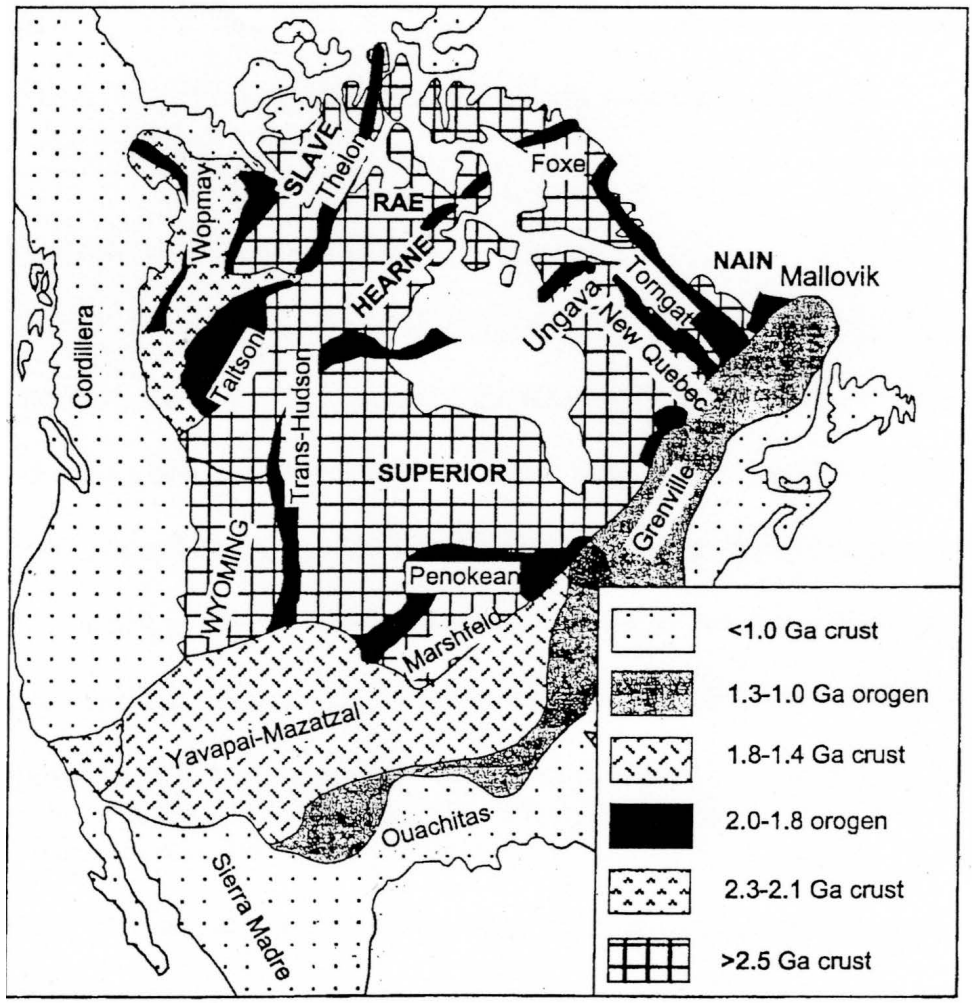

Figure 4.2 Map showing cratons and orogenic events in North America from (Zhao et al., 2002)

Orogens of Siberia, the Capricorn Orogen of Western Australia, the Transantarctic Mountains Orogen of Antarctica, the Trans-North China Orogen in North China, and the Trans-Hudson Orogen and age equivalents in North America (Figure 4.3).

4.2 Kaapvaal and Zimbabwe Cratons

The Limpopo Mobil Belt separates the Kaapvaal and Zimbabwe Cratons. The Limpopo Belt is a belt of high grade metamorphic orogen with NE-SW orientation, a length of 650 km and a width of 200 km. Two interpretations of this belt have been proposed. This belt is referred to as a classic example of an Archean collisional belt that was created when the Kaapvaal and Zimbabwe cratons collided (Zhao et al., 2002). It has been proposed that the two cratons may have been separated by as much as 1,000 km of Limpopo oceanic crust, which was subsequently subducted during collision at 2,600 Ma (Light 1982). The second interpretation is that a tectonothermal event occurred at ca. 2,000-1,900 Ma. This is the same style as the main collision of the cratons in a Himalayan style collision with initial crustal thickening, followed by uplift and exhumation. The late Archean event ca. 2,600-2,500 Ma of granulite facies metamorphism is caused by deep crustal processes related to intrusion of mantle-derived magma and crustal growth of the cratons (Holzer et al., 1998).

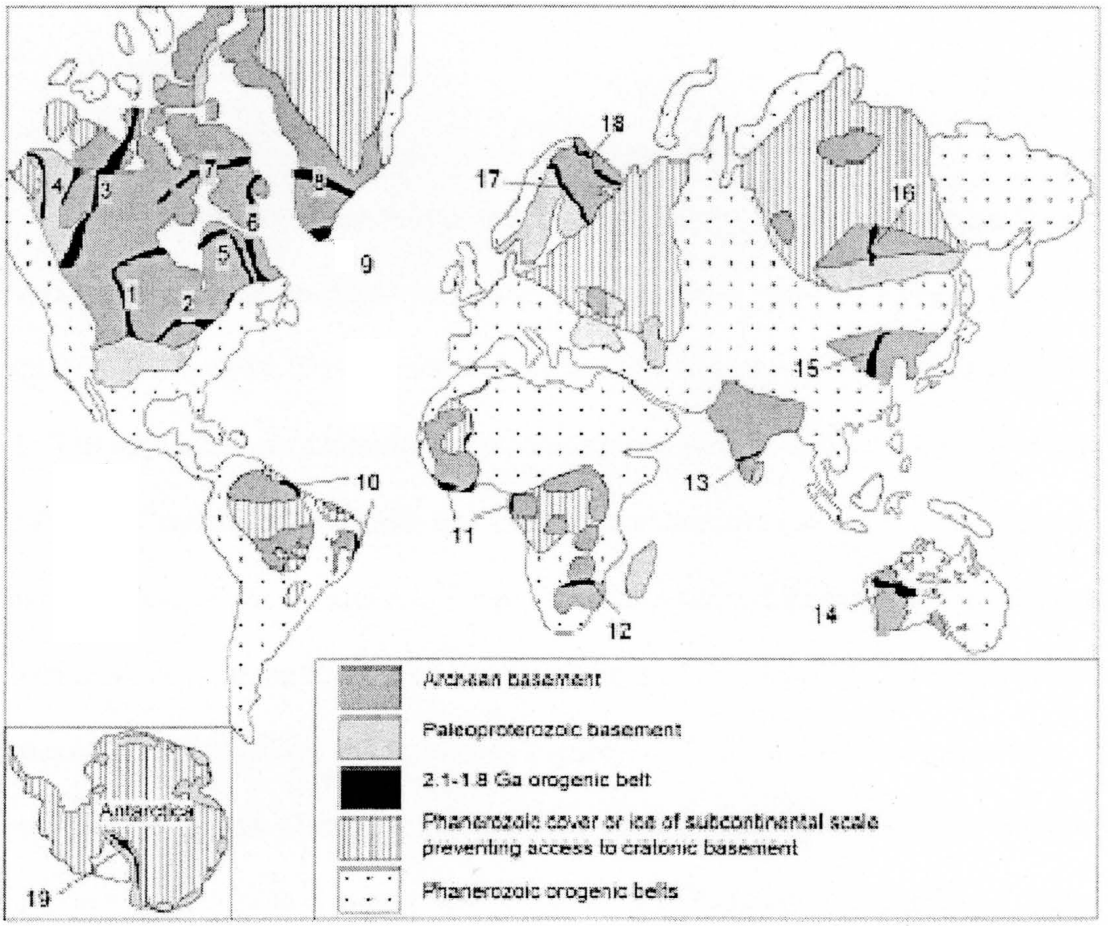

Figure 4.3 Map showing cratons of the world and dates of orogenic events. Orogens: Trans-Hudson (1), Penokean (2), Taltson-Thelon (3), Wopmay (4), Cape Smith-New Quebec (5), Torngat (6), Foxe (7), Nagssugtoqidian (8), Makkovikian (9), Transamazonian (10), Eburnian (11), Limpopo Belt (12), Moyar Belt (13), Capricorn Orogen (15), Central Aldan Belt (16), Svecofennian (17), Kola-Karelian (18), Transantarctic (19), from (Zhao et al., 2002).

4.3 Kaapvaal Reconstructions

A link between South Africa and Western Australia has been proposed based on several lines of evidence. The connects the Kaapvaal and Pilbara cratons on the basis of sequence stratigraphy. Three sequences are used for the correlation as outlined in Figure 4.4. The sequences are supported by paleomagnetic studies of the Millinda Complex in the Pilbara Craton (2860±20 Ma) and Usushwana Complex (2871±30 Ma) in the Kaapvaal Craton. The Pilbara and Kaapvaal cratons formed a continent named Vaalbara, which collided with the Zimbabwe Craton along the Limpopo Belt, forming Zimvaalbara. The reconstruction of this can be seen in Figure 4.5. This continent may also have contained the Yilgarn Craton, which was sutured to the Pilbara Craton at ca. 2,000-1,800 Ma. Some authors have also proposed that cratons in India and Sao Francisco, Amazon, Guiana, Congo and West African Cratons were involved (Aspler and Chiarenelli 1998). Figure 4.6 shows a possible reconstruction of Columbia.

Rogers and Santosh (2002) show reconstructions of the Columbia at ca. 1,500 Ma with close proximity of the Kaapvaal (Kalahari) Craton in Figure 4.7. The location of east Antarctica is not well known due to ice cover on the continent.

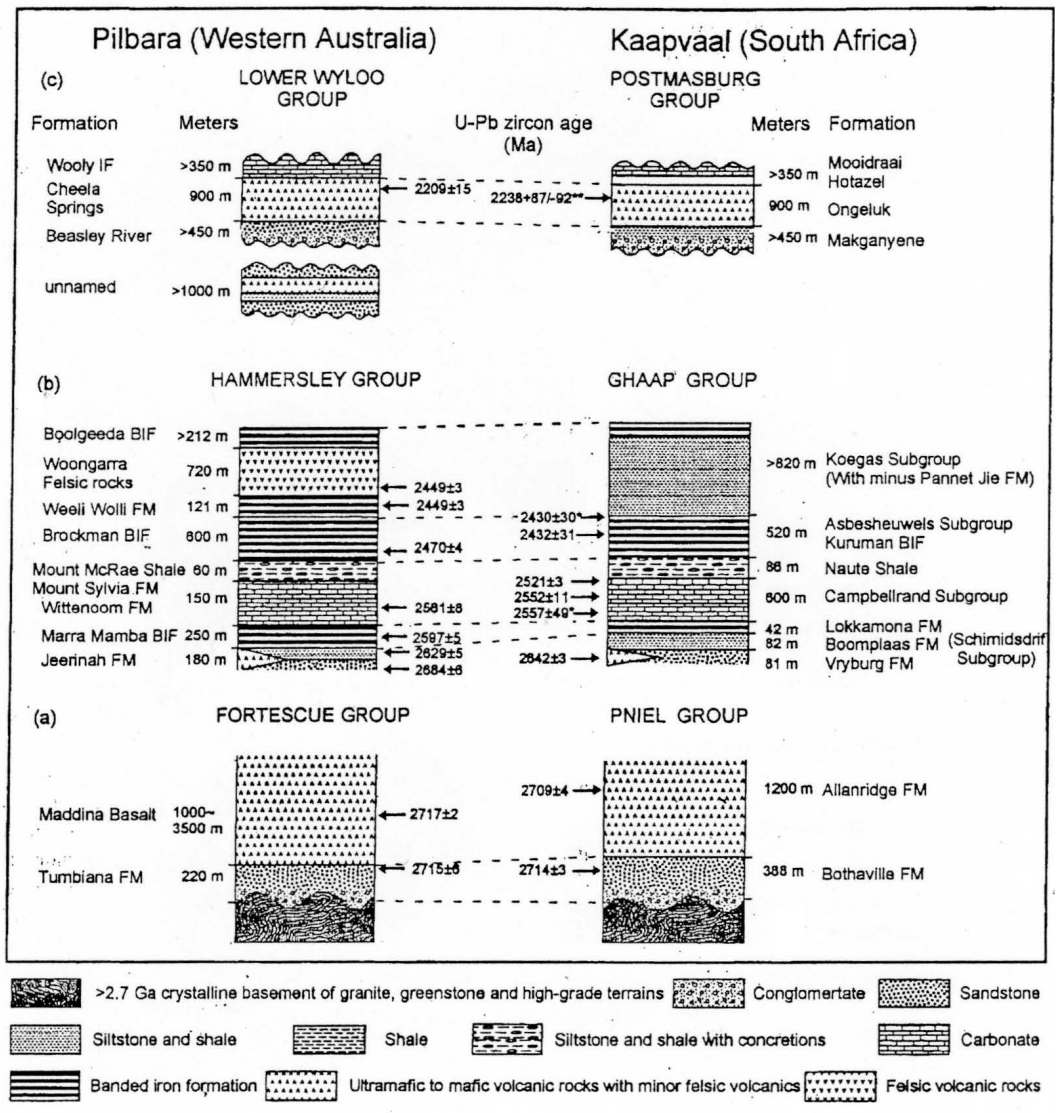

Figure 4.4 Correlation of the Pilbara Craton to the Kaapvaal Craton from (Zhao et al., 2002).

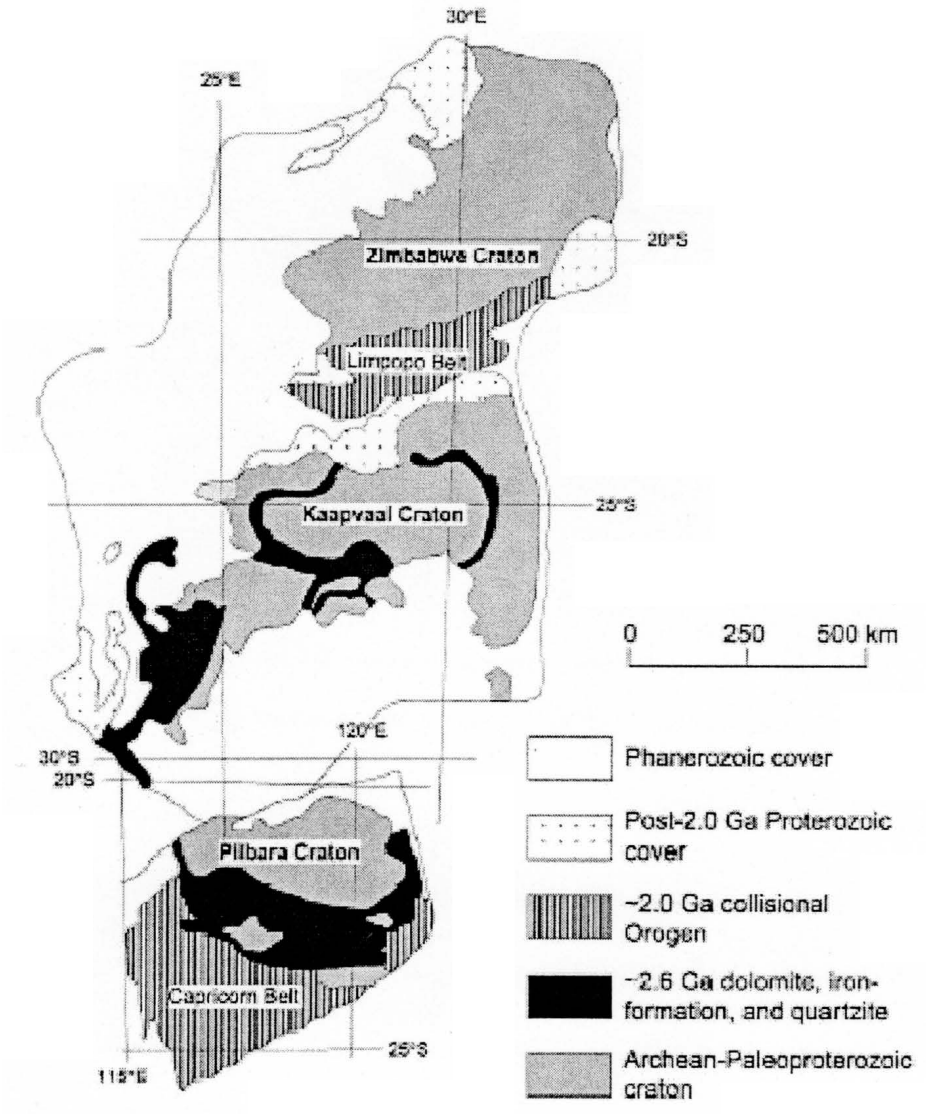

Figure 4.5 Reconstruction of the Kaapvaal and Pilbara Cratons from (Zhao et al., 2002).

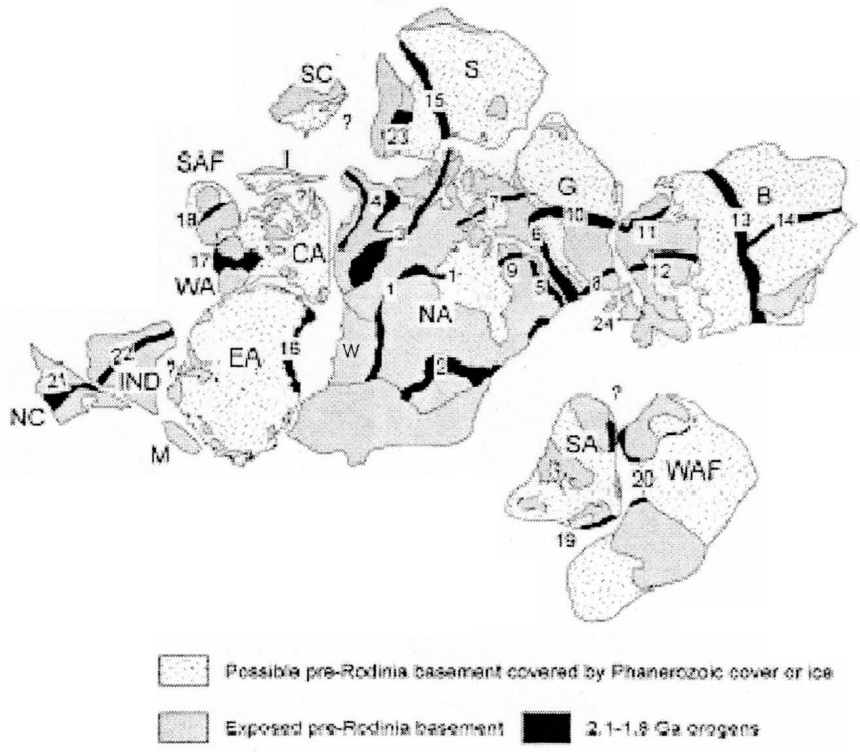

Figure 4.6 Possible reconstruction of Columbia. Orogens: Trans-Hudson (1), Penokean (2), Taltson-Thelon (3), Wopmay (4), New Quebec (5), Torngat (6), Foxe (7), Makkovik-Ketilidian (8), Ungava (9), Nugssugtoqidian (10), Kola-Karelian (11), Svecofennian (12), Volhyn-Central Russian (13), Pachelma (14), Akitkan (15), Transantarctic (16), Capricorn (17), Limpopo Belt (18), Transamazonian (19), Eburnian (20), Trans-North China (21), Central Indian Tectonic Zone (22), Central Aldan Orogen Zone (24), Scotland (25). Symbols: Baltica (B), Central Australia (CA), East Antarctica (EA), Greenland (G), India (IND), Madagascar (M), North America (NA), North China (NC), Siberia (S), South America (SA), South Africa (SAF), South China (SC), Tarim (T), West Australia (WA), West Africa (WAF) from (Zhao et al., 2002), Wyoming (W) added.

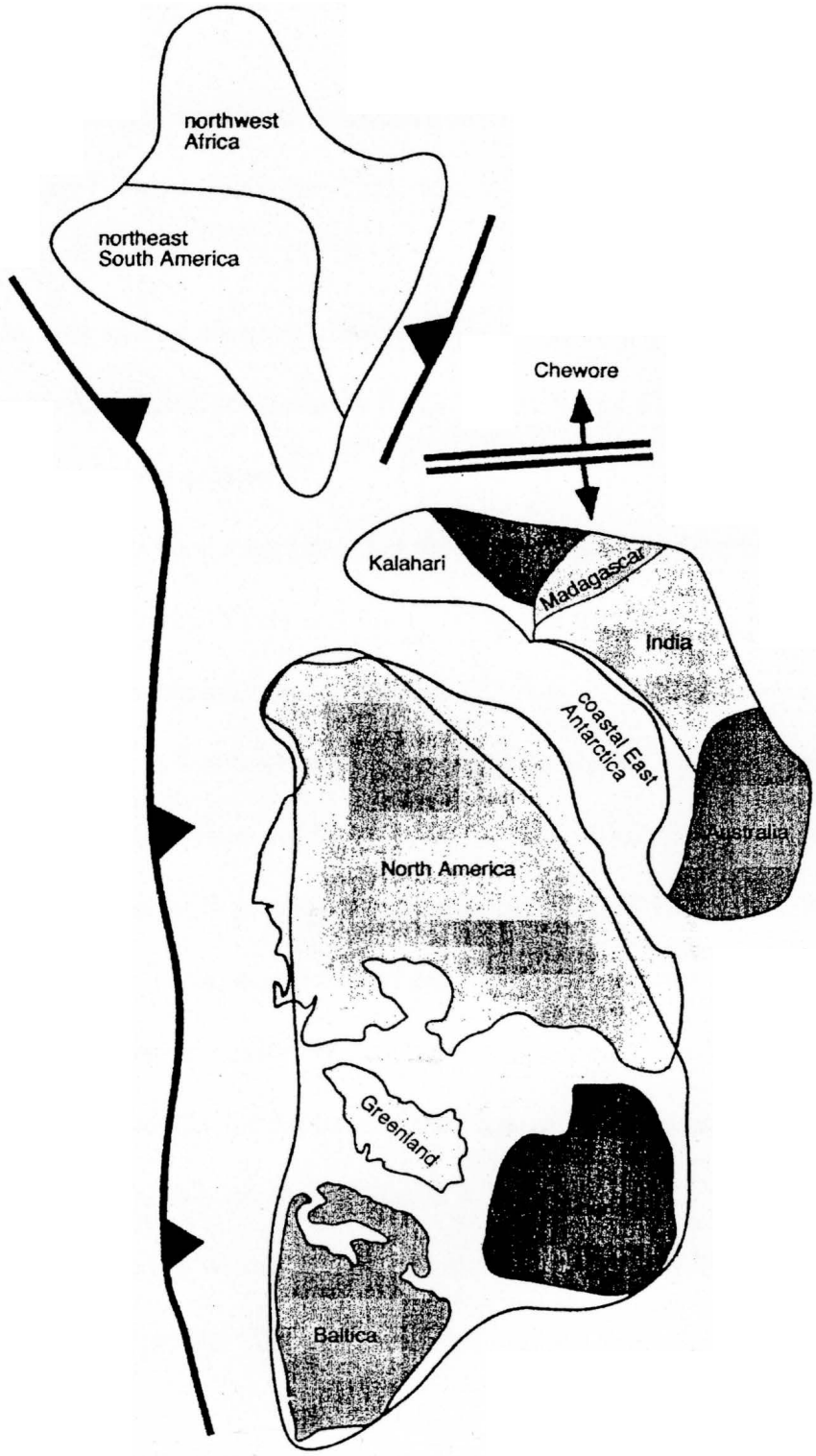

Figure 4.7 Reconstruction of Columbia from (Rogers and Santosh 2002)

4.4 North America Orogens

Orogens in North America joined the Superior, Hearne, Rae, Slave, and Wyoming Cratons between 2,000 and 1,800 Ma. Rocks in these cratons have ages greater than 2,500
Ma. Dominant rock types are low grade greenstone belts, intrusive granitoids, high grade gneiss and clastic sedimentary rocks. Figure 4.2 of Zhao et al. (2002) shows the ages of North America cratons.

It has been suggested that the Aldan Craton of Siberia should be linked to the Wyoming Craton (Sears and Price, 1978), but this view has been neglected by different authors in reconstructions of Rodinia (Zhao et al., 2002). New evidence has shown that this fit may, in fact have occurred. Figure 4.8 shows 3 possible reconstructions.

Recontructions of Rogers and Santosh (2002) place the western edge of the North America cratons in proximity to an assemblage of Kaapvaal (Kalahari), Zimbabwe, Madagascar, India, Australia and coastal East Antarctica cratons ca. 1500 Ma. Zhao et al. (2002) also review evidence that the Transantarctic Mountains may represent a continental source for the base of the Mojave Province of Laurentian basement at 2000-2400 Ma, which is given in Figure 4.9. The Mojave and Yavapai provinces were connected to the Wyoming Craton around 1700 Ma (Willis and Willis 2000). This suturing formed the Cheyenne Belt that extends from Nevada through Utah, and into Wyoming.

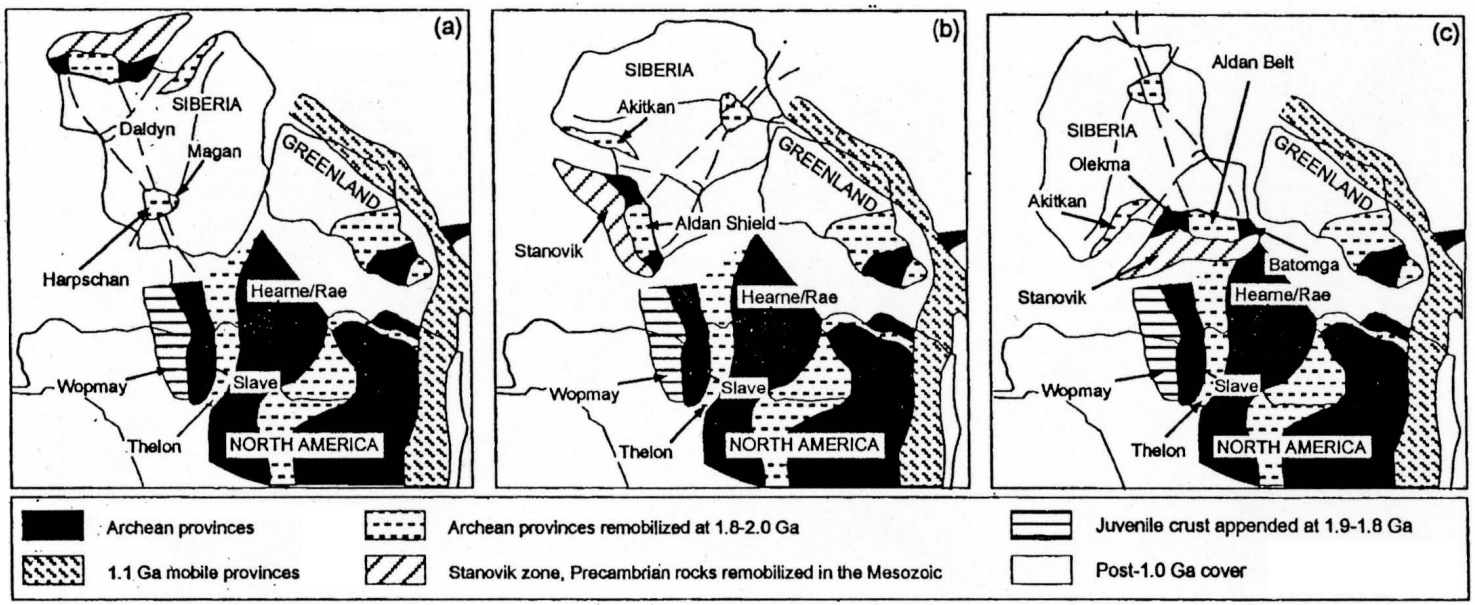

Figure 4.8 Three possible reconstructions of Siberia and North America from (Zhao et al., 2002).

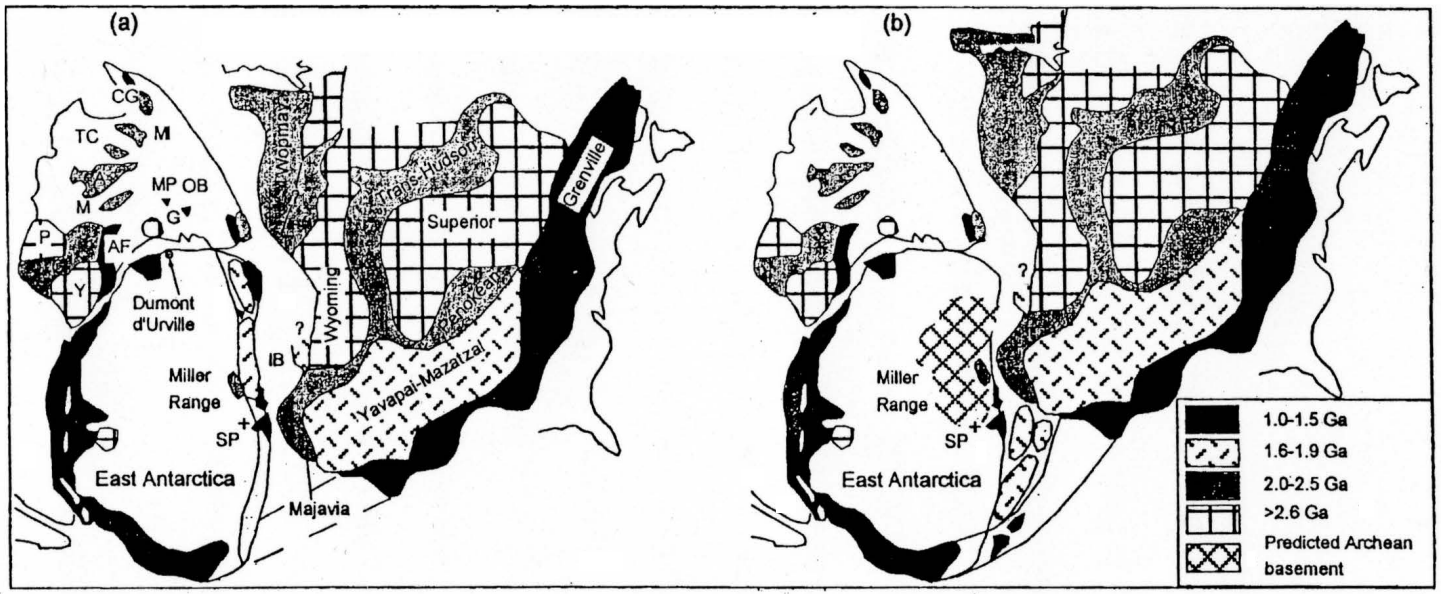

Figure 4.9 Two possible reconstructions of North America, Arunta Inlier (A), Albany-Fraser Orogen (AF), Capricorn Orogen (C), Coen-Georgetown Inlier (CG), Gawler Craton (G), Musgrave Orogen (M), Mt. Isa Inlier (MI), Mt. Painter Inlier (MP), Olary-Broken Hill Inlier (OB), Pilbara Craton (P), Tennant Creek Inlier (TC), South Pole (SP), Yilgarn Craton (Y), from (Zhao et al., 2002)

Chapter 5

Results

5.1 Lab Results

Samples of the UG-2 and J-M Reef were submitted to the Microscopic and chemical Analysis Research Center (MARC) laboratory of the Ohio State University Department of Geological Sciences using Inductively Coupled Plasma- Mass Spectrometry (ICP-MS). Both samples were taken from high grade ore sections of the respective mines (H. C. Noltimier, pers. comm. 2002). The UG2 sample was taken from the Rustenburg Mine, South Africa and the J-M Reef from the Stillwater Mine, MT. Analyses were conducted for Pd, Pt, Sb, Os, Cr, Ni, V, and Ru. The reported values are given in table 5.1. Values for the J-M are artificially high due to concentration of the sample before analysis; it is unknown why the UG2 value is lower than that of average grade. Calculated ratios from the final results are 1:5.3, Pt:Pd for Stillwater and 1:26.4 for Bushveld. It is not known why the proportions are so high.

Samples also were examined under the Scanning Electron Microscope (SEM) in the MARC facility. All samples of the J-M Reef, UG2, Merensky Reef and surrounding layers were under the detection limit for platinum group elements. Results for the J-M Reef are given in Appendix A.

The proportion of Pt:Pd can play an important role in understanding initial conditions within both the SIC and BIC. Virtually the entire range of values has been

Element	J-M Reef ug/g (g/t)	UG2 ug/g (g/t)
Pd	246	1.4
Pt	46	0.053
Sb	0.01	0.015
Os	<.002	<.002
Cr	634	868
Ni	8136	1759
V	26	242
Ru	0.3	0.01

Table 5.1 ICP-MS results for the J-M Reef and UG2.

observed from cooperite to vysotskite. The ideal formula of cooperite is PtS and vysotskite is PdS. Both cooperite and vysotskite have an effective chemical formula of (Pt,Pd,Ni)S. A miscibility gap has been observed between cooperite and braggite (Verryn and Merkle, 2002); however, braggite and vysotskite do occur in solid solution. The chemical formula for braggite is (Pt,Pd,Ni)S, but the ideal formula is close to equal proportions Pt and Pd. Figure 5.1a shows the weight percentages of Pd:Pt from analytical methods, Figure 5.1b shows the Merensky Reef and Figure 5.1c for the UG2 for cooperite, braggite, and vysotskite (Verryn and Merkle, 2002). Figure 5.2 gives the phase relations of melt to cooperite, braggite, and vysotskite from 1200°C to 700°C from Verryn and Merkle (2002).

From this diagrams provided in Figure 5.2, a clear shift to Ni rich melt is seen as Pt and Pd form minerals. A miscibility gap can also be seen between cooperite and braggite. This gap makes it unlikely that the same melt could form two larger areas, one with a Pt:Pd ratio of 1:3 and the other with a ratio of 2.4:1. This is unlikely because a melt should finish with the same overall proportion of Pt:Pd as it started. The high ratio of Pt:Pd cannot be explained by fractionation alone. Outside factors has played a role to drive this ratio to 2.4:1 (Peregoedova and Ohnentetter, 2002).

5.2 Microscope Study

The mineralogy of chromitite samples is fairly simple, with three to four major components and several minor components. All samples contain idiomorphic to hypidiomorphic chromite surrounded by silicate material. The chromite crystals were

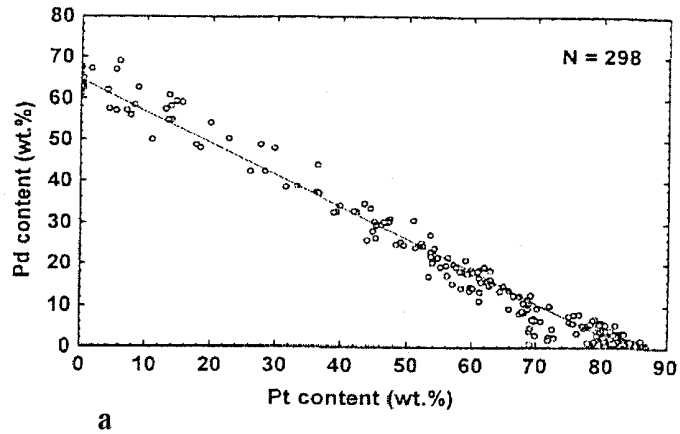

a

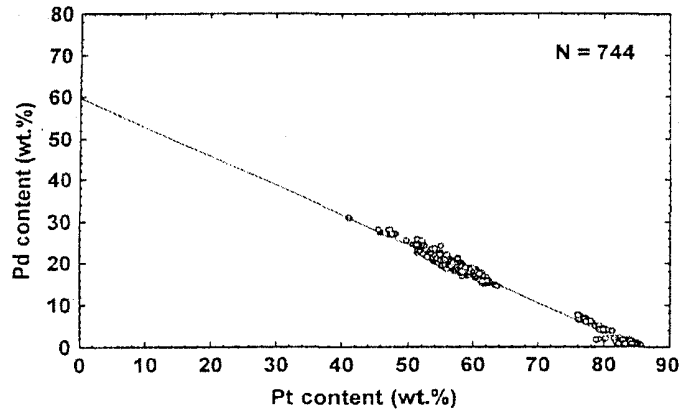

b

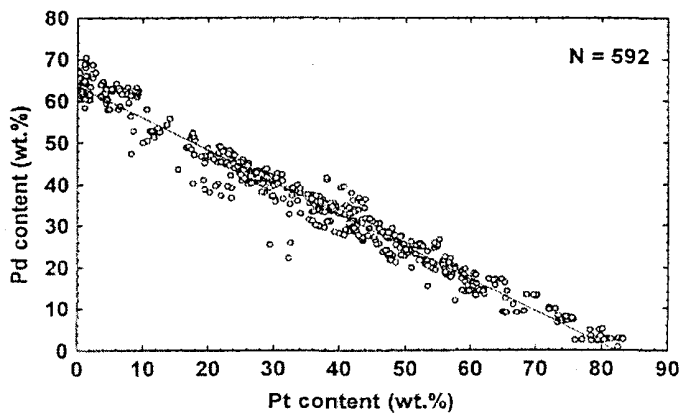

c

Figure 5.1 Pt:Pd ratio based on weight percent, analytical data (a), Merensky Reef (b), UG2 (c) from (Verryn and Merkle, 2002).

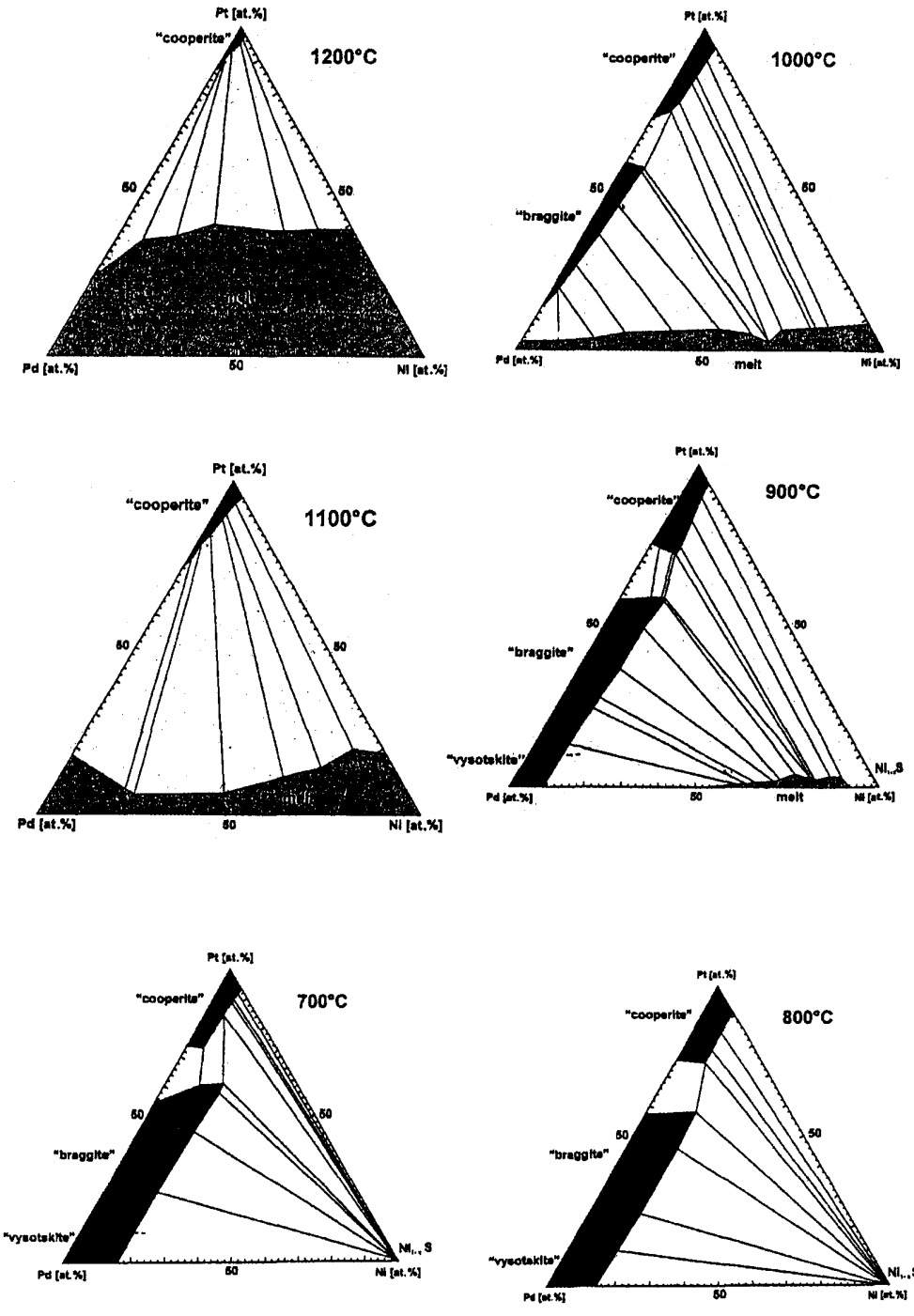

Figure 5.2 Phase diagram of Pt-Pd-Ni from 1200°C to 700°C from (Verryn and Merkle (2002).

rounded by this material in most samples. When several crystals of chromite are present the texture of the chromite is polygonal with triple point junctions at 120 degrees in most samples (Figure 5.3). Most of the time, when the polygonal texture is seen, so are synneusis structures. Synneusis chains along with a PGM can be seen in Figure 5.4. These are long chains that are formed by the chromite crystals and sometimes travel throughout the rock in an interlocking pattern similar to a cross or braid. However, no relationship can be drawn with the synneusis and polygonal textures other than the amount of chromite present. When one grain is present it resembles an ice cake (Figure 5.5), when a few are present they are polygonal, when still more are present they are usually in a synneusis chain and when even more are present they are polygonal only, covering large areas of the slide. Due to the crystal shape and the rounding, the chromite formed at or before the time of the surrounding material. In some cases the gangue minerals can be seen replacing or "eating" into the chromite. These areas show replacement within grains that resemble inclusions, replacement along the edges of grains that stay within the original idiomorphic grain boundaries, and others that destroy the original shape of the crystal. In thin section view, the different types of replacement do not seem to be characteristic of a certain type of gangue mineral, except fractured chromite grains with later stage alteration minerals that appear to flow into the fractures.

The PGM's show a complicated pattern of intergrowth with other PGM's and sometimes with chromite. Platinum minerals form a complex set of solid solution and alteration to new PGM's. To further complicate things, they have very similar properties and to common sulfides such as pyrite, chalcopyrite, and pyrrhotite. It is likely that some of what has been identified as PGM's, in this study is in fact one of these other minerals.

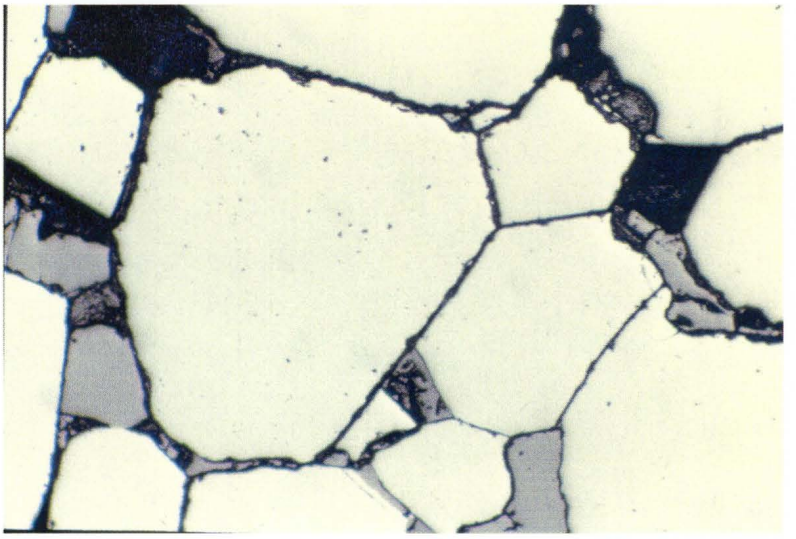

Figure 5.3 Chromite crystals showing triple point junction. Shown at 200X magnification under plane polarized light (photo by A. Rathbun).

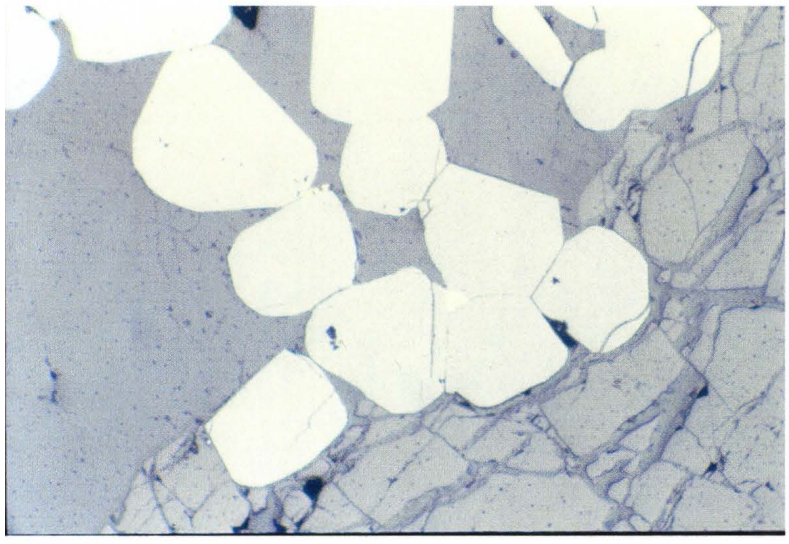

Figure 5.4 Chromite crystals showing triple point junctions forming a synneusis chain. PGM is filling a triple junction in the center of the figure. Shown at 100X magnification under plane polarized light (photo by A. Rathbun).

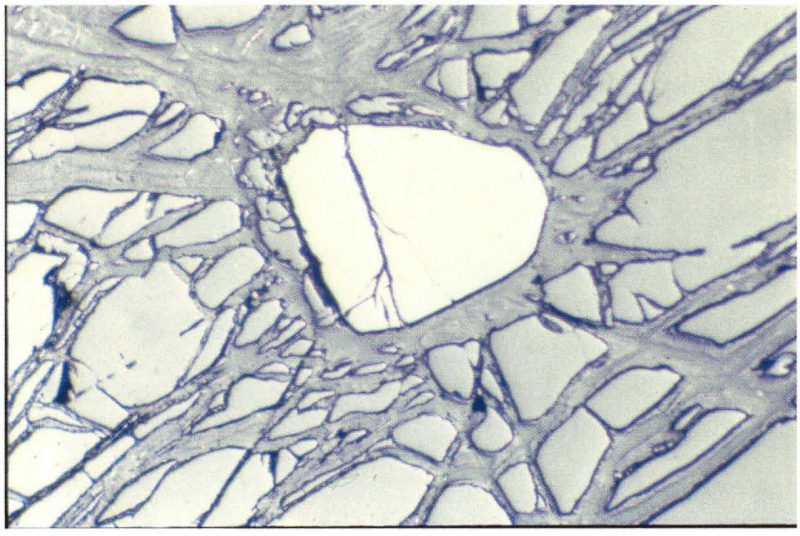

Figure 5.5 Chromite grain (center) surrounded by late stage alteration. This texture is termed ice cake because of the floating appearance of the chromite. Shown at 100X magnification under plane polarized light (photo by A. Rathbun).

The PGM's usually occur as allotriomorphic masses with graphic intergrowth along boundaries of chromite grains. The masses are yellow or white and usually show a high reflectivity next to chromite. It is hard to tell if the reflectivity is that of a sulfide or native metal due to the comparison with the low reflective mineral chromite. With the 400X power lens, it is possible to see the different phases and their intergrowths. Three PGM's can be seen in Figure 5.6. With this high power lens, three and possibly four mineral phases can be seen altogether. It is not possible to tell the paragenesis of the phases; however, but some can be inferred from the composition. Possible minerals are cooperite (PtS), hollingworthite ((Rh,Pt,Pd,Ru,Ir)AsS), irarsite ((Ir,Ru,Rh,Pt)AsS), stibiopalladinite (Pd_3Sb),sperrylite ($PtAs_2$), geversite ($PtSb_2$), and native platinum (Pt). Some grains are white and very reflective (native platinum or stibiopalladinite) and have similar properties except for anisotropism and reflectivity. Due to the small size and close proximity to gangue components it is not possible to tell if they are anisotropic, or if gangue phases are giving the anisotropic appearance. One of the minerals appears to be blue or brownish and is probably cooperite. This mineral also is harder than the surrounding minerals and does not exbit surface scratches. The minerals around it probably are geversite and Pt/stibiopalladinite due to the observed differences in hardness and color. Other areas show a hard mineral and a soft mineral in close proximity, with very similar colors. These are likely to be hollingworthite altering to irarsite, Pt, or intergrown with Pt and sperrylite. Some grains show rods of a very hard reflective substance, which most likely is sperrylite.

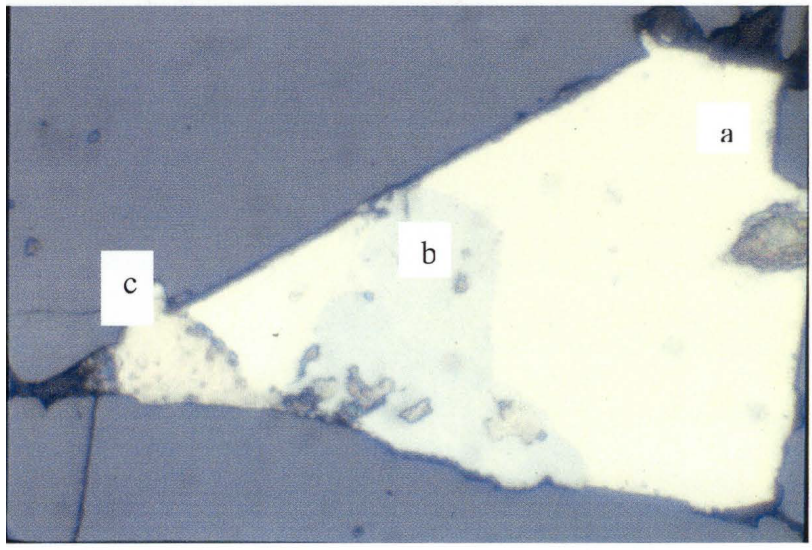

Figure 5.6 Three possible PGM's surrounded by chromite. Platinum? or stibiopalladinite? (a), hollingworthite? (b), cooperite? (c). Shown under crossed polars at 400X magnification (photo by A. Rathbun).

5.3 Reconstructions

Figure 5.7 presents a reconstruction has based on the reconstructions of Zhao et al., (2002) and given in Figure 4.6. Figure 5.7 inverts the location of South Africa, Western Australia, and Central Australia, placing South Africa in proximity to the Wyoming Craton. This also lowers the block of East Antarctica, India, and North China. No reconstruction has been created based on Figure 4.7 because the original diagram from Rogers and Santosh, (2002) was never adequately explained.

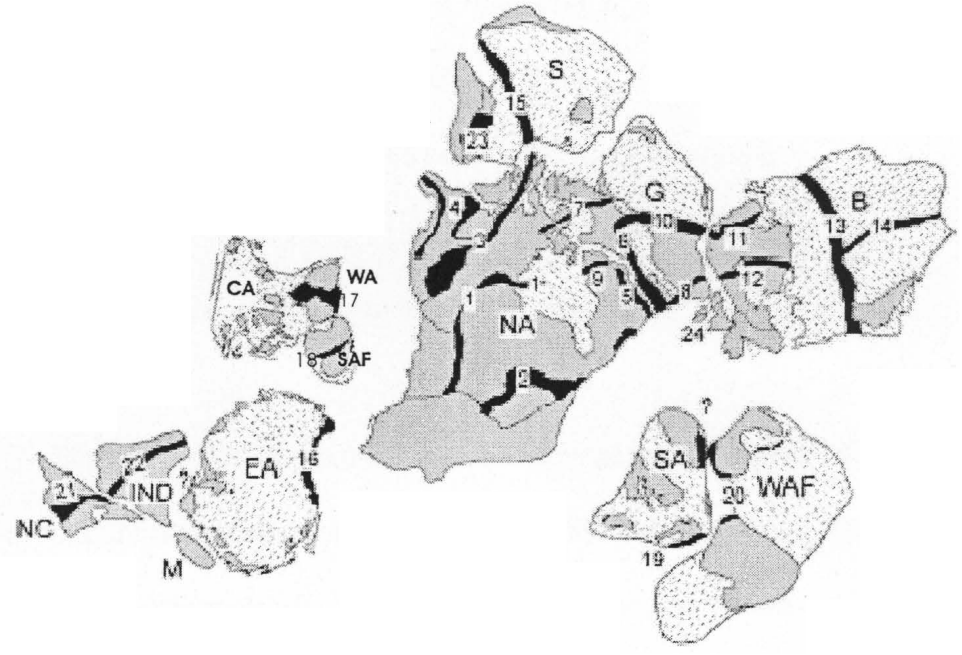

Figure 5.7 Possible reconstruction of Columbia (this study). Orogens: Trans-Hudson (1), Penokean (2), Taltson-Thelon (3), Wopmay (4), New Quebec (5), Torngat (6), Foxe (7), Makkovik-Ketilidian (8), Ungava (9), Nugssugtoqidian (10), Kola-Karelian (11), Svecofennian (12), Volhyn-Central Russian (13), Pachelma (14), Akitkan (15), Transantarctic (16), Capricorn (17), Limpopo Belt (18), Transamazonian (19), Eburnian (20), Trans-North China (21), Central Indian Tectonic Zone (22), Central Aldan Orogen Zone (24), Scotland (25). Symbols: Baltica (B), Central Australia (CA), East Antarctica (EA), Greenland (G), India (IND), Madagascar (M), North America (NA), North China (NC), Siberia (S), South America (SA), South Africa (SAF), South China (SC), Tarim (T), Wyoming (W), West Australia (WA), West Africa (WAF) after (Zhao et al., 2002).

Chapter 6

Discussion

6.1 Comparison of the Bushveld and Stillwater Complexes

6.1.1 Emplacement

Both the Stillwater and Bushveld complexes were emplaced into sedimentary basins with metamorphism occurring before and during intrusion. Country rock of the SIC is metasedimentary pelitic schist, iron formation, graywacke, quartzite and argillite referred to as the Boulder River Complex. Maximum conditions of contact metamorphism are 825° C and 200 MPa (Labotka and Kath, 2001). The Bushveld Complex intrudes into the Pretoria Group of the Transvaal Supergroup. Ages for the Transvaal Supergroup are 2,551 to 2,204 Ma (Cawthorn and Walraven, 1998), with an age near the base of the Pretoria Group at 2350 Ma (Eriksson et al., 1995). Metamorphic conditions were likely between 646 and 740°C and pressures under 220 MPa (Engelbrecht, 1990), with partial melting of country rocks near the top of the complex (Engelbrecht, 1990). Rocks of the Pretoria Group are quartzites, ironstone, shales, and basaltic and acid volcanic rock at the top.

The conditions of metamorphism and the characteristics of the country rocks are both similar and different. The Boulder Complex and the Pretoria Group are similar in they both contain iron formation and consist largely of clastic sedimentary rock. However, the basaltic and andesite layers are not seen in the Boulder River Complex as

they are in the Pretoria Group. The country rock around the SIC has been heavily intruded and deformed since intrusion of the SIC, and in most cases it is not directly in contact with the complex (Labotka and Kath, 2001). Calculated temperatures of contact metamorphism are different for the BIC and SIC complexes. In the far western portion of the BIC maximum temperatures were 646-740°C, whereas temperatures of contact metamorphism associated with the SIC were 825° C. Extreme temperatures of metamorphism as high as 1200° C are seen in xenoliths of the Marginal and Critical Zones, but these are related to temperatures of emplacement not contact metamorphism (Wallmach et al., 1989).

6.1.2 Ages

Three different age studies have yielded similar ages for the SIC: 2701±8 Ma, 2713±3 Ma, and 2705±4 Ma (DePaolo and Wasserburg, 1979, Nunes, 1981, Premo et al., 1990). The ages all were calculated with different methods and refine much earlier, but similar ages reported in earlier papers and reviewed by Lambert et al., (1985). The age of the BIC is 2060 Ma with a cooling time of 200,000 years (Cawthorn and Walraven, 1998). This age makes the BIC ca. 700 Ma younger than the SIC. The Pretoria Group itself is much younger than the SIC. Ages for the Rooiberg Group, the uppermost group of the Transvaal Supergroup, have an identical age to the BIC at 2,060 Ma (Eales and Cawthorn 1996).

6.1.3 Stratigraphy

The stratigraphy of the BIC and SIC are remarkably similar yet with some striking differences. The Basal Series of the SIC is similar in rock type to the Marginal Zone of the BIC. In both cases the rocks are norite and pyroxenite (bronzitite). Above the Basal Series is the Ultramafic Series. This series consists of ultramafic rock with all of the chromitite layers of the SIC. The chromitite layers contain small amounts of Pt-Pd mineralization, which are well below economic values. This series ends with the first occurrence of cumulus plagioclase rocks. The BIC analog of the Ultramafic Series is the Lower Zone and Lower Critical Zone. These zones contain chromitite layers with mafic to ultramafic rocks. Once again Pt-Pd is present in the chromitite layers, but is subeconomic. The C_LZ ends with the first occurrence of cumulus plagioclase.

With both the BIC and SIC the Pt-Pd bearing reefs occur after the occurrence of plagioclase cumulates. In the SIC, the J-M Reef is in the Lower Banded Series and in the BIC the Merensky Reef is located in the Upper Critical Zone. The hanging wall stratigraphy of the reef packages is macroscopically indistinguishable (Turner et al., 1985). In both cases, the reefs are "housed" in a variety of rock types with anorthosites overlying the ore zone. The major difference are the association of chromitite with Pt-Pd ore in the Merensky Reef and throughout the BIC. In the SIC, no chromitite occurs after the occurrence of plagioclase cumulates. In the BIC, chromitite layers are present in the C_UZ. In some cases the Merensky Reef even occurs in a chromitite layer. The other most obvious difference is the UG2 layer. The SIC does not contain a layer of chromitite that

is economic in Pt-Pd. Pt-Pd grades in the UG2 are comparable to the Merensky Reef, with averages ca. one g/t lower (Cawthorn et al., 2002

6.1.4 Ore Mineralogy

The ore mineralogy is different for the two complexes. The first difference is the difference in proportion of Pt-Pd. In the SIC the ratio is 1:3.4, whereas in the in the BIC the ratio is ca. 2.4:1. The minerals formed from the PGE's also are different for the complexes. In the SIC palladium is in solid solution for 80 percent of the ore. Platinum, however, occurs as a distinct mineral nearly 100 percent of the time (Stillwater information sheet, 2002). In the BIC, Pt-Pd occurs in many different minerals and alloys, not as solid solution mixtures. These occurrences can be seen in Figure 2.3.

6.2 Tectonics

The SIC was intruded into the Wyoming Craton, and the BIC into the Kaapvaal Craton. Both cratons are Archean age and contain rocks older than 2,700 Ma. Several ideas have been presented about the tectonic history of these two cratons. In the classic view of the Kaapvaal Craton, it collided with the Zimbabwe Craton at 2,600 Ma forming the Limpopo Belt. Another idea has recently been presented, but is not widely recognized. Holzer et al., (1998) argued that the Limpopo belt was formed by a Himalayan style collision ca. 2,000-1,900 Ma, making the suturing coeval with the global orogens of Zhao et al., (2002). It is likely that the Pilbara Craton of Australia and

Kaapvaal Cratons were connected as cited from several lines of evidence reviewed in Zhao et al., (2002). However, the inclusion of the cratons in India, Sao Francisco, Amazon, Guiana, Congo and West African Cratons is widely debated.

Little is discussed in relation to the Wyoming Craton with the orogens and possible pre-Rodinia supercontinent. The Wyoming Craton was involved in part of the Trans-Hudson Orogeny. Sears and Price (1978) argued for a link of the Aldan Craton in Siberia to the Wyoming Craton, a view that was largely unaccepted until recently (Zhao et al., 2002). Most reconstructions still ignore the Wyoming Craton, locations, and connections it could have had in the pre-Rodinia supercontinent. Rogers and Santosh (2002) do show a close proximity of North America and the Kaapvaal (Kalahari) Craton at around 1500 Ma a view that is based largely on the connection of the Madagascar Craton to both India and the Zimbabwe Craton, with subsequent rifting between India and North America during the breakup of Columbia (Figure 4.7).

Chapter 7

Conclusions

7.1 Conclusions

Based on several lines of evidence, it seems clear that the SIC and BIC were not formed as a single body in Archean time. The stratigraphy of the complexes is different, indicating that the SIC was not rifted off the BIC after formation. In addition, the ages of the complexes are almost 700 Ma different (SIC older), making the possibility of coeval formation remote. The mineralogy and Pt:Pd ratios also are different, which indicates that the same magma source probably could not supply the PGE enriched magmas to the complexes, even at different times. Large variations of ratios occur in each complex, but it is unlikely that injections of magma from the same source hundreds of millions of years apart could have formed the complexes. The SIC and BIC probably formed from independent magma sources at different times. Country rock of the complexes is not similar enough to infer equivalent before intrusion. Thick sequences of igneous rock are seen in the Pretoria Group and throughout the Transvaal Supergroup, which are not observed, or known surrounding the SIC. The possibility does remain that the SIC represents the remaining fragment of a large parent PGE rich ore body that subsequently rifted apart.

Thus it is not possible to provide specific evidence for the reconstructions of Archean Columbia. This study cannot provide definitive information before the orogens of Zhao et al., (2002). Neither is it possible to provide definitive evidence during the subsequent rifting of Columbia that is proposed Rogers and Santosh, (2002). The remarkably similar overall petrologies and concentrations of PGE's of these two ancient

cratons remains a geologic mystery. Further investigations of the formation of the BIC and SIC and their relation should include the Great Dyke of Zimbabwe (2532 Ma) and the relation of the Great Dyke to the formation of the Limpopo Mobil Belt (Jensen and Bateman, 1979).

References

Bastin, E. S., 1950, Interpretation of ore textures: GSA Memoir 45, 101p.

Cawthorn, R. G., Lee, C. A., Schouwstra, R. P., and Mellowship, P., 2002, Relationship between PGE and PGM in the Bushveld Complex: The Canadian Mineralogist, v. 40, p. 311-328.

Cawthorn, R. G., and Walraven, F., 1998, Emplacement and crystallization time for the Bushveld Complex: Journal of Petrology, v. 39(9), p. 1669-1687.

Coleman, D. S, Barth, A. P., and Wooden, J. L., 2002, Early to Middle Proterozoic construction of the Mojave Province, Southwestern United States: Gondwana Research, v. 5(1), p. 75-78.

Condie, K. C., 2002, Breakup of a Paleoproterozoic supercontinent: Gondwana Research, v. 5(1), p. 41-43.

Cooper, R. W.,1985, Geology and structure of the Fishtail Creek area *in* Czamanske, G. K., and Zientek, M. L. (eds.), The Stillwater Complex, Montana: Geology and Guide, Special Publication Montana Bureau of Mines and Geology 92, p.118-124.

Eales, H. V., and Cawthorn, R. G., 1996, The Bushveld Complex *in* Cawthorn, R. G., ed., Layered Intrusions: Elsevier, p. 181-229.

Engelbrecht, J. P., 1990, The Marico Hypabyssal Suite, and the marginal zone of the Bushveld Complex in the Marico District, western Transvaal, South Africa: South African Journal of Geology, v. 93(2), p. 318-328.

Eriksson, P. G., Hattingh, P. J., and Altermann, W., 1995, An overview of the geology of the Transvaal Sequence and Bushveld Complex, South Africa: Mineralium Deposita, v. 30, p. 98-111.

Frost, B. R., 1982, Contact metamorphic effects of the Stillwater Complex, Montana: the concordant iron formation: a discussion of the role of buffering in metamorphism of iron-formation: American Mineralogist, v. 67, p. 142-148.

Guilbert, J. M., and Park, C. F. Jr., 1986, The Geology of Ore Deposits: W. H. Freeman and Company, New York, 983p.

Hartmann, L. A., 2002, The Mesoproterozoic supercontinent Atlantica in the Brazilian Shield-review of geological and U-Pb zircon and Sm-Nd isotopic evidence: Gondwana Research, v. 5(1), p. 157-163.

Heliz, R., T., 1995, The Stillwater Complex, Montana: A subvolcanic magma chamber?: American Mineralogist, v. 80(11-12), p. 1343-1346.

Howland, A. L., 1955, Chromite deposits in the central part of the Stillwater Complex, Montana: US Geological Survey Bulletin, 1015-D, p. 99-121.

Hunter, D. R., 1976, Some enigmas of the Bushveld Complex: Economic Geology, v. 71, p. 229-248.

Irvine, T. N., Keith, D. W., and Todd, S. G., 1983, The J-M platinum-palladium reef of the Stillwater Complex, Montana: II. Origin by Double-diffusive convective magma mixing and implications for the Bushveld Complex: Economic Geology, v. 78(7), p. 1287-1334.

Jackson, E. D., 1961, Primary textures and associations in the ultramafic zone of the Stillwater Complex, Montana: US Geological Survey Professional Paper 358, 106p.

Jackson, E. D., 1968, The chromite deposits of the Stillwater Complex, Montana *in* Ridge, J. D., (ed.) Ore Deposits of the United States 1933-1967: The Graton-Sales Volume, American Institute of Mining Metallurgical Engineers, v. 2, p. 1496-1510.

Jensen, M. L., and Bateman, A. M., 1979, Economic Mineral Deposits, Edition III, Wiley, 593p.

Jones, W. R., Peoples, J. W., and Howland, A. L., 1960, Igneous and tectonic structures of the Stillwater Complex, Montana: US Geological Survey Bulletin, 1071-H, p. 281-340.

Kinloch, E., D., 1982, Regional trends in the platinum-group mineralogy of the critical zone of the Bushveld Complex, South Africa: Economic Geology, v. 77, p. 1328-1347.

Labotka, T. C., 1985, Petrogenesis of the metamorphic rocks beneath the Stillwater Complex: Assemblages and conditions of metamorphism *in* Czamanske, G. K., and Zientek, M. L. (eds.), The Stillwater Complex, Montana: Geology and Guide, Special Publication Montana Bureau of Mines and Geology 92, p.70-76.

Labotka, T. C., and Kath, R. L., 2001, Petrogenesis of the contact-metamorphic rocks beneath the Stillwater Complex, Montana: GSA Bulletin, v. 113(10), p. 1312-1323.

Labotka, T. C., Vaniman, D. T., and Papike, J. J., 1982, , Contact metamorphic effects of the Stillwater Complex, Montana: the concordant iron formation: a reply to the

role of buffering in metamorphism of iron-formation: American Mineralogist, v. 67, p. 149-152

Lambert, D. D., Unruth, D. M., and Simmons, E. C., 1985, Isotopic investigations of the Stillwater Complex: A review, *in* Czamanske, G. K., and Zientek, M. L. (eds.), The Stillwater Complex, Montana: Geology and Guide, Special Publication Montana Bureau of Mines and Geology 92, p.46-54.

LeRoy, L. W., 1985,Troctolite-Anorthosite zone I and the J-M Reef: Frog Pond adit to the Graham Creek area *in* Czamanske, G. K., and Zientek, M. L. (eds.), The Stillwater Complex, Montana: Geology and Guide, Special Publication Montana Bureau of Mines and Geology 92, p.325-333.

Majzlan, J., Makovicky, M., Makovicky, E., and Rose-Hansen, J., 2002, The system Fe-Pt-S at 1100°: The Canadian Mineralogist, v. 40, p. 509-517.

Mann, E. L., and Lin, Chong-Pin, 1985, Geology of the West Fork adit *in* Czamanske, G. K., and Zientek, M. L. (eds.), The Stillwater Complex, Montana: Geology and Guide, Special Publication Montana Bureau of Mines and Geology 92, p.247-252.

Mann, E. L., Lipin, B. R., Page, N. J., Foose, M. P., and Loferski, P. J., Guide to the Stillwater Complex exposed in the West Fork area *in* Czamanske, G. K., and Zientek, M. L. (eds.), The Stillwater Complex, Montana: Geology and Guide, Special Publication Montana Bureau of Mines and Geology 92, p.231-246.

McCourt, S., 1995, The crustal architecture of the Kaapvaal crustal block South Africa, between 3.5 and 2.0, A synopsis: Mineralium Deposita, v.30, p. 89-97.

McCullum, I. S., 1996, The Stillwater Complex *in* Cawthorn, R. G., ed., Layered Intrusions: Elsevier, p. 441-483.

McLaren, C. H., and Villiers, J. P. R., 1982. The platinum-group chemistry and mineralogy of the UG-2 Chromitite Layer of the Bushveld Complex: Economic Geology, v. 77, p. 1348-1366.

Meert, J. G., 2002, Paleomagnetic evidence for a Paleo-Mesoproterozoic supercontinent Columbia: Gondwana Research, v. 5(1), p. 207-215.

Page, N. J., Zientek, M. L., 1985a, Geologic and structural setting of the Stillwater Complex, *in* Czamanske, G. K., and Zientek, M. L. (eds.), The Stillwater Complex, Montana: Geology and Guide, Special Publication Montana Bureau of Mines and Geology 92, p.1-8.

Page, N. J., Zientek, M. L., 1985b, Petrogenesis of the metamorphic rocks beneath the Stillwater Complex: Lithologies and structures *in* Czamanske, G. K., and Zientek,

M. L. (eds.), The Stillwater Complex, Montana: Geology and Guide, Special Publication Montana Bureau of Mines and Geology 92, p.55-69.

Page, N. J., Zientek, M. L., Czamanske, G. K., and Foose, M. P., 1985, Sulfide mineralization in the Stillwater Complex and underlying rocks metamorphism *in* Czamanske, G. K., and Zientek, M. L. (eds.), The Stillwater Complex, Montana: Geology and Guide, Special Publication Montana Bureau of Mines and Geology 92, p.93-96.

Peregoedova, A., and Ohnenstetter, M., 2002, Collectors of Pt, Pd, and Rh in a S-poor Fe-Ni-Cu sulfide system at 760°C: experimental data and application to ore deposits: The Canadian Mineralogist, v. 40, p. 527-561.

Rogers, J. J. W., and Santosh, M., 2002, Configuration of Columbia, a Mesoproterozoic supercontinent: Gondwana Research, v. 5(1), p. 5-22.

Raedeke, L. D., 1983, Platinum group metals in the Stillwater Complex, *in* Proceedings of the Denver Region Exploration Geologists Society Symposium, The genesis of Rocky Mountain ore deposits: Changes with time and tectonics, 1982, p. 31-37.

Sears, J. W., and Price, R. A., 2002, The hypothetical Mesoproterozoic supercontinent Columbia: implications of the Siberian-West Laurentian Connection: Gondwana Research, v. 5(1), p. 35-39.

Todd, S. G., Keith, D. W., Le Roy, L. W., Schissel, D. J., Mann, E. L., and Irvine, T. N., 1982, The J-M platinum-palladium reef of the Stillwater Complex, Montana: I. Stratigraphy and petrology: Economic Geology, v. 77, p. 1454-1480.

Turner, A. R., Wolfgram, D., and Barnes, S. J., 1985, Geology of the Stillwater County sector of the J-M Reef including the Minneapolis adit *in* Czamanske, G. K., and Zientek, M. L. (eds.), The Stillwater Complex, Montana: Geology and Guide, Special Publication Montana Bureau of Mines and Geology 92, p.210-230.

Viljoen, M. J., and Schurmann, L. W.,1998, Platinum group metals *in* Wilson, M. J. C., and Anhaeusser, C. R. (eds.), The Mineral Resources of South Africa 6th Edition: Council for Geoscience Handbook 16, p.532-568.

Verryn, S. M. C., and Merkle, R. K. W., 2002, The system PtS-PdS-NiS between 1200°C and 700°: The Canadian Mineralogist, v. 40, p. 571-584.

Wallmach, T., Hatton, C. J., and Droop, G. T. R., 1989, Extreme facies of contact metamorphism developed in calc-silicate xenoliths in the eastern Bushveld Complex: The Canadian Mineralogist, v. 27(3), p. 509-524.

Willis, J. B., and Willis, G. C., 2000, Geology of the Wasatch Mountain State Park, Utah *in* Sprinkel, D. A., Chidsey, T. C. Jr., and Anderson, P. B. (eds.), Geology of Utah Parks and Monuments: Utah Geological Association Publication 28, p. 495-516.

Uytenbogaardt, W., and Burke, E. A. J., 1985, Tables for Microscopic Identification of Ore Minerals: Dover Publications, Inc., New York, 430p.

Zhao, G., Cawood, P. A., Wilde, S. A., and Sun, M., 2002, Review of global 2.1-1.8 orogens: implications for a pre-Rodinia supercontinent: Earth-Science Reviews v.59, p. 125-162.

Zientek, M. L., Czamanske, G. K., and Irvine, T. N., 1985, Stratigraphy and nomenclature for the Stillwater Complex, *in* Czamanske, G. K., and Zientek, M. L. (eds.), The Stillwater Complex, Montana: Geology and Guide, Special Publication Montana Bureau of Mines and Geology 92, p.9-20.

Zingg, A. J., 1996, Recrystallization and the origin of layering in the Bushveld Complex: Lithos, v. 37, p. 15-37.

Appendix A

ICP-MS Results

Microscopic and chemical Analysis Research Center (MARC)
The Ohio State University
125 S. Oval Mall, 026 Mendenhall Laboratory
Columbus, OH 43210

(614) 292-6954
olesik.2@osu.edu
www.geology.ohio-state.edu/marc

July 29, 2003

03-3155

Quantitative Analysis Results using Inductively Coupled Plasma Mass Spectrometry (ICP-MS)
ThermoFinnigan Element 2 ICP-sector field-MS

Concentration uncertainties are typically +/- 1 to 10% relative,
so in some cases more significant digits are shown than are actually significant.

Element	SMC4	UG2
Pd	246	1.4 ug/g
Pt	46	0.053
Sb	0.01	0.15
Os	<0.002	<0.002
Cr	634	868
Ni	8186	1759
V	26	242
Ru	0.3	0.1

	method bla	std 4 as ch	smc4 all stds	smc 4 Pd low 3 stds	smc 4 Ni linear	TQ results smc4	ug2 all stds
Pd106(LR)	-0.228	48.9	519	490.392		849.0	6.4
Pd108(LR)	0.329	46.8	487	487.814			3.1
Pd105(LR)	-0.093	47.1	495	484.06			7.3
Pt194(LR)	0.001	5.2	89.737			81.0	0.151
Pt195(LR)	-0.188	5.4	97.1				-0.064
Pt196(LR)	-0.045	5.3	90.398				0.16
Sb121(LR)	0.002	0.004	0.027			0.033	0.311
Sb123(LR)	0.001	0.003	0.553	PdO			0.425
Os187(LR)	0.001	0.005	5.004			0.0028	11.156
Os188(LR)	0	0.005	0.0010				0.0030
Os189(LR)	0	0.005	0.0020				0.0030
Cr52(MR)	1.525	200	1246			1729	1756
Cr53(MR)	0.553	200	1246				1766
Ni60(MR)	-9.272	1288	17962		17962.04	27200	3305
Ni62(MR)	-2.621	1527	15737				3491
V51(MR)	0.158	51	104			140	493
Ru101(MR)	0.001	0.152	0.573			0.95	0.15
Ru100(MR)	0.006	0.15	1.464				1.405
Ru101(HR)	0	0.155	0.561				0.145
Ru100(HR)	0.011	0.144	0.578				2.713
Ru99(LR)	0.007	0.157	0.67				0.339

solution concentrations

	smc4	**ug2**	***TQ-smc4***	***TQ-ug2***
Pd	545	3.28	*849.0*	*2.3*
Pt	101	0.12	*81.0*	*0.1*
Sb	0.02	0.335	*0.033*	*0.57*
Os	0.002	0.004	*0.0028*	*0.000*
Cr	1405	1986	*1729*	*2687*
Ni	18140	4024	*27200*	*6574*
V	57	554	*140*	*834*
Ru	0.62	0.2	*0.95*	*0.35*
sample	0.111	0.1144		
solution	50.09	50.02		

ug2 Pd low 3 stds	ug2 Ni linear	TQ results ug2	std 4 as ch	theoretical std 4		
6.671		2.3	43.7	51.4	1.118356	ppb
3.034			41.6		1.1242	ppb
7.633			39.3		1.198941	ppb
		0.1	4.7	5.1	1.092214	ppb
			4.9		1.093782	ppb
			4.8		1.09509	ppb
		0.57	0.0050	0.005	0.8	ppb
			0.021		0.142857	ppb
		0	0.007	0.005	0.714286	ppb
			0.004		1.25	ppb
			0.005		1	ppb
		2687	178	206	1.127718	ppb
			178		1.127242	ppb
		6574	1090	1541	1.181778	ppb
			1325		1.152697	ppb
		834	45	51.4	1.123704	ppb
		0.35	0.14	0.154	1.085714	ppb
			0.127		1.181102	ppb
			0.137		1.131387	ppb
			0.136		1.058824	ppb
			0.137		1.145985	ppb

S

	method blank	std 4 as check	smc4	ug2	std 4 as check 2	
Isotope	Concentration AVG	Concentration AVG	Concentration AVG	Concentration AVG	Concentration AVG	
Pd106(LR)	0.392	46.736	490.392	6.671	41.854	ppb
Pd108(LR)	0.281	46.783	487.814	3.034	41.609	ppb
Pd105(LR)	0.443	46.572	484.06	7.633	38.933	ppb
Pt194(LR)	0.024	5.007	86.441	0.168	4.587	ppb
Pt195(LR)	0.026	5.022	86.997	0.137	4.608	ppb
Pt196(LR)	0.024	5.028	84.916	0.217	4.598	ppb
Sb121(LR)	0.002	0.004	0.024	0.276	0.005	ppb
Sb123(LR)	0.001	0.003	0.493	0.378	0.019	ppb
Os187(LR)	0.001	0.005	4.659	10.386	0.006	ppb
Os188(LR)	0	0.005	0.001	0.003	0.004	ppb
Os189(LR)	0	0.005	0.002	0.003	0.005	ppb
Ru99(LR)	0.007	0.158	0.676	0.342	0.138	ppb
Cr52(MR)	0.612	199.737	1246.783	1757.975	177.011	ppb
Cr53(MR)	0.653	200.059	1243.014	1762.015	177.489	ppb
Ni60(MR)	2.236	1264.219	17486.01	3226.288	1071.491	ppb
Ni62(MR)	2.45	1494.19	15349.164	3408.577	1296.919	ppb
V51(MR)	0.304	49.759	101.917	483.162	44.297	ppb
Ru101(MR)	0.002	0.147	0.553	0.145	0.135	ppb
Ru100(MR)	0.006	0.15	1.468	1.409	0.128	ppb
Ar40Ar40(MR)						not calib.
Ru101(HR)	0	0.152	0.548	0.142	0.135	ppb
Ru100(HR)	0.012	0.138	0.548	2.564	0.13	ppb
Ar40Ar40(HR)						not calib.

	method blank	std 4 as check	smc4	ug2	std 4 as check 2	
Isotope	Concentration AVG	Concentration AVG	Concentration AVG	Concentration AVG	Concentration AVG	
Pd106(LR)	-0.228	48.918	519.4	6.431	43.741	ppb
Pd108(LR)	0.329	46.751	487.03	3.077	41.586	ppb
Pd105(LR)	-0.093	47.104	494.724	7.263	39.288	ppb
Pt194(LR)	0.001	5.176	89.737	0.151	4.739	ppb
Pt195(LR)	-0.188	5.4	97.1	-0.064	4.937	ppb
Pt196(LR)	-0.045	5.286	90.398	0.16	4.827	ppb
Sb121(LR)	0.002	0.004	0.027	0.311	0.005	ppb
Sb123(LR)	0.001	0.003	0.553	0.425	0.021	ppb
Os187(LR)	0.001	0.005	5.004	11.156	0.007	ppb
Os188(LR)	0	0.005	0.001	0.003	0.004	ppb
Os189(LR)	0	0.005	0.002	0.003	0.005	ppb
Ru99(LR)	0.007	0.157	0.67	0.339	0.137	ppb
Cr52(MR)	1.525	200.33	1245.695	1756.067	177.642	ppb
Cr53(MR)	0.553	200.454	1246	1766.291	177.827	ppb
Ni60(MR)	-9.272	1287.901	17962.04	3304.683	1089.799	ppb
Ni62(MR)	-2.621	1527.325	15737.145	3490.741	1325.001	ppb
V51(MR)	0.158	50.615	103.83	492.803	45.043	ppb
Ru101(MR)	0.001	0.152	0.573	0.15	0.14	ppb
Ru100(MR)	0.006	0.15	1.464	1.405	0.127	ppb
Ar40Ar40(MR)						not calib.
Ru101(HR)	0	0.155	0.561	0.145	0.137	ppb
Ru100(HR)	0.011	0.144	0.578	2.713	0.136	ppb
Ar40Ar40(HR)						not calib.

03-3155 Rathburn 1 std only
Data from Sept 26, 2003
Reprocessed Sept. 29, 2003

	blank	std1	blank1	ug2
Isotope	Concentration AVG	Concentration AVG	Concentration AVG	Concentration AVG
Pd104(LR)			0.087 ppb	3.458 ppb
Pd108(LR)			-0.455 ppb	3.102 ppb
Sb121(LR)			0 ppb	0.276 ppb
Pt192(LR)			-0.036 ppb	0.806 ppb
Pt194(LR)			0.008 ppb	0.164 ppb
Pt195(LR)			0.01 ppb	0.127 ppb
Pt196(LR)			0.014 ppb	0.23 ppb
Pt198(LR)			0.016 ppb	0.123 ppb
V50(MR)			0.245 ppb	1855.821 ppb
V51(MR)			-0.018 ppb	541.557 ppb
Pd104(MR)			-0.056 ppb	3.232 ppb
Pd108(MR)			0.096 ppb	3.483 ppb
Sb121(MR)			0.002 ppb	0.304 ppb
Pt192(MR)			0.102 ppb	0.574 ppb
Pt194(MR)			-0.017 ppb	0.097 ppb
Pt195(MR)			0.02 ppb	0.115 ppb
Pt196(MR)			-0.004 ppb	0.182 ppb
Pt198(MR)			0.041 ppb	0.142 ppb
Ar40Ar40(MR)			not calib.	not calib.
Ru101(HR)			0.002 ppb	0.162 ppb
Pd104(HR)			-0.065 ppb	2.532 ppb
Pd108(HR)			0.201 ppb	3.04 ppb
Ar40Ar40(HR)			not calib.	not calib.

	blank1		ug2	
Isotope	Concentration AVG		Concentration AVG	
Pd104(LR)	0.053	ppb	3.447	ppb
Pd108(LR)	-0.299	ppb	3.204	ppb
Sb121(LR)	0	ppb	0.335	ppb
Pt192(LR)	-0.064	ppb	0.802	ppb
Pt194(LR)	-0.008	ppb	0.151	ppb
Pt195(LR)	0.003	ppb	0.122	ppb
Pt196(LR)	0.013	ppb	0.23	ppb
Pt198(LR)	-0.021	ppb	0.091	ppb
V50(MR)	-1.233	ppb	1977.05	ppb
V51(MR)	-0.134	ppb	544.222	ppb
Pd104(MR)	-0.263	ppb	3.154	ppb
Pd108(MR)	-0.755	ppb	3.053	ppb
Sb121(MR)	0.002	ppb	0.298	ppb
Pt192(MR)	0.048	ppb	0.557	ppb
Pt194(MR)	-0.065	ppb	0.051	ppb
Pt195(MR)	0.006	ppb	0.102	ppb
Pt196(MR)	-0.068	ppb	0.129	ppb
Pt198(MR)	-0.006	ppb	0.103	ppb
Ar40Ar40(MR)		not calib.		not calib.
Ru101(HR)	0.001	ppb	0.163	ppb
Pd104(HR)	-0.893	ppb	1.799	ppb
Pd108(HR)	0.047	ppb	2.963	ppb
Ar40Ar40(HR)		not calib.		not calib.

ug2
Data acquired 9/27/03

	blank1	ug2	std 2 as ch	blank2	std2 as check 3		std8
Isotope	Concentrat	Concentrat	Concentrat	Concentrat	Concentration AVG		Concentrat
Pd104(LR)	0.087	3.458	9.861	0.039	9.734	ppb	
Pd108(LR)	-0.455	3.102	9.81	-0.513	9.799	ppb	
Sb121(LR)	0	0.276	0	0	0	ppb	
Pt192(LR)	-0.036	0.806	0.994	-0.036	0.969	ppb	
Pt194(LR)	0.008	0.164	0.975	0.007	0.985	ppb	
Pt195(LR)	0.01	0.127	0.988	0.009	0.973	ppb	
Pt196(LR)	0.014	0.23	0.984	0.011	0.981	ppb	
Pt198(LR)	0.016	0.123	0.983	0.015	0.971	ppb	
V50(MR)	0.245	1855.821	10.301	0.194	9.914	ppb	
V51(MR)	-0.018	541.557	9.788	-0.076	9.701	ppb	
Pd104(MR	-0.056	3.232	9.459	-0.099	9.855	ppb	
Pd108(MR	0.096	3.483	9.712	0.044	9.638	ppb	
Sb121(MR	0.002	0.304	0	-0.001	0.001	ppb	
Pt192(MR)	0.102	0.574	1.033	0.083	1.052	ppb	
Pt194(MR)	-0.017	0.097	0.989	-0.017	0.973	ppb	
Pt195(MR)	0.02	0.115	0.978	0.019	0.98	ppb	
Pt196(MR)	-0.004	0.182	0.974	-0.005	1.006	ppb	
Pt198(MR)	0.041	0.142	1.02	0.031	1.011	ppb	
Ar40Ar40(MR)						not calib.	
Ru101(HR	0.002	0.162	0.03	0.002	0.031	ppb	
Pd104(HR)	-0.065	2.532	9.682	-0.109	9.91	ppb	
Pd108(HR)	0.201	3.04	9.814	0.165	9.789	ppb	
Ar40Ar40(HR)						not calib.	

ion AVG	data this worksheet	data with 1 std	data with std 1-4 8	
Pd	3.28	3.28		Pt 104, 108 ratio matches, not others
Pt	0.0105	0.121667		Pt 195,198 isotopes match expected ratio; others too high
Sb			0.335	
Ru	0.162	0.162		

Appendix B

SEM Results of the J-M Reef

Sample: Sample 1
Type: Default
ID:

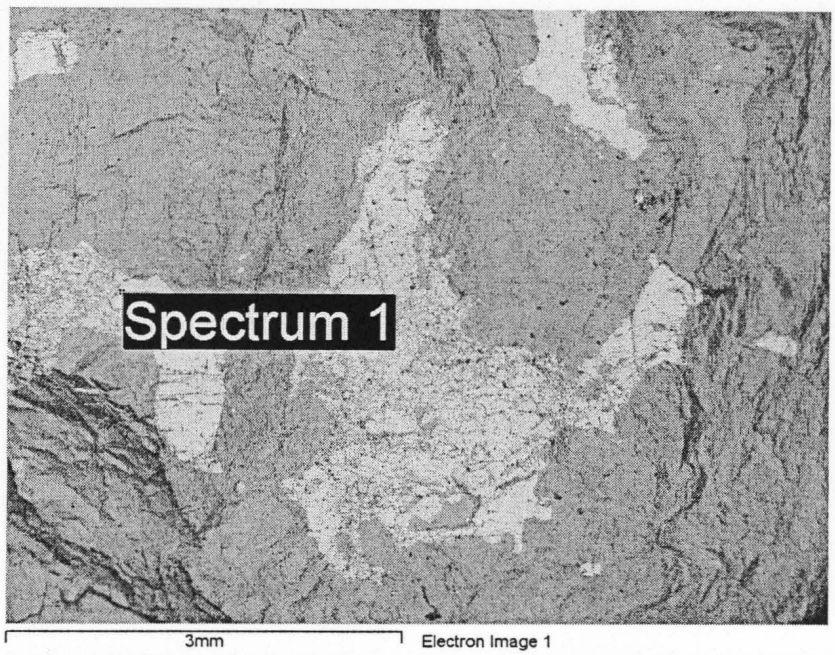

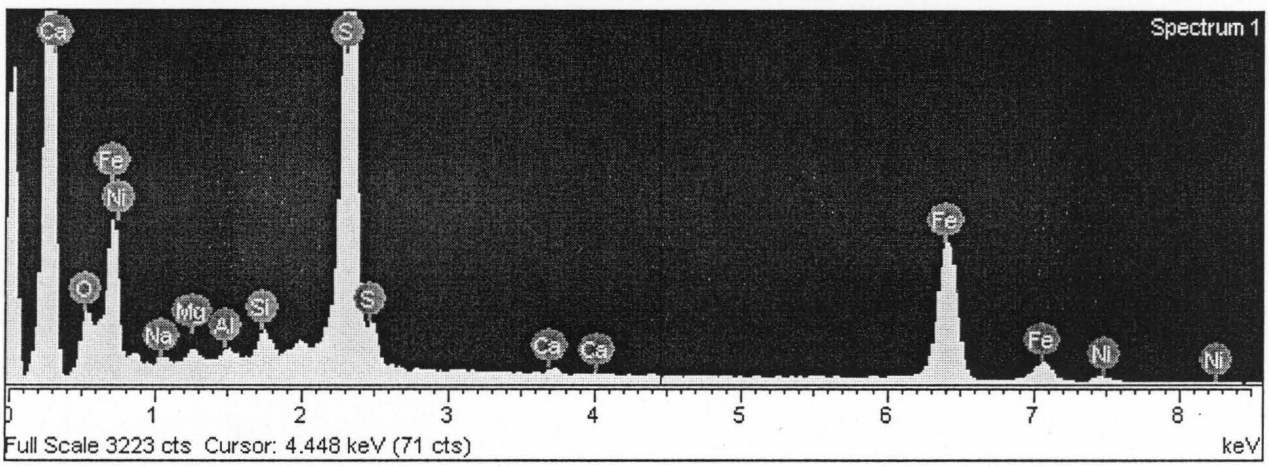

Spectrum processing :
No peaks omitted

Processing option : All elements analyzed (Normalised)
Number of iterations = 2

Standard :
O SiO2 6-Feb-2003 01:20 PM
Na NaAlSi2O6 7-Feb-2003 10:30 AM
Mg Mg Metal 5-Feb-2003 04:08 PM
Al Al Metal 5-Feb-2003 03:43 PM
Si SiO2 6-Feb-2003 01:20 PM
S FeS2 6-Feb-2003 01:51 PM
Ca CaF2 6-Feb-2003 01:16 PM
Fe Fe Metal 5-Feb-2003 04:14 PM
Ni Ni Metal 5-Feb-2003 04:01 PM

ement	App Conc.	Intensity Corrn.	Weight%	Weight% Sigma	Atomic%
O K	0.55	0.9606	5.23	0.36	12.70

a K	0.05	0.7022	0.67	0.20	1.14
Mg K	0.09	0.5144	1.54	0.34	2.46
Al K	0.04	0.6278	0.61	0.14	0.87
Si K	0.14	0.9194	1.34	0.14	1.86
S K	3.78	0.9930	34.52	0.50	41.86
Ca K	0.07	0.9898	0.65	0.14	0.63
Fe K	5.29	0.9232	51.92	0.64	36.15
Ni K	0.35	0.8981	3.52	0.49	2.33
Totals			100.00		

Sample: Sample 1
Type: Default
ID:

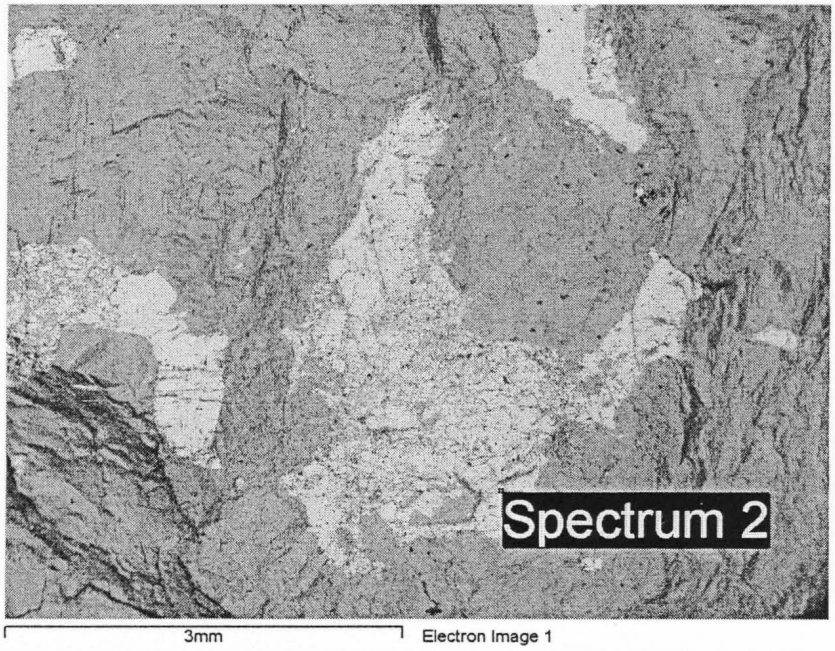

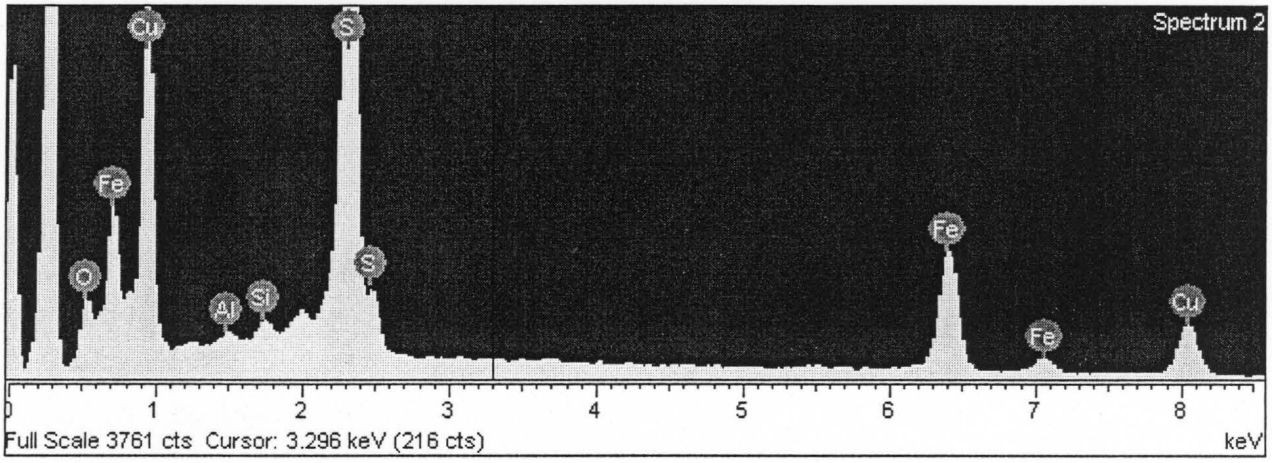

Spectrum processing :
Peaks possibly omitted : 0.267, 3.680 keV

Processing option : All elements analyzed (Normalised)
Number of iterations = 2

Standard :
O SiO2 6-Feb-2003 01:20 PM
Al Al Metal 5-Feb-2003 03:43 PM
Si SiO2 6-Feb-2003 01:20 PM
S FeS2 6-Feb-2003 01:51 PM
Fe Fe Metal 5-Feb-2003 04:14 PM
Cu Cu Metal 5-Feb-2003 03:47 PM

Element	App Conc.	Intensity Corrn.	Weight%	Weight% Sigma	Atomic%
O K	0.86	0.9520	4.86	0.24	12.64
' K	0.04	0.5867	0.39	0.11	0.60
Si K	0.11	0.8764	0.68	0.10	1.00
S K	6.09	0.9766	33.45	0.43	43.42

Fe K	5.24	0.9697	28.99	0.50	21.61
Cu K	5.25	0.8902	31.65	0.68	20.73
Totals			100.00		

Sample: Sample 1
Type: Default
ID:

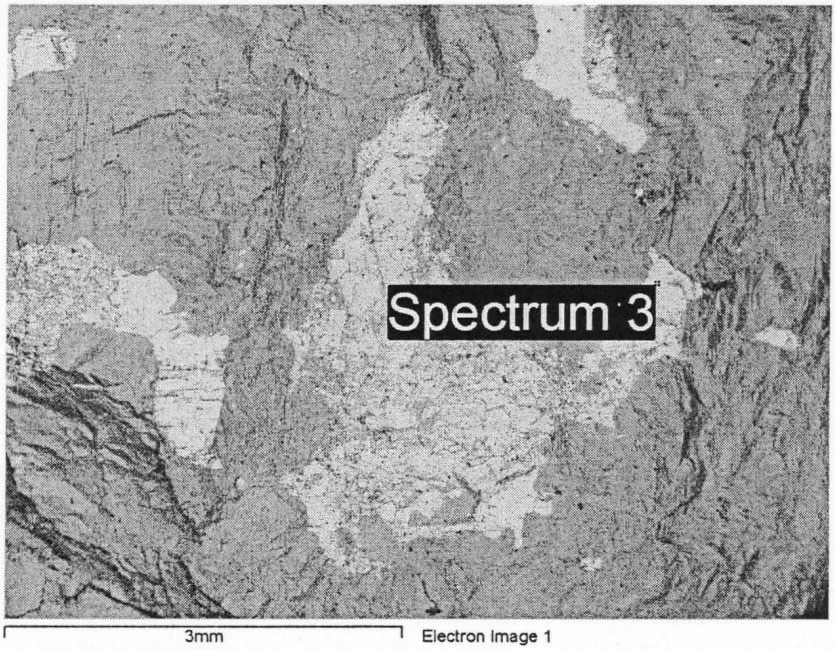

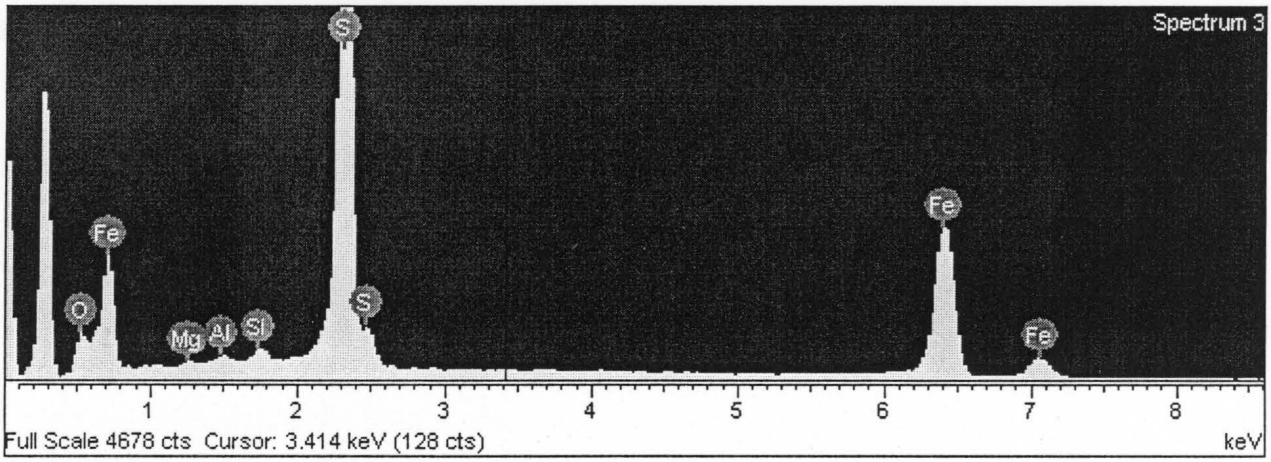

Spectrum processing :
Peak possibly omitted : 0.268 keV

Processing option : All elements analyzed (Normalised)
Number of iterations = 2

Standard :
O SiO2 6-Feb-2003 01:20 PM
Mg Mg Metal 5-Feb-2003 04:08 PM
Al Al Metal 5-Feb-2003 03:43 PM
Si SiO2 6-Feb-2003 01:20 PM
S FeS2 6-Feb-2003 01:51 PM
Fe Fe Metal 5-Feb-2003 04:14 PM

Element	App Conc.	Intensity Corrn.	Weight%	Weight% Sigma	Atomic%
O K	0.65	1.0105	4.42	0.24	11.23
g K	0.05	0.5043	0.66	0.24	1.10
Al K	0.03	0.6240	0.34	0.10	0.51
Si K	0.08	0.9190	0.62	0.10	0.90

K	4.85	1.0006	33.13	0.39	41.99
Fe K	8.27	0.9288	60.82	0.46	44.26
Totals			100.00		

Sample: Sample 1
Type: Default
ID:

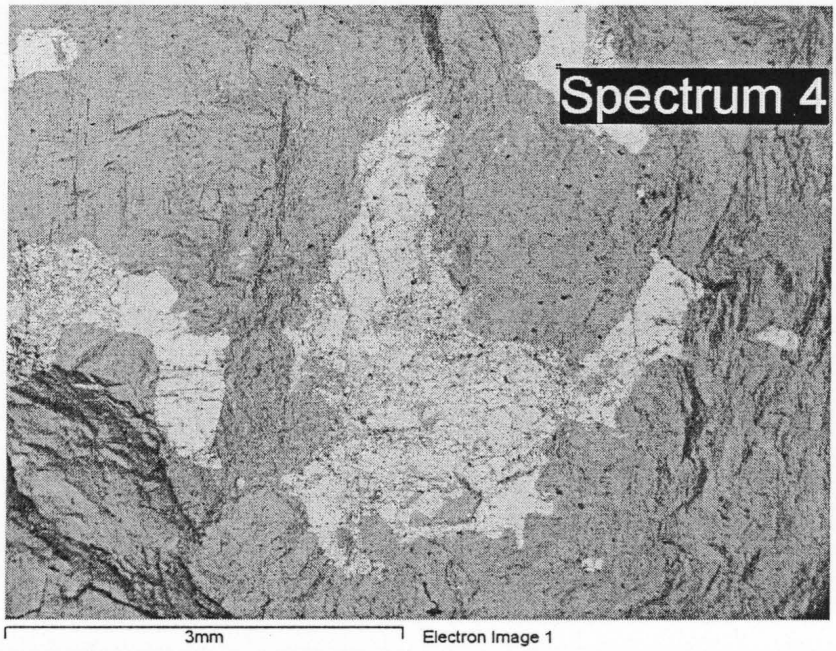

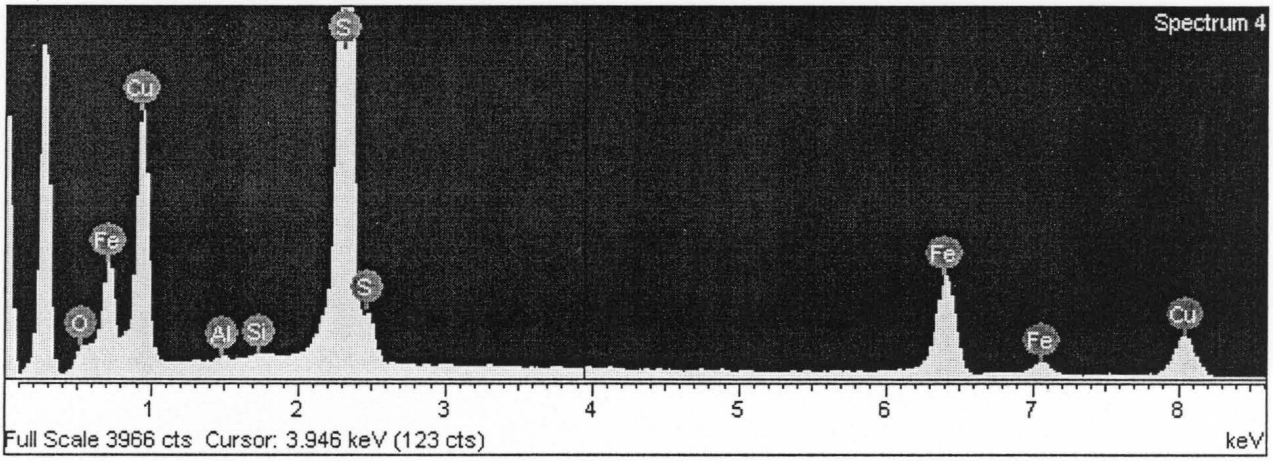

Spectrum processing :
Peak possibly omitted : 0.268 keV

Processing option : All elements analyzed (Normalised)
Number of iterations = 2

Standard :
O SiO2 6-Feb-2003 01:20 PM
Al Al Metal 5-Feb-2003 03:43 PM
Si SiO2 6-Feb-2003 01:20 PM
S FeS2 6-Feb-2003 01:51 PM
Fe Fe Metal 5-Feb-2003 04:14 PM
Cu Cu Metal 5-Feb-2003 03:47 PM

Element	App Conc.	Intensity Corrn.	Weight%	Weight% Sigma	Atomic%
O K	0.39	0.9528	2.74	0.21	7.48
' K	0.02	0.5808	0.23	0.10	0.38
ɔ1 K	0.02	0.8718	0.13	0.09	0.20
S K	4.87	0.9791	33.44	0.48	45.49

Fe K	4.46	0.9772	30.63	0.56	23.92
Cu K	4.38	0.8963	32.83	0.76	22.53
Totals			100.00		

Sample: Sample 1
Type: Default
ID:

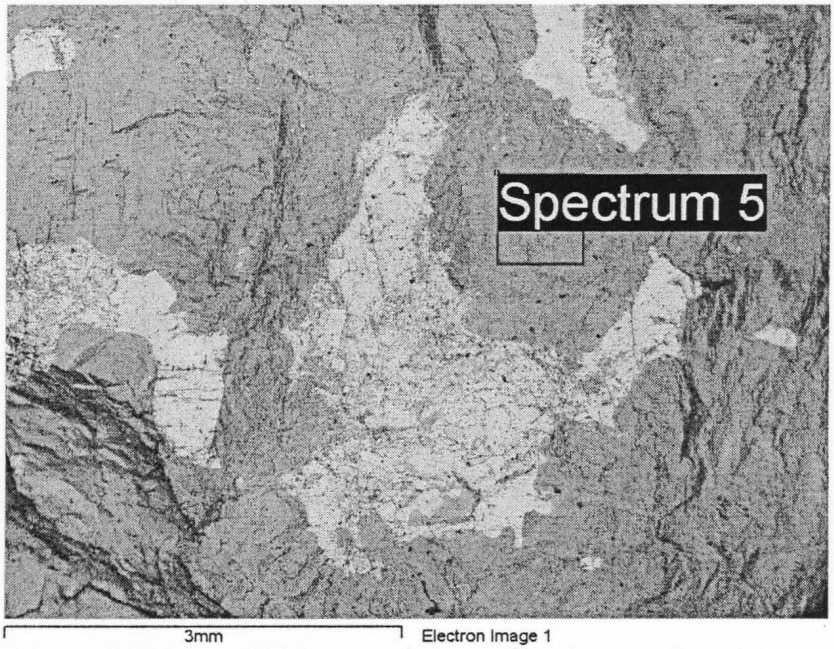

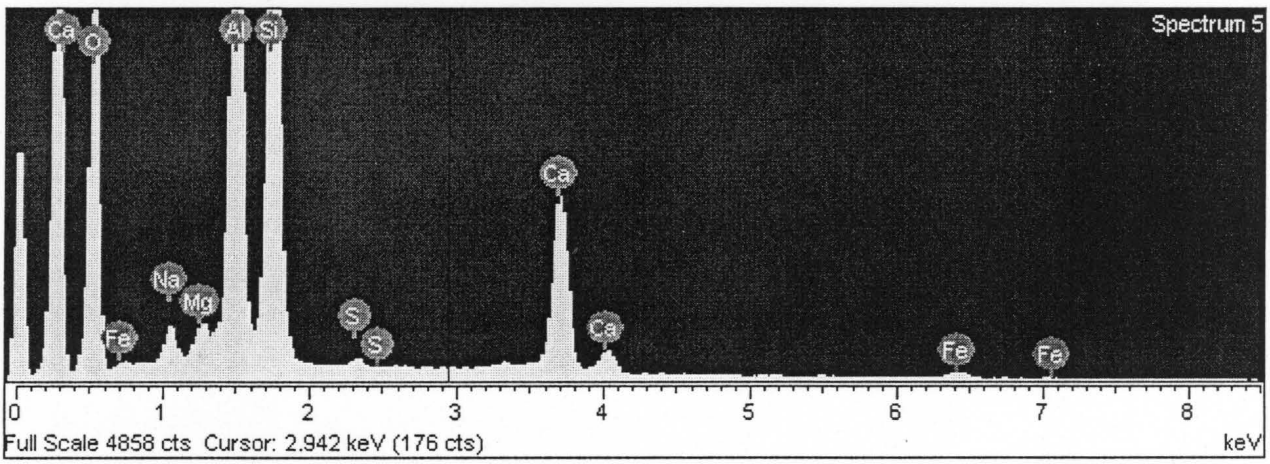

Spectrum processing :
No peaks omitted

Processing option : All elements analyzed (Normalised)
Number of iterations = 3

Standard :
O SiO2 6-Feb-2003 01:20 PM
Na NaAlSi2O6 7-Feb-2003 10:30 AM
Mg Mg Metal 5-Feb-2003 04:08 PM
Al Al Metal 5-Feb-2003 03:43 PM
Si SiO2 6-Feb-2003 01:20 PM
S FeS2 6-Feb-2003 01:51 PM
Ca CaF2 6-Feb-2003 01:16 PM
Fe Fe Metal 5-Feb-2003 04:14 PM

Element	App Conc.	Intensity Corrn.	Weight%	Weight% Sigma	Atomic%
O K	6.87	0.7935	37.83	0.35	53.27
Na K	0.33	1.0670	1.33	0.10	1.30

Mg K	0.23	0.6953	1.46	0.19	1.35
Al K	3.36	0.7660	19.15	0.20	15.99
Si K	4.83	0.8855	23.83	0.23	19.12
S K	0.08	0.8375	0.39	0.08	0.28
Ca K	2.97	0.9211	14.06	0.20	7.91
Fe K	0.36	0.8193	1.94	0.21	0.78
Totals			100.00		

Sample: Sample 1
Type: Default
ID:

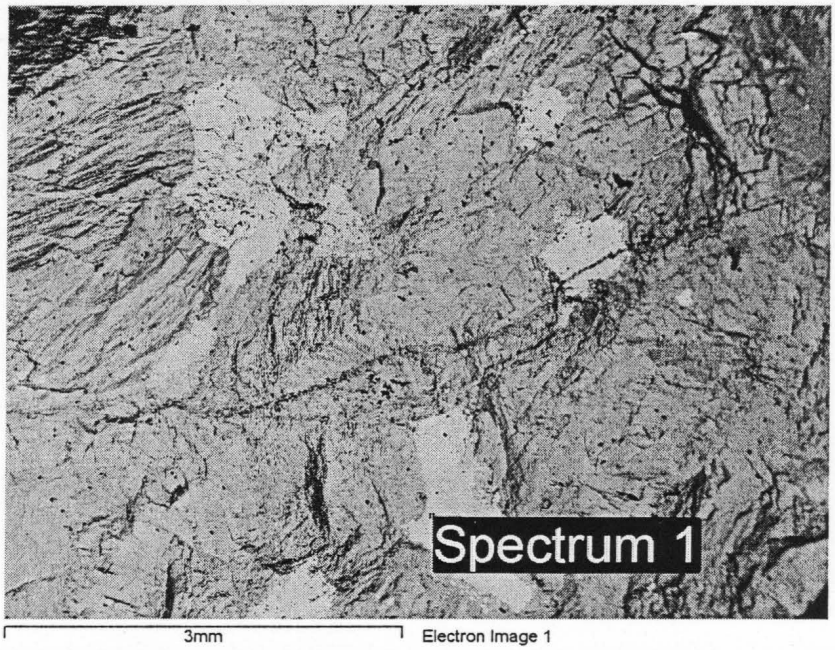

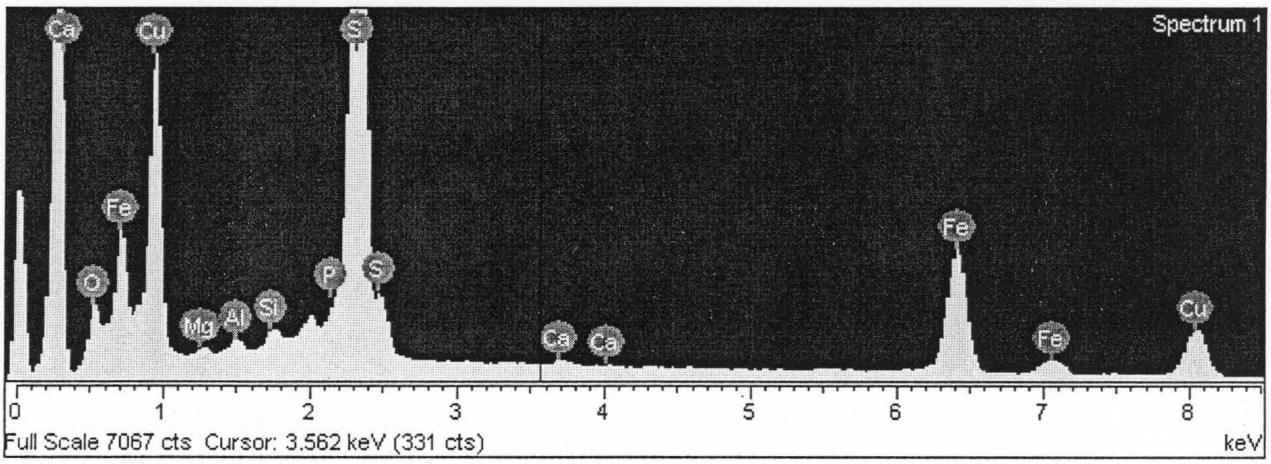

Spectrum processing :
Peaks possibly omitted : 5.500, 7.451 keV

Processing option : All elements analyzed (Normalised)
Number of iterations = 2

Standard :
O SiO2 6-Feb-2003 01:20 PM
Mg Mg Metal 5-Feb-2003 04:08 PM
Al Al Metal 5-Feb-2003 03:43 PM
Si SiO2 6-Feb-2003 01:20 PM
P Ca5(PO4)3F 7-Feb-2003 10:36 AM
S FeS2 6-Feb-2003 01:51 PM
Ca CaF2 6-Feb-2003 01:16 PM
Fe Fe Metal 5-Feb-2003 04:14 PM
Cu Cu Metal 5-Feb-2003 03:47 PM

ement	App Conc.	Intensity Corrn.	Weight%	Weight% Sigma	Atomic%
O K	1.23	0.9433	3.78	0.18	9.94

Mg K	0.11	0.4664	0.70	0.18	1.21
Al K	0.10	0.5864	0.49	0.07	0.76
Si K	0.17	0.8757	0.58	0.07	0.87
P K	0.14	0.9566	0.42	0.10	0.57
S K	11.08	0.9749	33.06	0.32	43.39
Ca K	0.12	0.9961	0.34	0.08	0.36
Fe K	10.02	0.9688	30.08	0.38	22.67
Cu K	9.36	0.8905	30.56	0.51	20.24
Totals			100.00		

Sample: Sample 1
Type: Default
ID:

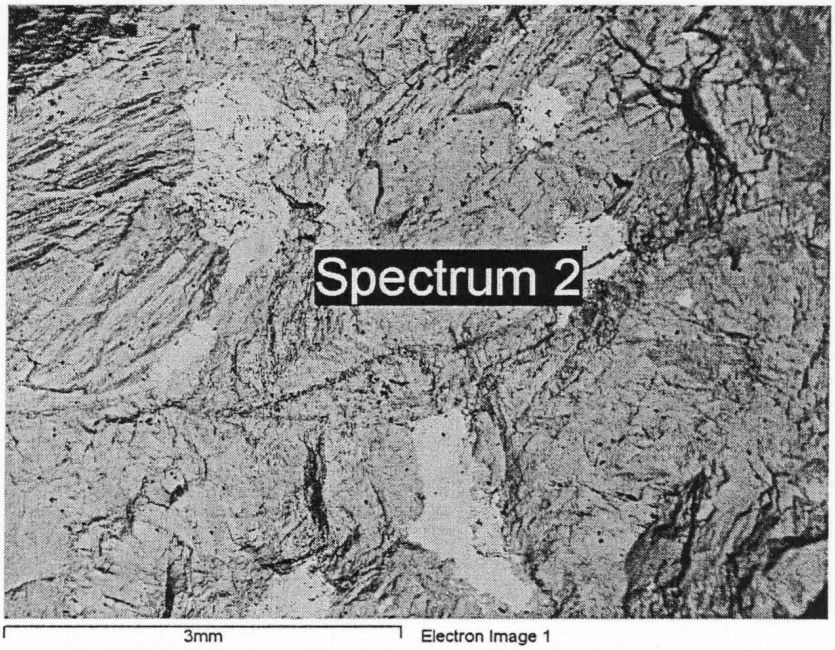

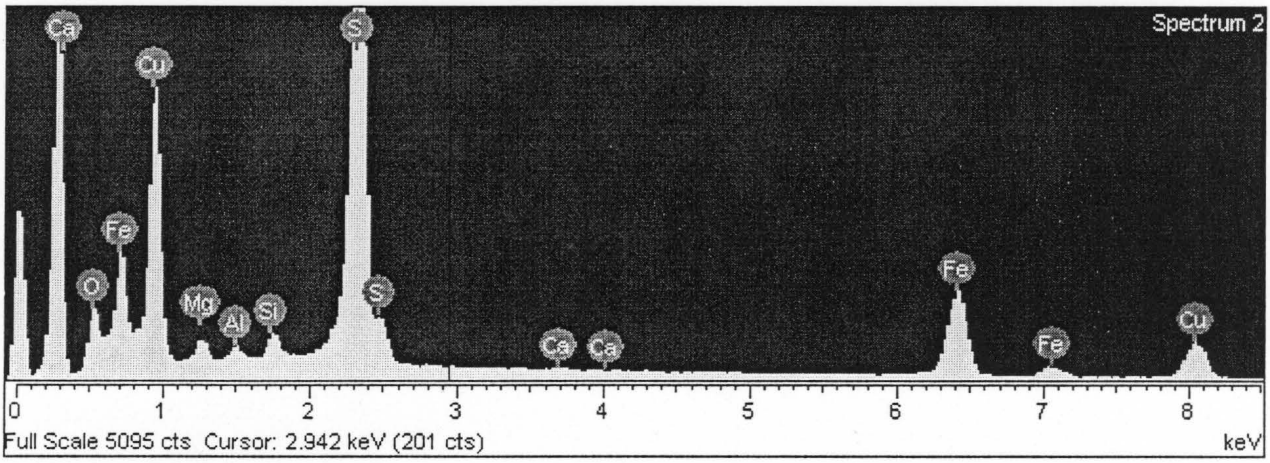

Spectrum processing :
No peaks omitted

Processing option : All elements analyzed (Normalised)
Number of iterations = 2

Standard :
O SiO2 6-Feb-2003 01:20 PM
Mg Mg Metal 5-Feb-2003 04:08 PM
Al Al Metal 5-Feb-2003 03:43 PM
Si SiO2 6-Feb-2003 01:20 PM
S FeS2 6-Feb-2003 01:51 PM
Ca CaF2 6-Feb-2003 01:16 PM
Fe Fe Metal 5-Feb-2003 04:14 PM
Cu Cu Metal 5-Feb-2003 03:47 PM

Element	App Conc.	Intensity Corrn.	Weight%	Weight% Sigma	Atomic%
O K	1.42	0.9544	5.47	0.25	13.73
Mg K	0.35	0.4737	2.69	0.27	4.45

Al K	0.10	0.5832	0.63	0.10	0.94
Si K	0.27	0.8696	1.13	0.10	1.62
S K	8.40	0.9681	31.98	0.41	40.05
Ca K	0.06	0.9910	0.23	0.10	0.23
Fe K	7.22	0.9630	27.64	0.48	19.88
Cu K	7.25	0.8850	30.22	0.66	19.10
Totals			100.00		

Sample: Sample 1
Type: Default
ID:

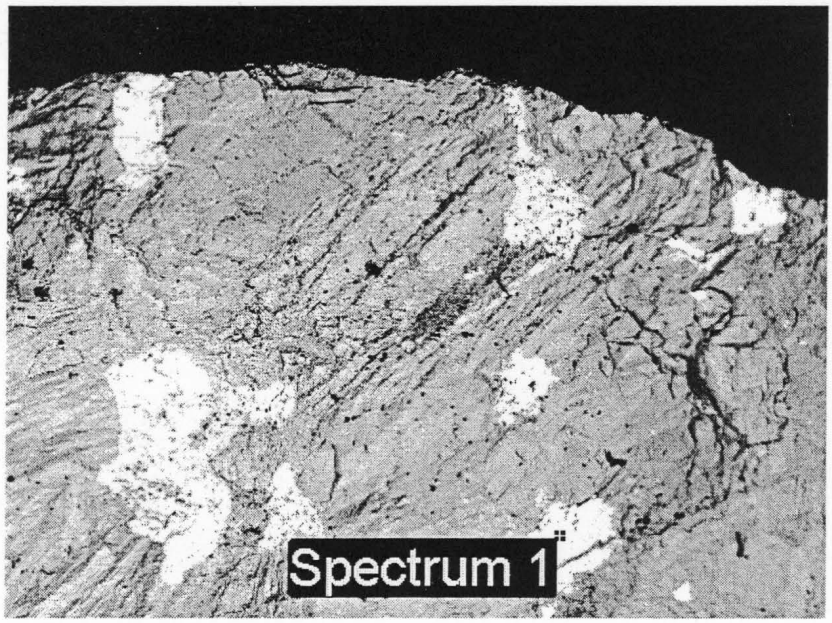

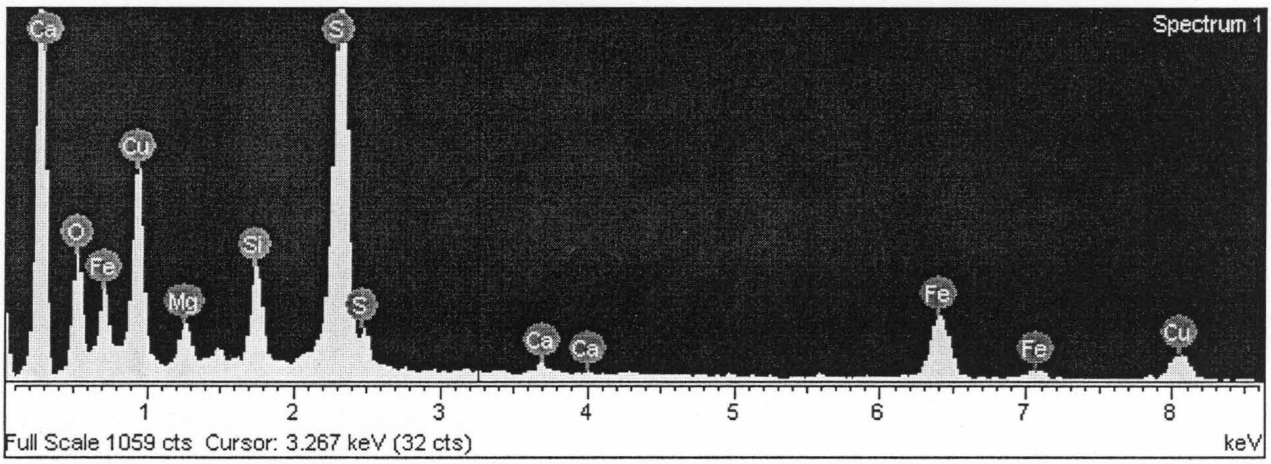

Spectrum processing :
No peaks omitted

Processing option : All elements analyzed (Normalised)
Number of iterations = 3

Standard :
O SiO2 6-Feb-2003 01:20 PM
Mg Mg Metal 5-Feb-2003 04:08 PM
Si SiO2 6-Feb-2003 01:20 PM
S FeS2 6-Feb-2003 01:51 PM
Ca CaF2 6-Feb-2003 01:16 PM
Fe Fe Metal 5-Feb-2003 04:14 PM
Cu Cu Metal 5-Feb-2003 03:47 PM

Element	App Conc.	Intensity Corrn.	Weight%	Weight% Sigma	Atomic%
K	4.19	0.9775	12.52	0.72	27.02
Mg K	1.05	0.5019	6.10	0.68	8.67
Si K	1.54	0.8767	5.15	0.33	6.33

K	8.79	0.9450	27.19	0.84	29.28
Ca K	0.30	0.9754	0.90	0.25	0.77
Fe K	7.63	0.9349	23.85	1.06	14.75
Cu K	7.17	0.8627	24.28	1.52	13.19
Totals			100.00		

Sample: Sample 1
Type: Default
ID:

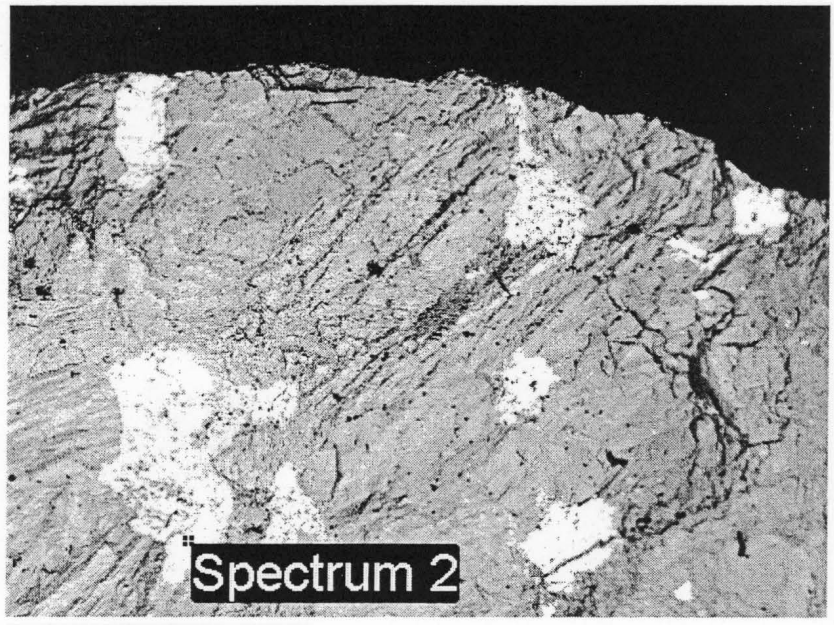

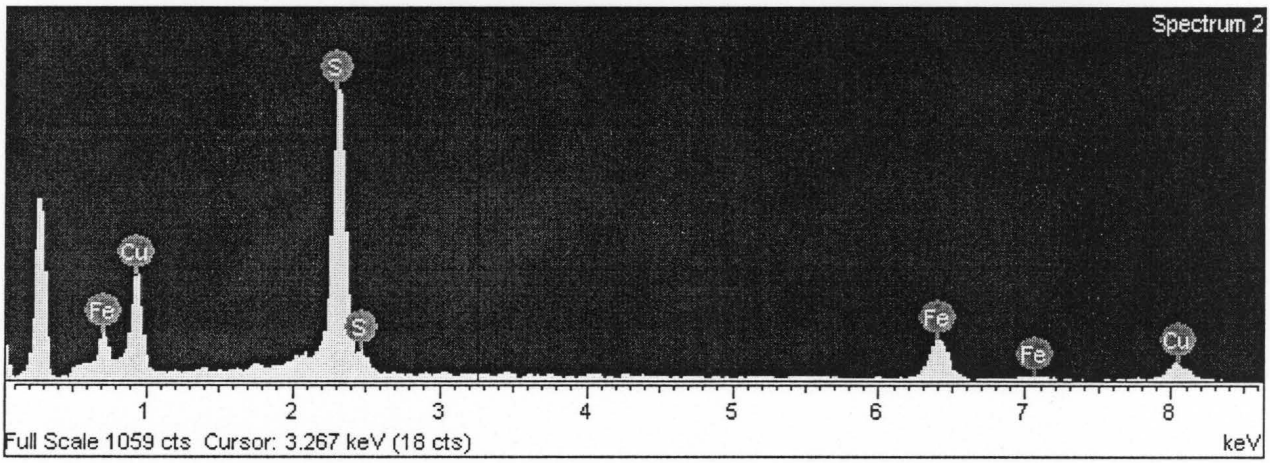

Spectrum processing :
Peak possibly omitted : 0.268 keV

Processing option : All elements analyzed (Normalised)
Number of iterations = 2

Standard :
S FeS2 6-Feb-2003 01:51 PM
Fe Fe Metal 5-Feb-2003 04:14 PM
Cu Cu Metal 5-Feb-2003 03:47 PM

Element	App Conc.	Intensity Corrn.	Weight%	Weight% Sigma	Atomic%
S K	12.22	0.9873	37.69	1.63	52.88
Fe K	9.87	0.9750	30.84	1.78	24.84
Cu K	9.27	0.8970	31.46	2.41	22.28
Totals			100.00		

Sample: Sample 1
Type: Default
ID:

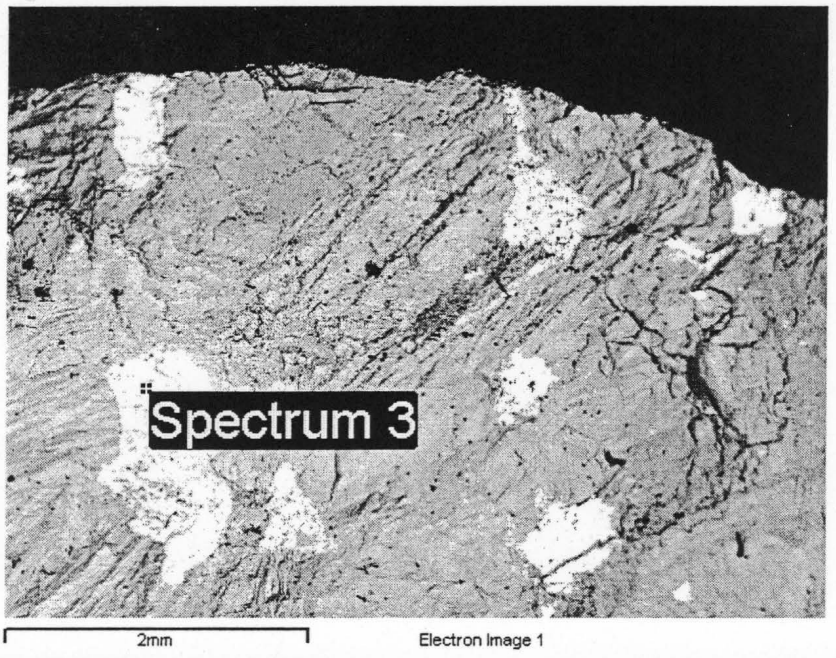

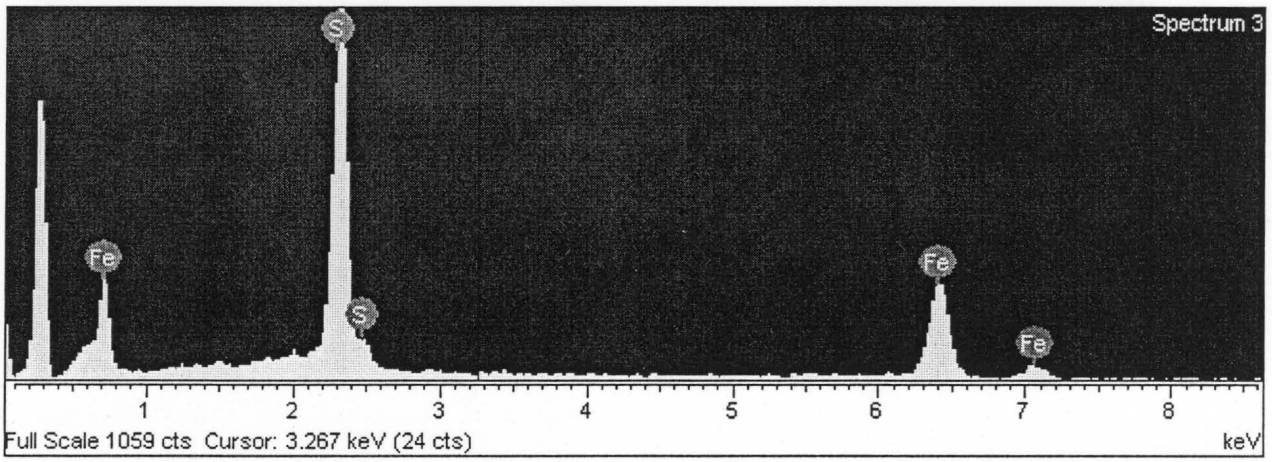

Spectrum processing :
Peak possibly omitted : 0.268 keV

Processing option : All elements analyzed (Normalised)
Number of iterations = 2

Standard :
S FeS2 6-Feb-2003 01:51 PM
Fe Fe Metal 5-Feb-2003 04:14 PM

Element	App Conc.	Intensity Corrn.	Weight%	Weight% Sigma	Atomic%
S K	12.86	1.0143	39.00	1.10	52.68
Fe K	18.50	0.9329	61.00	1.10	47.32
Totals			100.00		

Sample: Sample 1
Type: Default
ID:

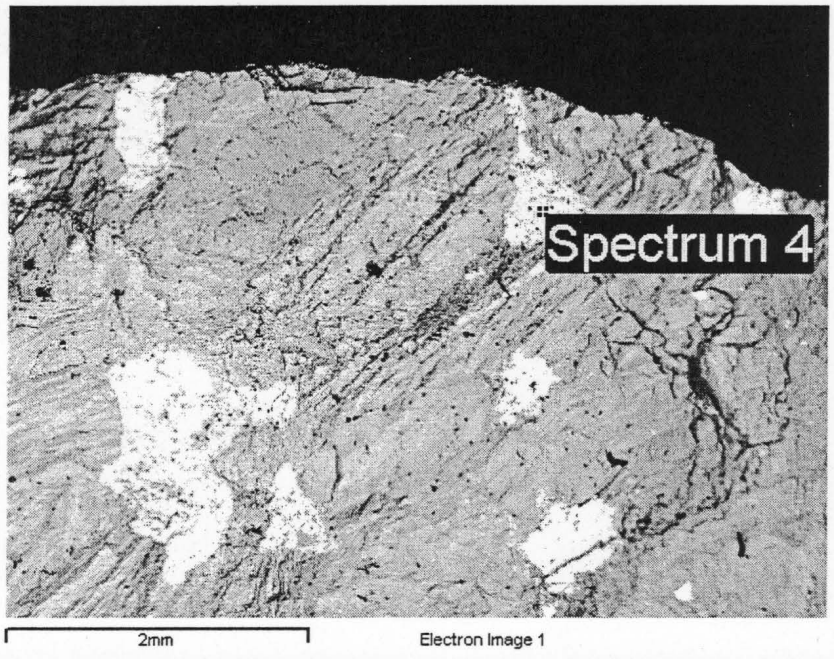

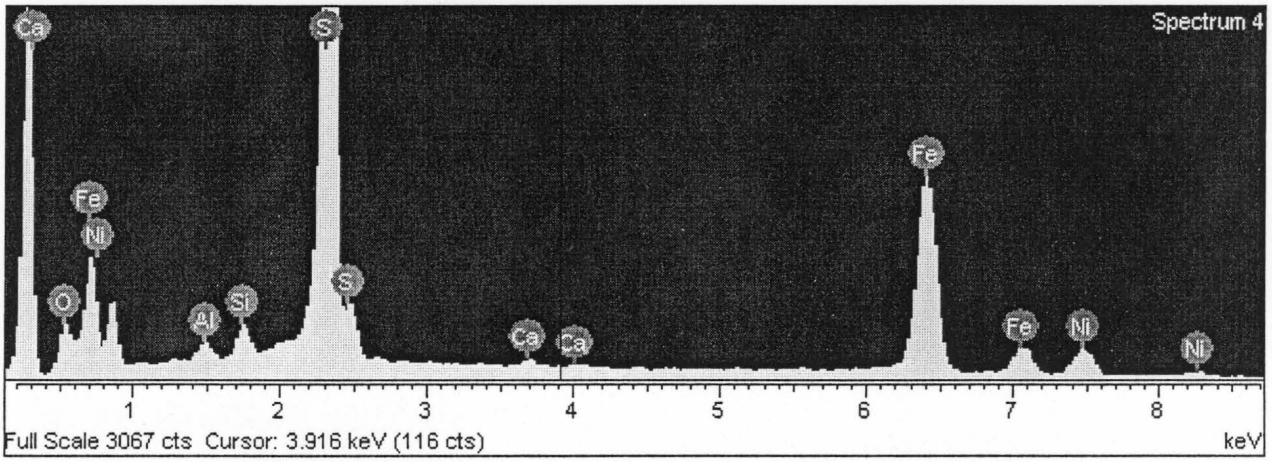

Spectrum processing :
No peaks omitted

Processing option : All elements analyzed (Normalised)
Number of iterations = 2

Standard :
O SiO2 6-Feb-2003 01:20 PM
Al Al Metal 5-Feb-2003 03:43 PM
Si SiO2 6-Feb-2003 01:20 PM
S FeS2 6-Feb-2003 01:51 PM
Ca CaF2 6-Feb-2003 01:16 PM
Fe Fe Metal 5-Feb-2003 04:14 PM
Ni Ni Metal 5-Feb-2003 04:01 PM

Element	App Conc.	Intensity Corrn.	Weight%	Weight% Sigma	Atomic%
K	0.76	1.0184	3.08	0.22	8.20
Al K	0.09	0.6022	0.64	0.10	1.01
Si K	0.25	0.8925	1.18	0.10	1.79

K	7.07	0.9846	29.75	0.40	39.52
Ca K	0.10	1.0080	0.41	0.12	0.43
Fe K	11.93	0.9506	51.99	0.56	39.65
Ni K	2.86	0.9137	12.95	0.57	9.39
Totals			100.00		

Sample: Sample 1
Type: Default
ID:

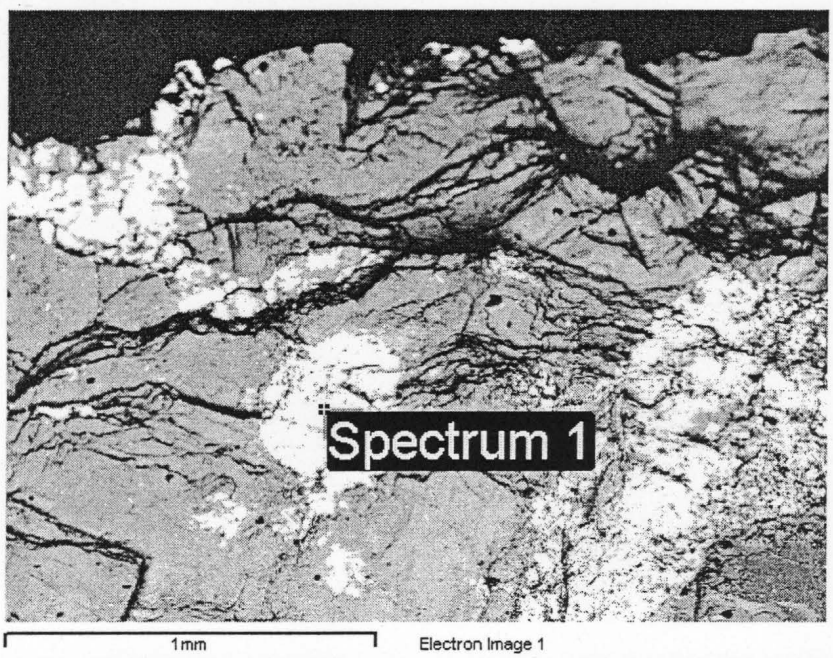

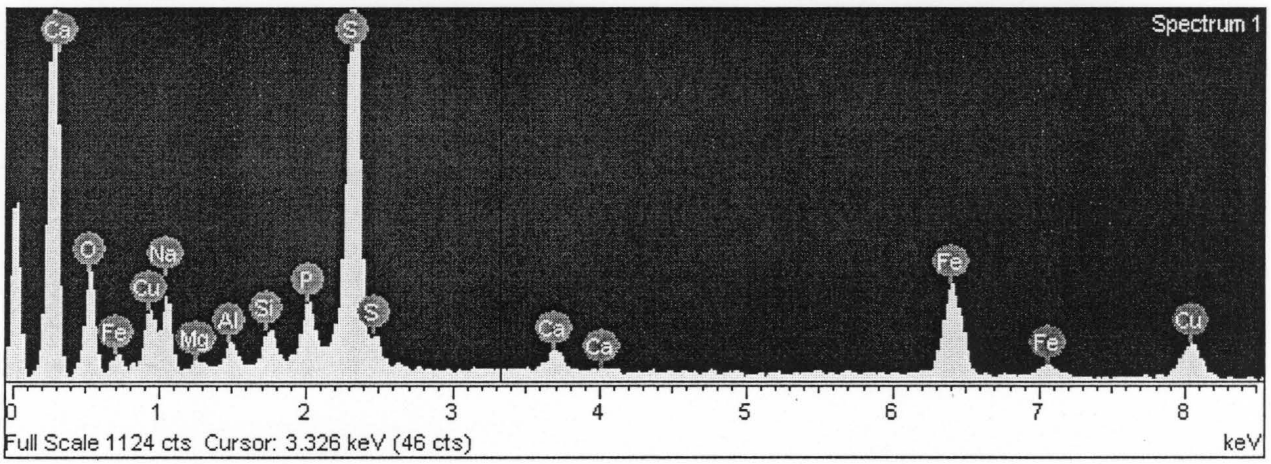

Spectrum processing :
No peaks omitted

Processing option : All elements analyzed (Normalised)
Number of iterations = 2

Standard :
O SiO2 6-Feb-2003 01:20 PM
Na NaAlSi2O6 7-Feb-2003 10:30 AM
Mg Mg Metal 5-Feb-2003 04:08 PM
Al Al Metal 5-Feb-2003 03:43 PM
Si SiO2 6-Feb-2003 01:20 PM
P Ca5(PO4)3F 7-Feb-2003 10:36 AM
S FeS2 6-Feb-2003 01:51 PM
Ca CaF2 6-Feb-2003 01:16 PM
Fe Fe Metal 5-Feb-2003 04:14 PM
Cu Cu Metal 5-Feb-2003 03:47 PM

Element	App Conc.	Intensity Corrn.	Weight%	Weight% Sigma	Atomic%

O K	2.16	1.0162	8.59	0.53	20.03
Na K	0.95	0.6883	5.61	0.47	9.10
Mg K	0.12	0.4599	1.05	0.46	1.62
Al K	0.17	0.5770	1.19	0.20	1.65
Si K	0.34	0.8574	1.61	0.21	2.14
P K	0.69	0.9297	3.00	0.31	3.62
S K	5.06	0.9421	21.71	0.68	25.27
Ca K	0.45	0.9982	1.83	0.27	1.71
Fe K	6.77	0.9538	28.68	1.05	19.17
Cu K	5.81	0.8772	26.73	1.47	15.70
Totals			100.00		

Sample: Sample 1
Type: Default
ID:

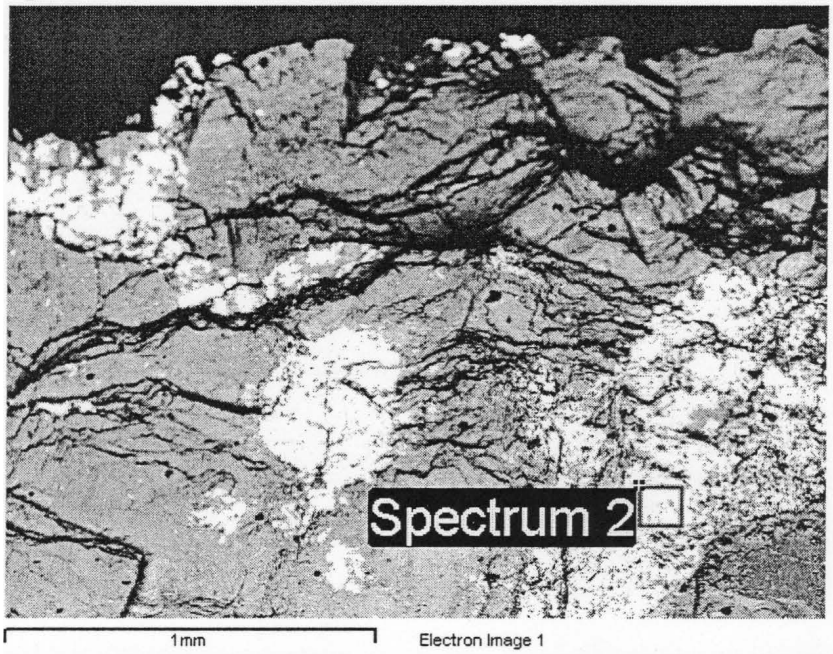

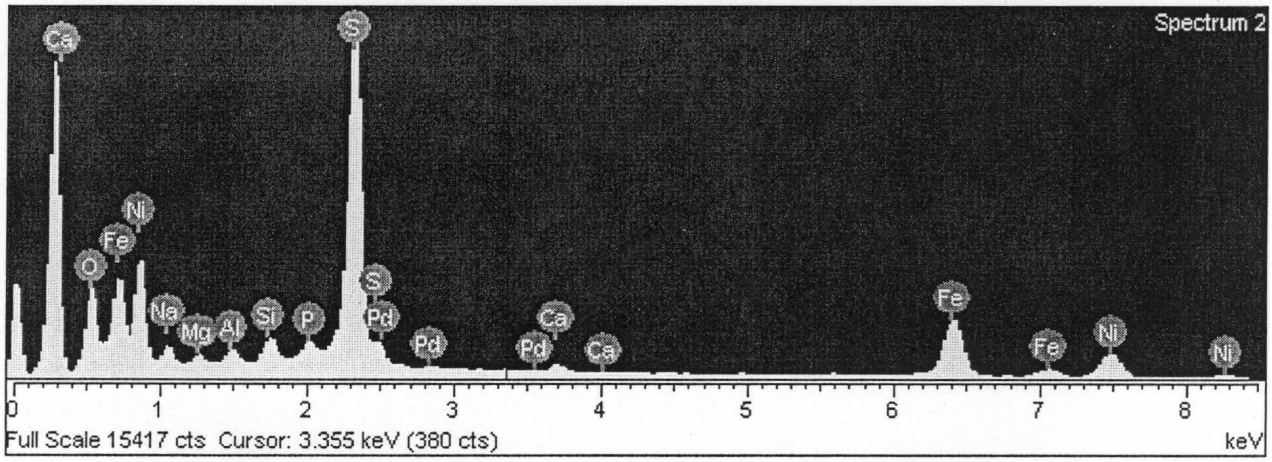

Spectrum processing :
No peaks omitted

Processing option : All elements analyzed (Normalised)
Number of iterations = 3

Standard :
O SiO2 6-Feb-2003 01:20 PM
Na NaAlSi2O6 7-Feb-2003 10:30 AM
Mg Mg Metal 5-Feb-2003 04:08 PM
Al Al Metal 5-Feb-2003 03:43 PM
Si SiO2 6-Feb-2003 01:20 PM
P Ca5(PO4)3F 7-Feb-2003 10:36 AM
S FeS2 6-Feb-2003 01:51 PM
Ca CaF2 6-Feb-2003 01:16 PM
Fe Fe Metal 5-Feb-2003 04:14 PM
Ni Ni Metal 5-Feb-2003 04:01 PM
1 Pd 1-Jun-1999 12:00 AM

Element	App	Intensity	Weight%	Weight%	Atomic%

	Conc.	Corrn.		Sigma	
O K	3.24	0.9436	9.23	0.24	21.43
Na K	0.57	0.6779	2.28	0.14	3.68
Mg K	0.33	0.4914	1.80	0.19	2.75
Al K	0.24	0.6032	1.08	0.08	1.48
Si K	0.57	0.8865	1.72	0.08	2.27
P K	0.41	0.9525	1.14	0.10	1.37
S K	9.84	0.9646	27.42	0.29	31.76
Ca K	0.37	0.9766	1.02	0.09	0.95
Fe K	10.17	0.9464	28.89	0.37	19.21
Ni K	7.43	0.9093	21.97	0.41	13.90
Pd L	0.95	0.7370	3.45	0.49	1.20
Totals			100.00		

Sample: Sample 1
Type: Default
ID:

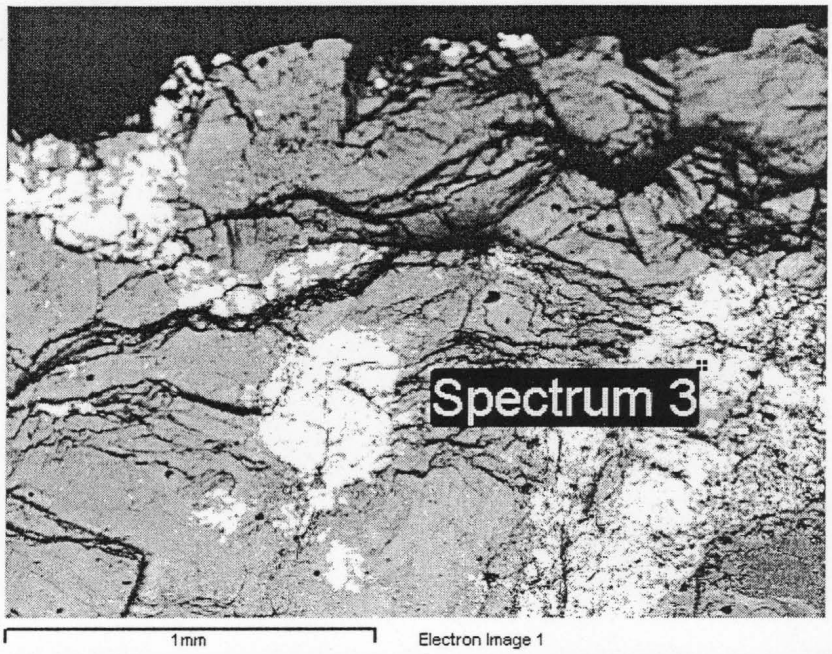

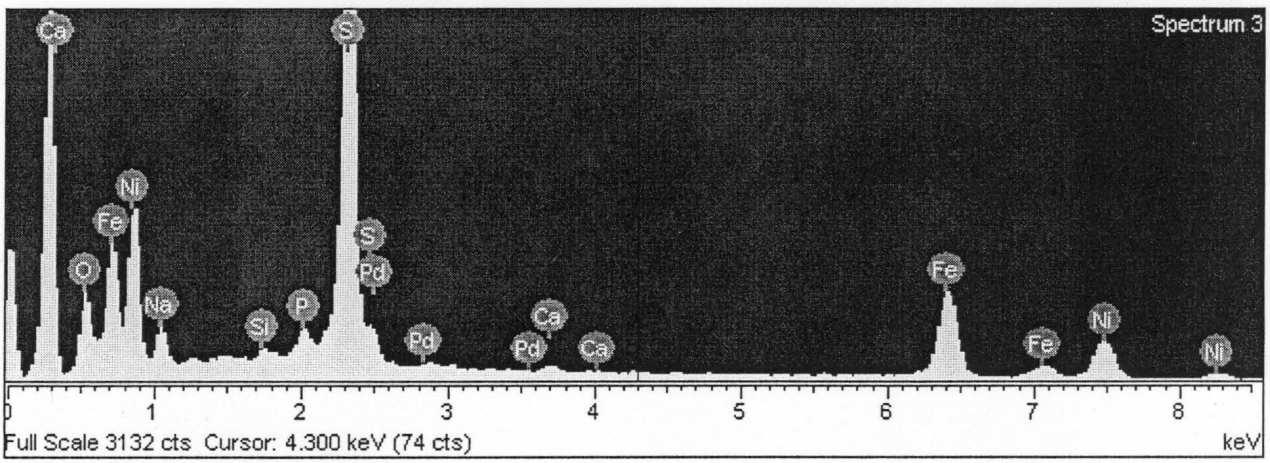

Spectrum processing :
Peak possibly omitted : 1.260 keV

Processing option : All elements analyzed (Normalised)
Number of iterations = 2

Standard :
O SiO2 6-Feb-2003 01:20 PM
Na NaAlSi2O6 7-Feb-2003 10:30 AM
Si SiO2 6-Feb-2003 01:20 PM
P Ca5(PO4)3F 7-Feb-2003 10:36 AM
S FeS2 6-Feb-2003 01:51 PM
Ca CaF2 6-Feb-2003 01:16 PM
Fe Fe Metal 5-Feb-2003 04:14 PM
Ni Ni Metal 5-Feb-2003 04:01 PM
Pd Pd 1-Jun-1999 12:00 AM

Element	App Conc.	Intensity Corrn.	Weight%	Weight% Sigma	Atomic%
O K	1.96	0.9356	6.14	0.39	15.08

Na K	0.76	0.6616	3.37	0.26	5.76
Si K	0.16	0.8911	0.53	0.12	0.75
P K	0.45	0.9657	1.37	0.18	1.74
S K	10.15	0.9739	30.49	0.56	37.36
Ca K	0.23	0.9810	0.68	0.14	0.67
Fe K	9.91	0.9561	30.31	0.69	21.33
Ni K	7.63	0.9154	24.37	0.77	16.31
Pd L	0.69	0.7350	2.74	0.91	1.01
Totals			100.00		

Sample: Sample 1
Type: Default
ID:

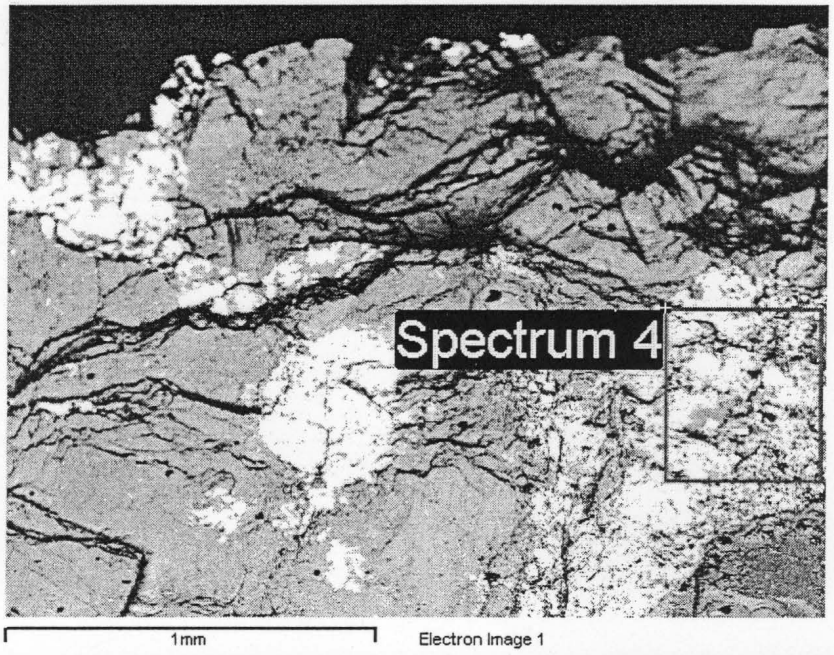

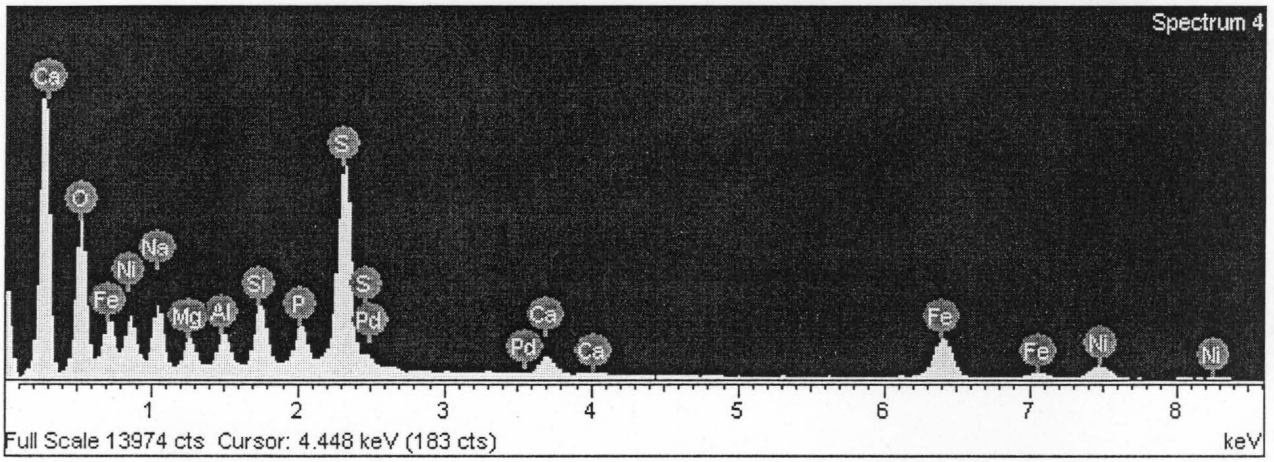

Spectrum processing :
No peaks omitted

Processing option : All elements analyzed (Normalised)
Number of iterations = 3

Standard :
O SiO2 6-Feb-2003 01:20 PM
Na NaAlSi2O6 7-Feb-2003 10:30 AM
Mg Mg Metal 5-Feb-2003 04:08 PM
Al Al Metal 5-Feb-2003 03:43 PM
Si SiO2 6-Feb-2003 01:20 PM
P Ca5(PO4)3F 7-Feb-2003 10:36 AM
S FeS2 6-Feb-2003 01:51 PM
Ca CaF2 6-Feb-2003 01:16 PM
Fe Fe Metal 5-Feb-2003 04:14 PM
Ni Ni Metal 5-Feb-2003 04:01 PM
Pd Pd 1-Jun-1999 12:00 AM

Element	App	Intensity	Weight%	Weight%	Atomic%

	Conc.	Corrn.		Sigma	
O K	6.34	0.9807	20.03	0.30	36.85
Na K	1.67	0.7926	6.51	0.16	8.33
Mg K	0.95	0.5314	5.55	0.22	6.72
Al K	0.52	0.6157	2.61	0.09	2.85
Si K	1.30	0.8823	4.57	0.11	4.79
P K	1.05	0.9211	3.53	0.12	3.35
S K	5.54	0.9229	18.59	0.22	17.07
Ca K	0.86	0.9561	2.79	0.11	2.05
Fe K	6.19	0.8992	21.34	0.34	11.25
Ni K	3.42	0.8766	12.10	0.37	6.07
Pd L	0.56	0.7300	2.39	0.47	0.66
Totals			100.00		